

# Making Stars

*Alyssa A. Goodman (Harvard-Smithsonian Center for Astrophysics)*

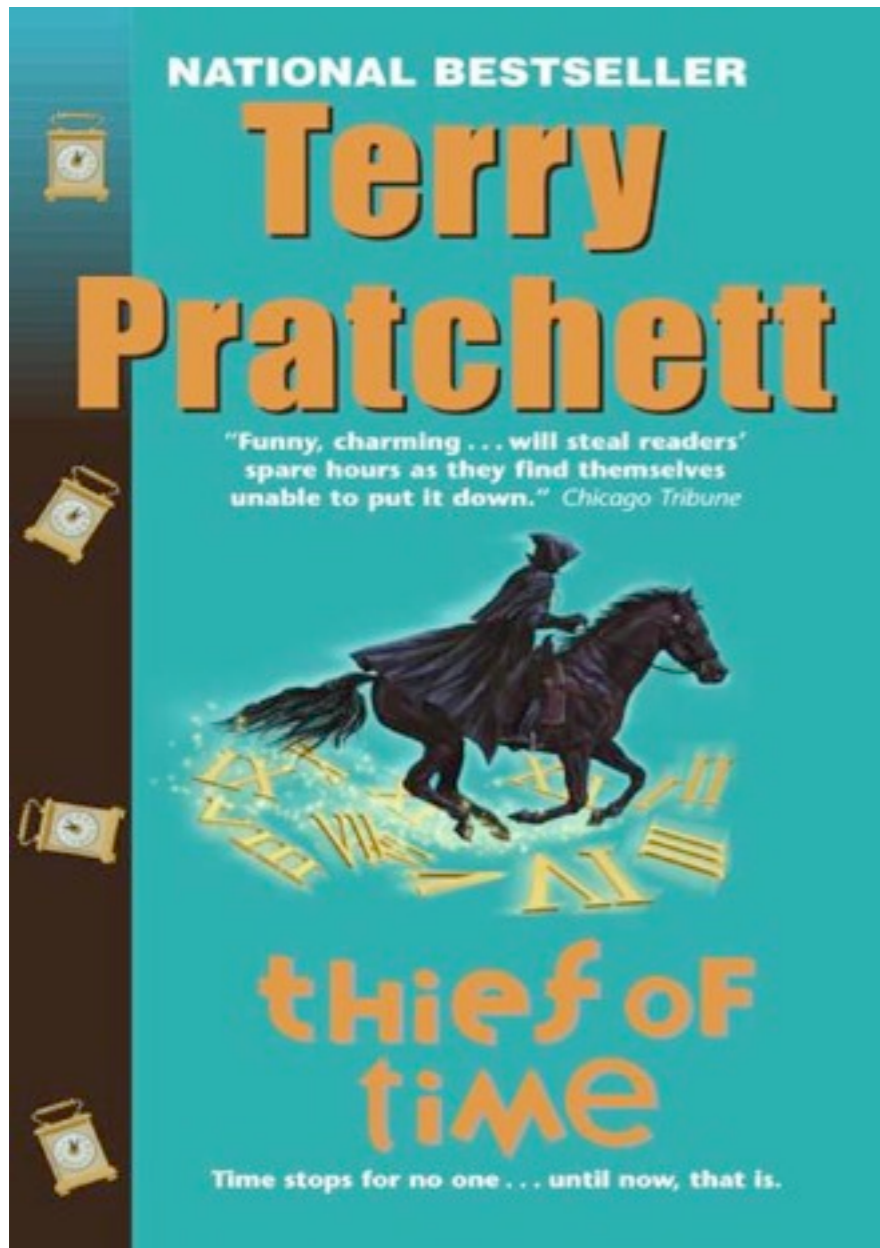
*with*

*João Alves, Héctor Arce, Frank Bertoldi, Michelle Borkin, Paola Caselli, David Collins, Jonathan Foster, Katherine Guenthner, Michael Halle, Jens Kauffmann, Helen Kirk, Elizabeth Lada, Phil Myers, Stella Offner, Jaime Pineda, Naomi Ridge, Carlos Román-Zúñiga, Erik Rosolowsky, Sana Sharma, Scott Schnee, & Rahul Shetty  
& thanks to Douglas Alan, Chris Beaumont, Kevin Covey, Nick Holliman, Doug Johnstone, Kaisey Mandel, Gus Muench, Paolo Padoan, & Tom Robitaille*





# FYI: “Accounting” won’t work



For something to exist, it has to be observed.

For something to exist, it has to have a position in time and space.

And this explains why nine-tenths of the mass of the universe is unaccounted for.

Nine-tenths of the universe is the knowledge of the position and direction of everything in the other tenth. Every atom has its biography, every star its file, every chemical exchange its equivalent of the inspector with a clipboard. It is unaccounted for because it is doing the accounting for the rest of it, and you cannot see the back of your own head.\*

---

\*Except in very small universes.



# Holistic Star Formation

holistic | hō'listik |

adjective chiefly Philosophy  
characterized by comprehension of the parts of  
something as intimately interconnected and  
explicable only by reference to the whole



Magnetic  
Fields

Gravity

Chemical & Phase  
Transformations

~ 1 pc

“Holistic Physics”

Radiation

Thermal  
Pressure

“Turbulence”  
(Random Kinetic Energy)

Outflows  
& Winds



...from 0.1 pc to 100 pc

Massive Star-Forming Regions

warm dust cold dust

HII regions(+SNR)

radio SNR

20 cm VLA from MAGPIS (Helfand et al. 2006) & MIR from Spitzer GLIMPSE (see Churchwell et al.)

3.6, 4.5, 8.0, 20cm (Luptonized, see Lupton et al. 2004)

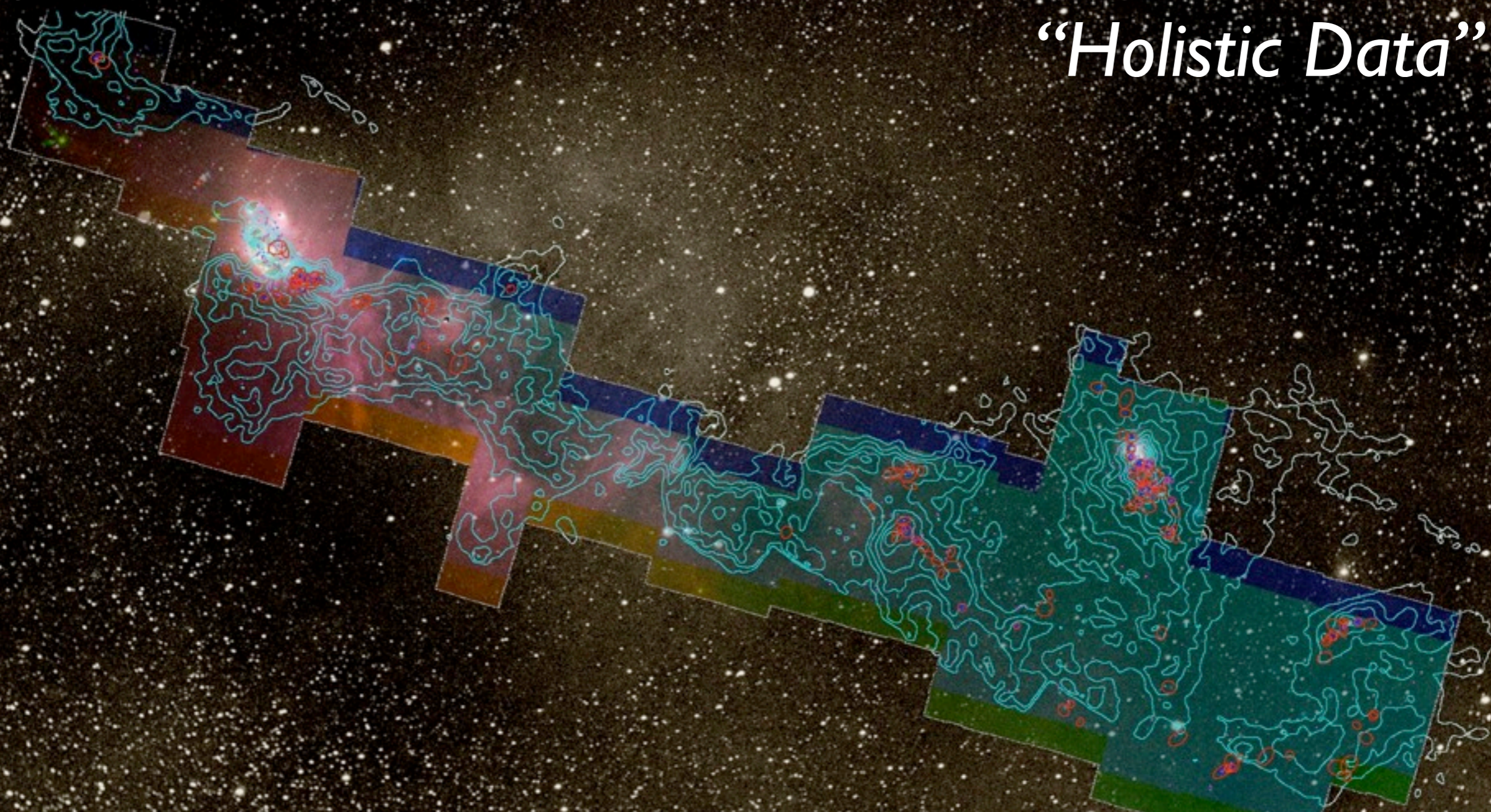
image "height" is 1.6 degrees (e.g. 140 pc at 5 kpc)



# COMPLETE =

**CO**ordinated **M**olecular **P**robe **L**ine **E**xinction **T**hermal  
**E**mission Survey of Star-Forming Regions

“Holistic Data”



COMPLETE Collaborators,  
2010:

Alyssa A. Goodman (CfA/IIC)

João Alves (Vienna)

Héctor Arce (Yale)

Michelle Borkin (Harvard SEAS/IIC)

Paola Caselli (Leeds, UK)

James DiFrancesco (HIA, Canada)

Jonathan Foster (B.U.)

Mark Heyer (UMASS/FCRAO)

Doug Johnstone (HIA, Canada)

Jens Kauffmann (JPL/Caltech)

Helen Kirk (CfA)

Di Li (JPL/Caltech)

Stella Offner (CfA)

Jaime Pineda (CfA, PhD Student)

Thomas Robitaille (CfA)

Erik Rosolowsky (UBC Okanagan)

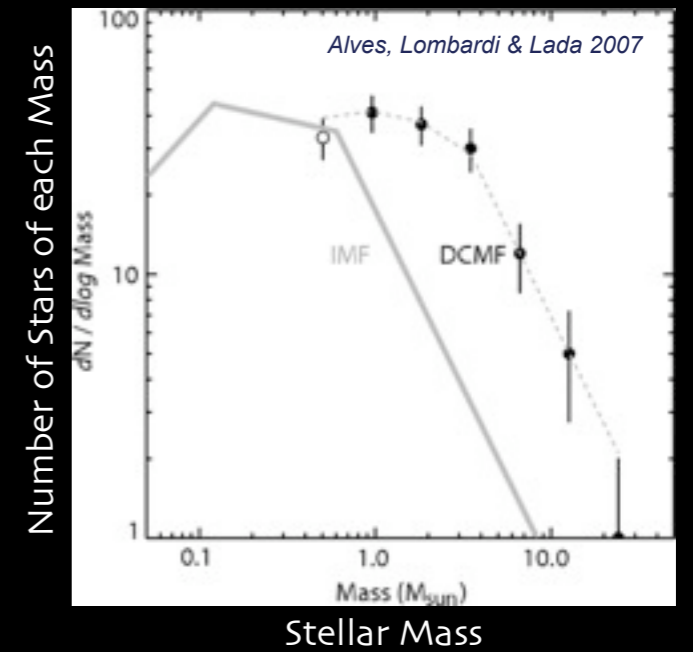
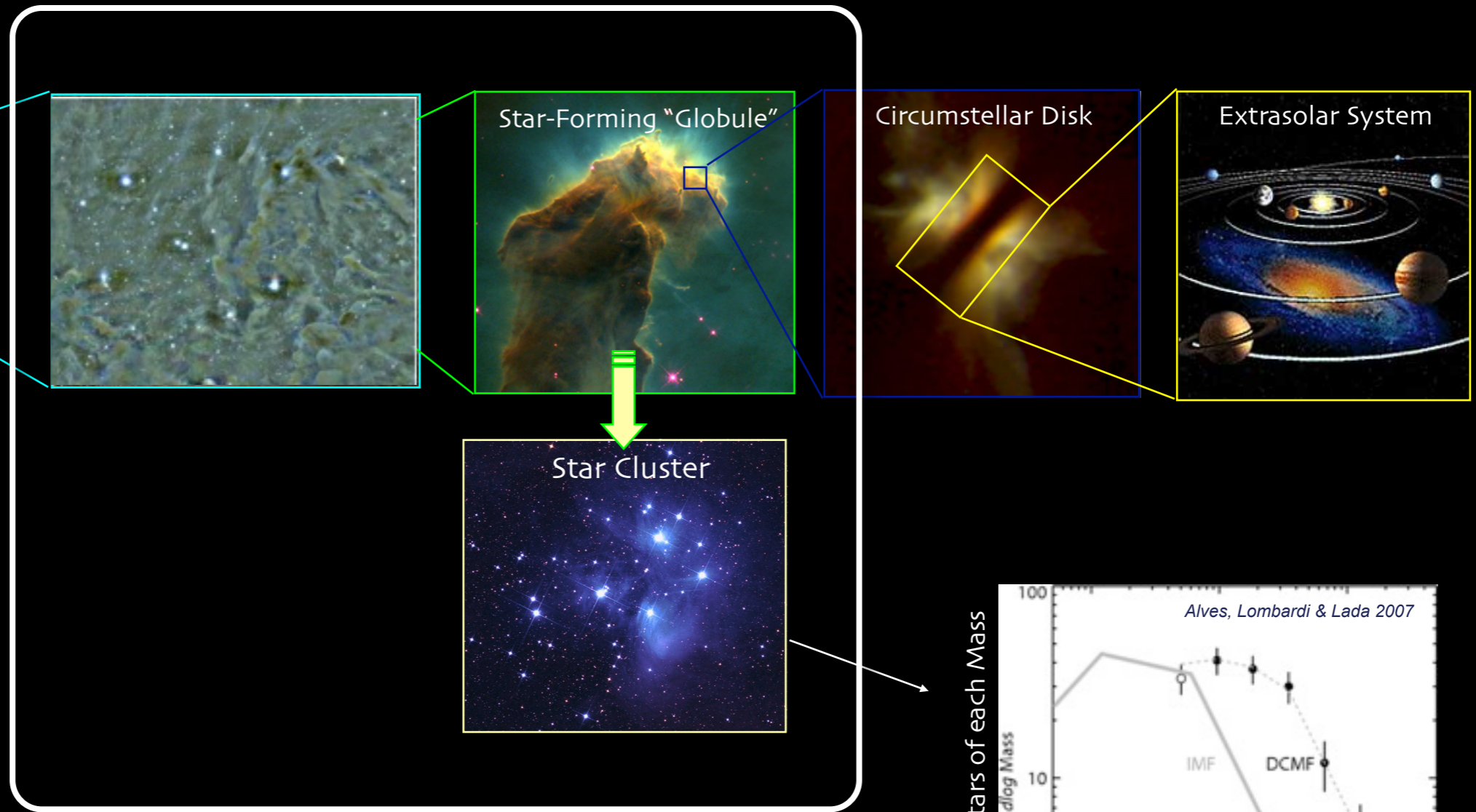
Rahul Shetty (ITA Heidelberg)

Scott Schnee (HIA Victoria)

Mario Tafalla (OAN, Spain)

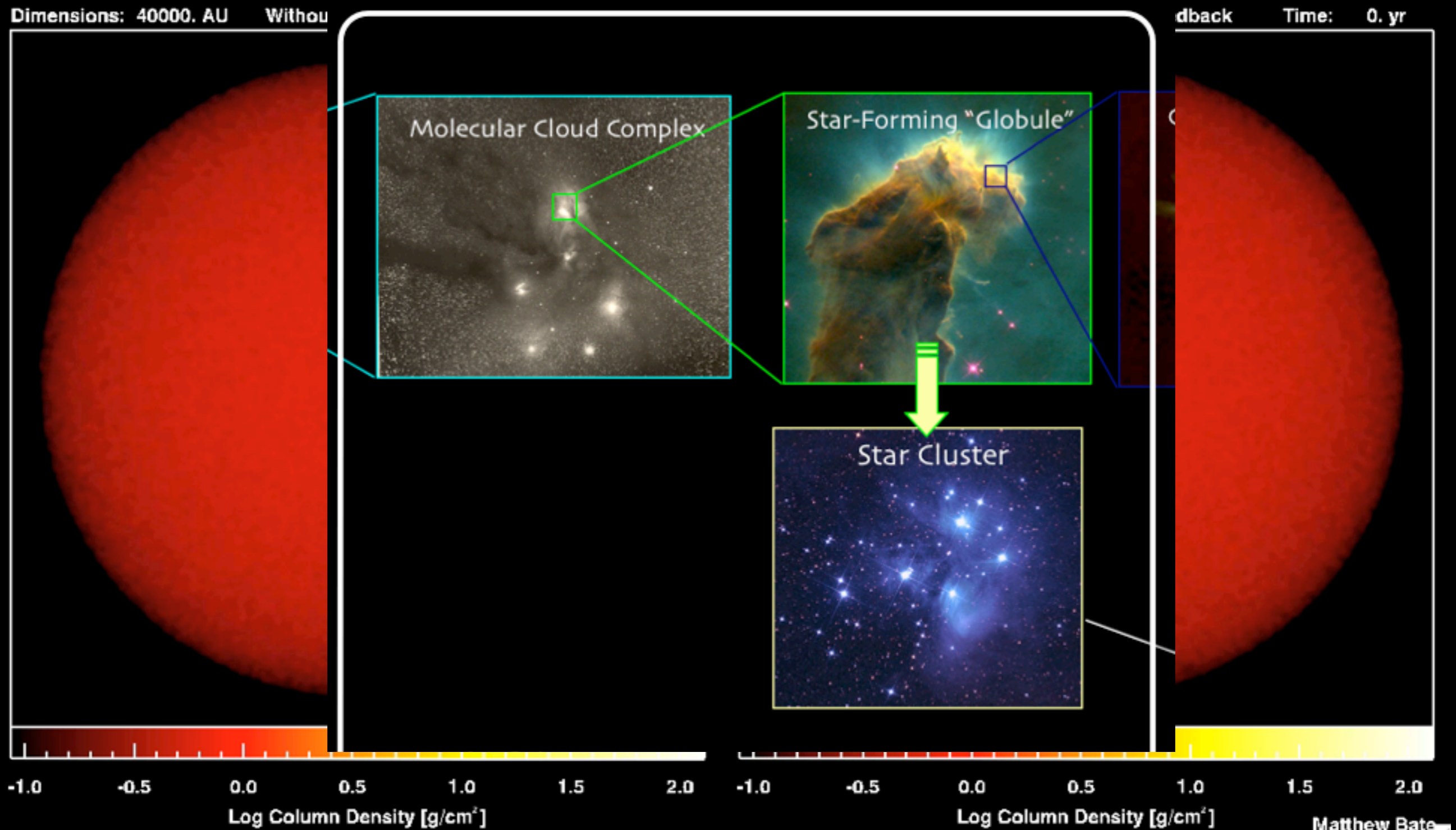


# Star (and Planet, and Moon) Formation 30 I



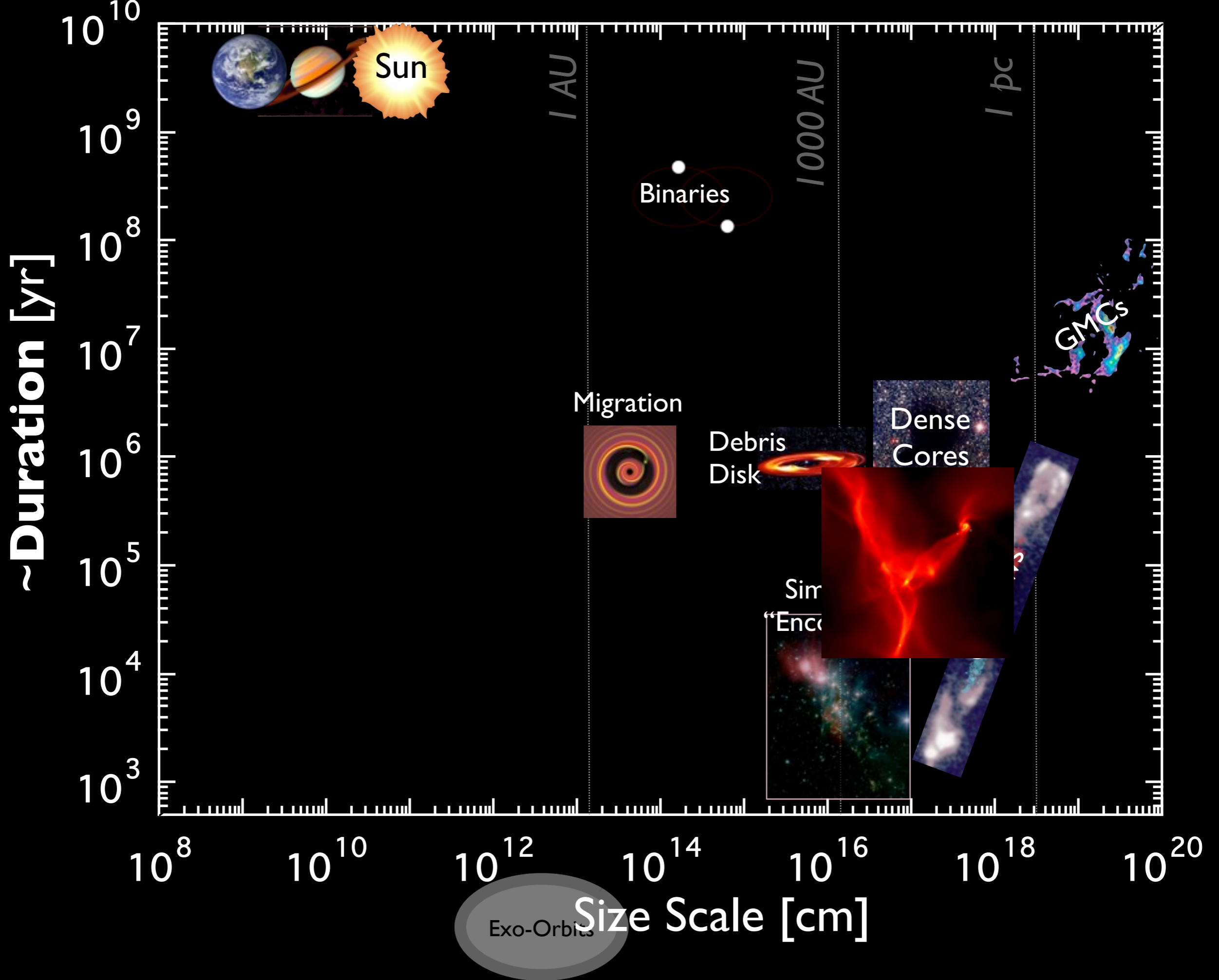


# Our Goal is to “Taste” Star Formation



*Simulations of Bate 2009*







# An Exemplar Dissection

LETTERS

## A role for self-gravity at multiple length scales in the process of star formation

Alyssa A. Goodman<sup>1,2</sup>, Ori W. Rosolowsky<sup>1,3</sup>, Michelle A. Barkin<sup>1</sup>, Jonathan S. Foster<sup>1</sup>, Michael Halle<sup>1,4</sup>, Jens Kauffmann<sup>1,5</sup> & Jaime E. Pineda<sup>1</sup>

Self-gravity plays a decisive role in the final stages of star formation, where dense cores (size ~0.1 parsec) within molecular clouds collapse to form star plus disk systems. But self-gravity's role at earlier times (and on larger length scales, such as ~1 parsec) in molecular cloud evolution remains unclear. We report a new self-gravity model that indicates that self-gravity plays a significant role over the full range of possible scales in the observed region. In particular, more than 80 per cent of the compact (pre-stellar cores) traced by peaks of dust emission are predicted to be self-gravitating. This model is consistent with observations of the 1.1 mm molecular cloud, but not consistent in the observed region. In particular, more than 80 per cent of the compact (pre-stellar cores) traced by peaks of dust emission are predicted to be self-gravitating. This model is consistent with observations of the 1.1 mm molecular cloud, but not consistent in the observed region. In particular, more than 80 per cent of the compact (pre-stellar cores) traced by peaks of dust emission are predicted to be self-gravitating. This model is consistent with observations of the 1.1 mm molecular cloud, but not consistent in the observed region.




Figure 1: A 3D visualization of the L1448 star-forming region. It shows a complex network of filaments and clumps. A central cluster of stars is visible, surrounded by a dense network of filaments. The visualization is color-coded to show different physical properties like density and velocity.

LETTERS

## TASTE TEST

The relationship between the observed and simulated self-gravitating regions is shown in Figure 4. The observed self-gravitating regions are shown in red, and the simulated self-gravitating regions are shown in blue. The plot shows the fraction of self-gravitating regions as a function of the ratio of the observed to simulated self-gravitating regions. The plot shows that the observed self-gravitating regions are generally smaller than the simulated self-gravitating regions, but that there is a significant overlap between the two sets of regions.



Figure 2: A plot showing the distribution of the observed and simulated self-gravitating regions. The x-axis is the ratio of the observed to simulated self-gravitating regions, and the y-axis is the number of regions. The plot shows two distributions: one for the observed regions (red) and one for the simulated regions (blue). The observed distribution is generally narrower and shifted towards lower ratios compared to the simulated distribution.

LETTERS

## LETTERS

Figure 1: Comparison of the observed and simulated self-gravitating regions. The plot shows the fraction of self-gravitating regions as a function of the ratio of the observed to simulated self-gravitating regions. The observed self-gravitating regions are shown in red, and the simulated self-gravitating regions are shown in blue. The plot shows that the observed self-gravitating regions are generally smaller than the simulated self-gravitating regions, but that there is a significant overlap between the two sets of regions.

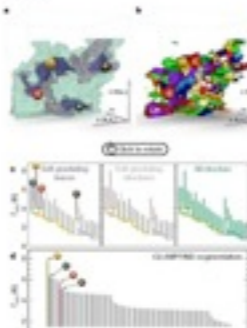
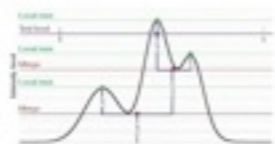


Figure 2: Substrate distribution of the observed and simulated self-gravitating regions. The plot shows the distribution of the observed and simulated self-gravitating regions as a function of the ratio of the observed to simulated self-gravitating regions. The observed self-gravitating regions are shown in red, and the simulated self-gravitating regions are shown in blue. The plot shows that the observed self-gravitating regions are generally smaller than the simulated self-gravitating regions, but that there is a significant overlap between the two sets of regions.



LETTERS

## LETTERS

Figure 1: Comparison of the observed and simulated self-gravitating regions. The plot shows the fraction of self-gravitating regions as a function of the ratio of the observed to simulated self-gravitating regions. The observed self-gravitating regions are shown in red, and the simulated self-gravitating regions are shown in blue. The plot shows that the observed self-gravitating regions are generally smaller than the simulated self-gravitating regions, but that there is a significant overlap between the two sets of regions.



Figure 2: Substrate distribution of the observed and simulated self-gravitating regions. The plot shows the distribution of the observed and simulated self-gravitating regions as a function of the ratio of the observed to simulated self-gravitating regions. The observed self-gravitating regions are shown in red, and the simulated self-gravitating regions are shown in blue. The plot shows that the observed self-gravitating regions are generally smaller than the simulated self-gravitating regions, but that there is a significant overlap between the two sets of regions.



Goodman, Rosolowsky, Barkin, Foster, Halle, Kauffmann & Pineda 2009, Nature, 457, 63.



“turbulent fragmentation”

“L1448”

“(magneto-)hydrodynamic simulation”

“Cloudshine”

“pre-stellar core”

“protostar”

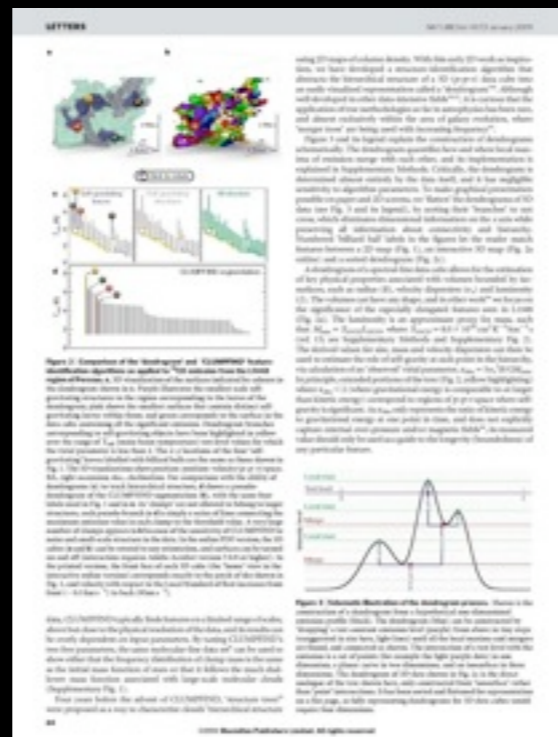
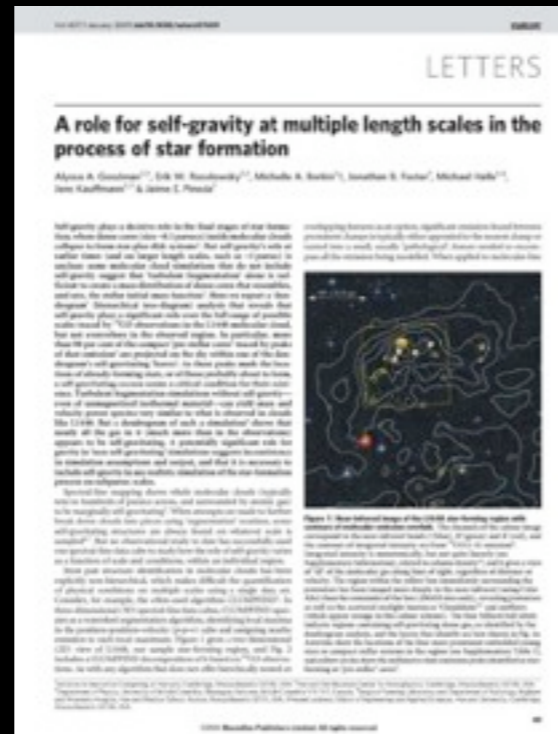
“integrated intensity”

“p-p-v cube”

“segmentation”

“CLUMPFIND”

“Dendrogram”



“COMPLETE”

“3D PDF”

“bi-jection”

“virial parameter”

“column density”

“turbulent power spectrum”

“synthetic observation”

“depletion, opacity”

“taste-test”

caveats



“turbulent fragmentation”

“L1448”

“(magneto-)hydrodynamic simulation”

“Cloudshine”

“pre-stellar core”

“protostar”

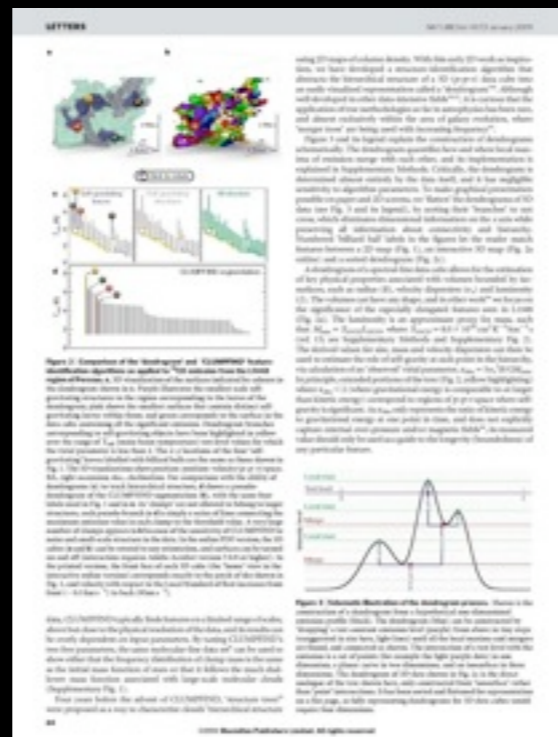
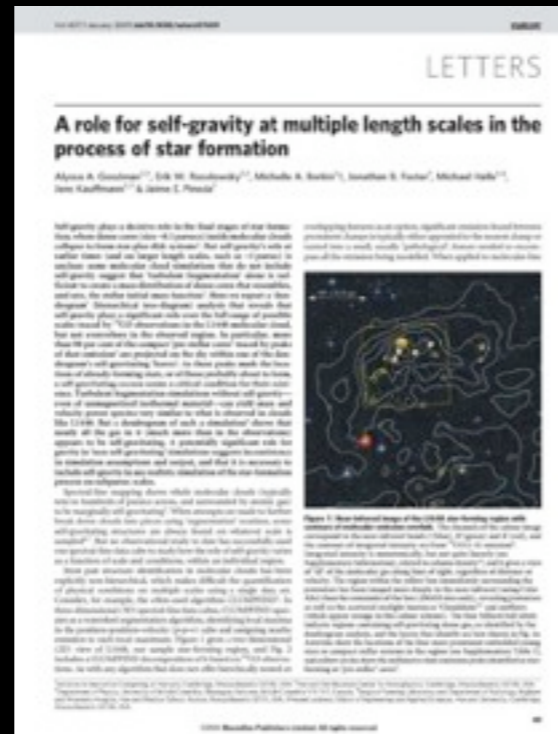
“integrated intensity”

“p-p-v cube”

“segmentation”

“CLUMPFIND”

“Dendrogram”



“COMPLETE”

“3D PDF”

“bi-jection”

“virial parameter”

“column density”

“turbulent power spectrum”

“synthetic observation”

“depletion, opacity”

“taste-test”

caveats



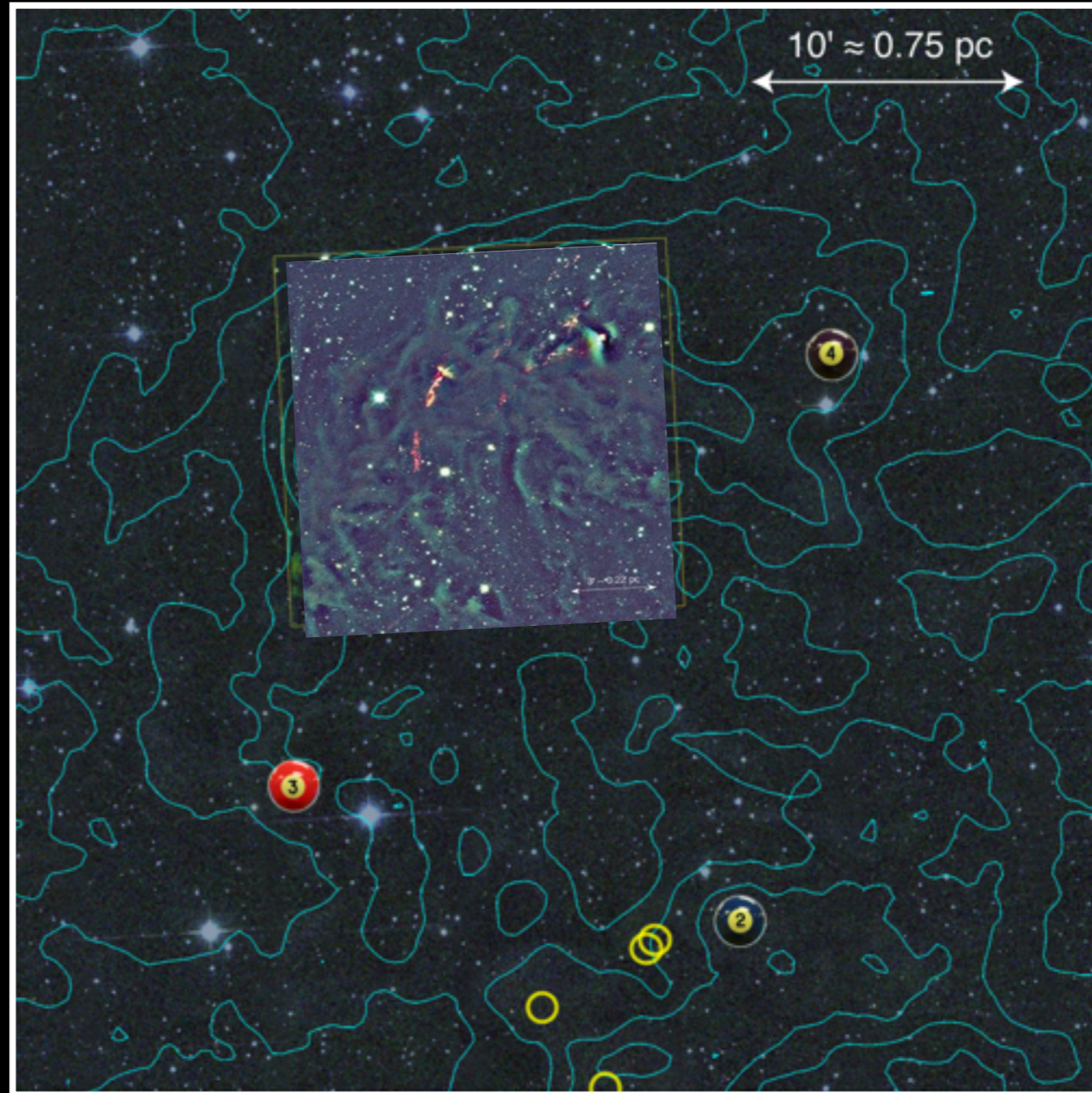
# “L1448”

“Cloudshine”

“pre-stellar core”

“protostar”

“integrated intensity”

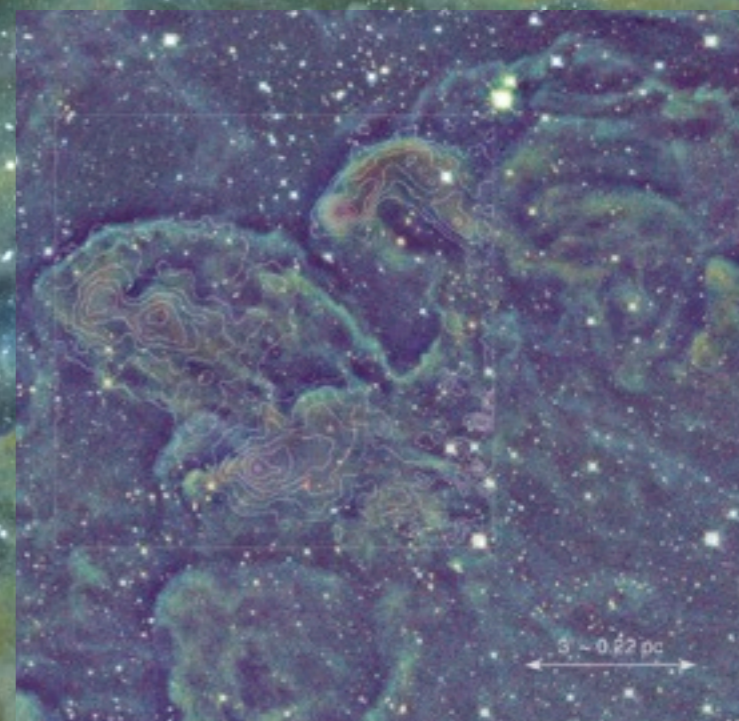
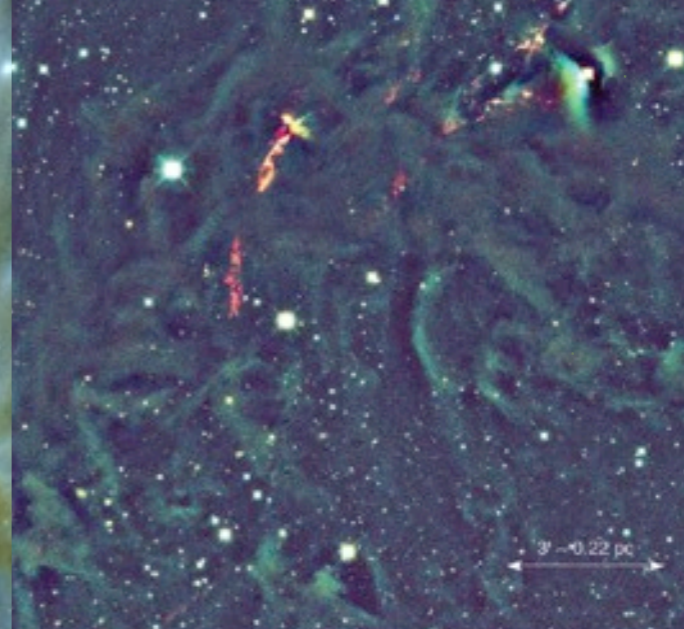


“column density”

“COMPLETE”



# “Cloudshine”



Background: to appear in Foster, Mandel, Pineda, Covey & Goodman 2010  
Insets: Foster & Goodman 2006, Calar Alto JHK



# ✓ “L1448”

“Cloudshine” ✓

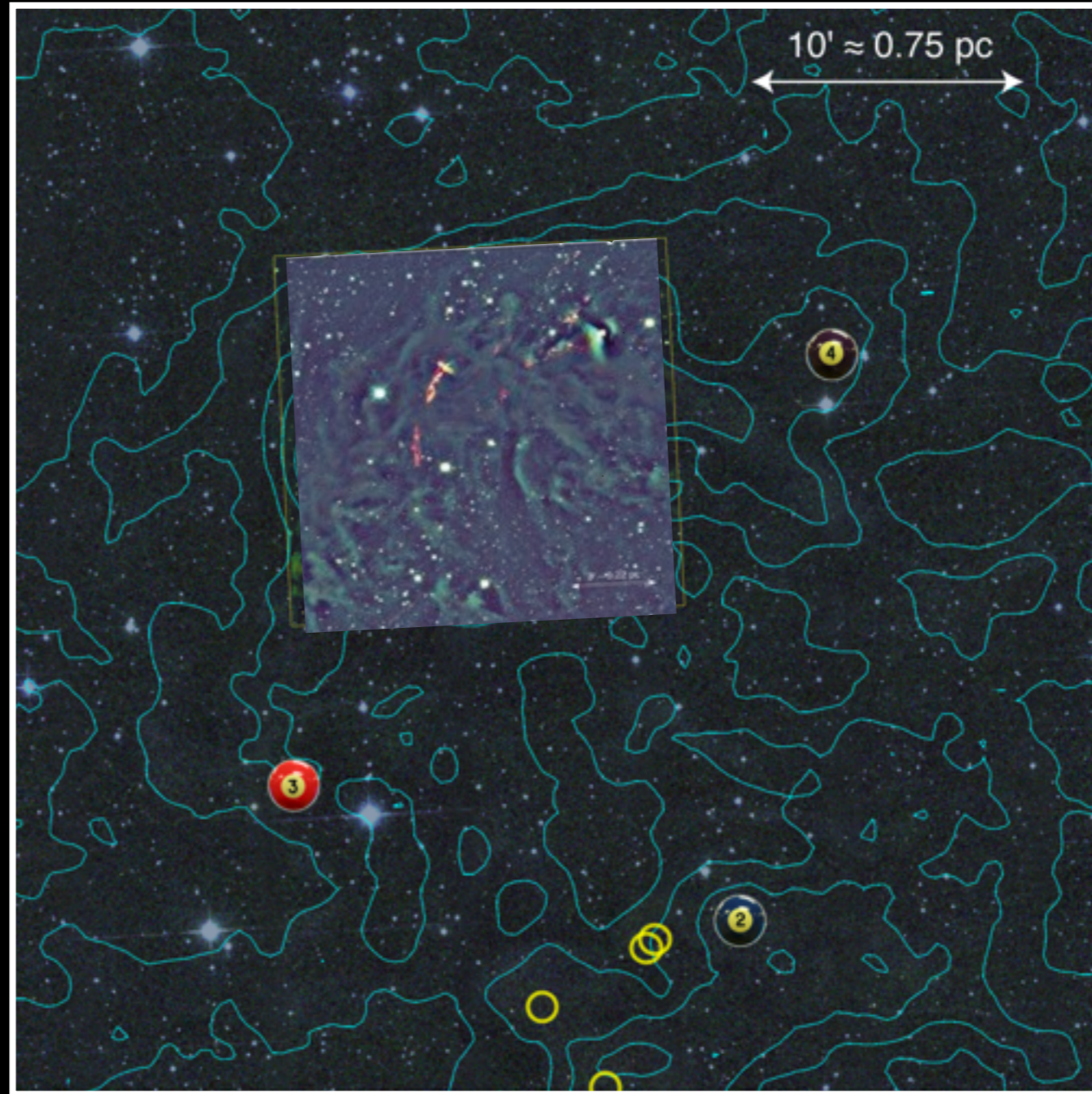
○ “pre-stellar core”

...compact  
thermal dust peak ✓

\* “protostar” ✓

...Spitzer c2d (MIR) point  
source with “right” SED

“integrated  
intensity”

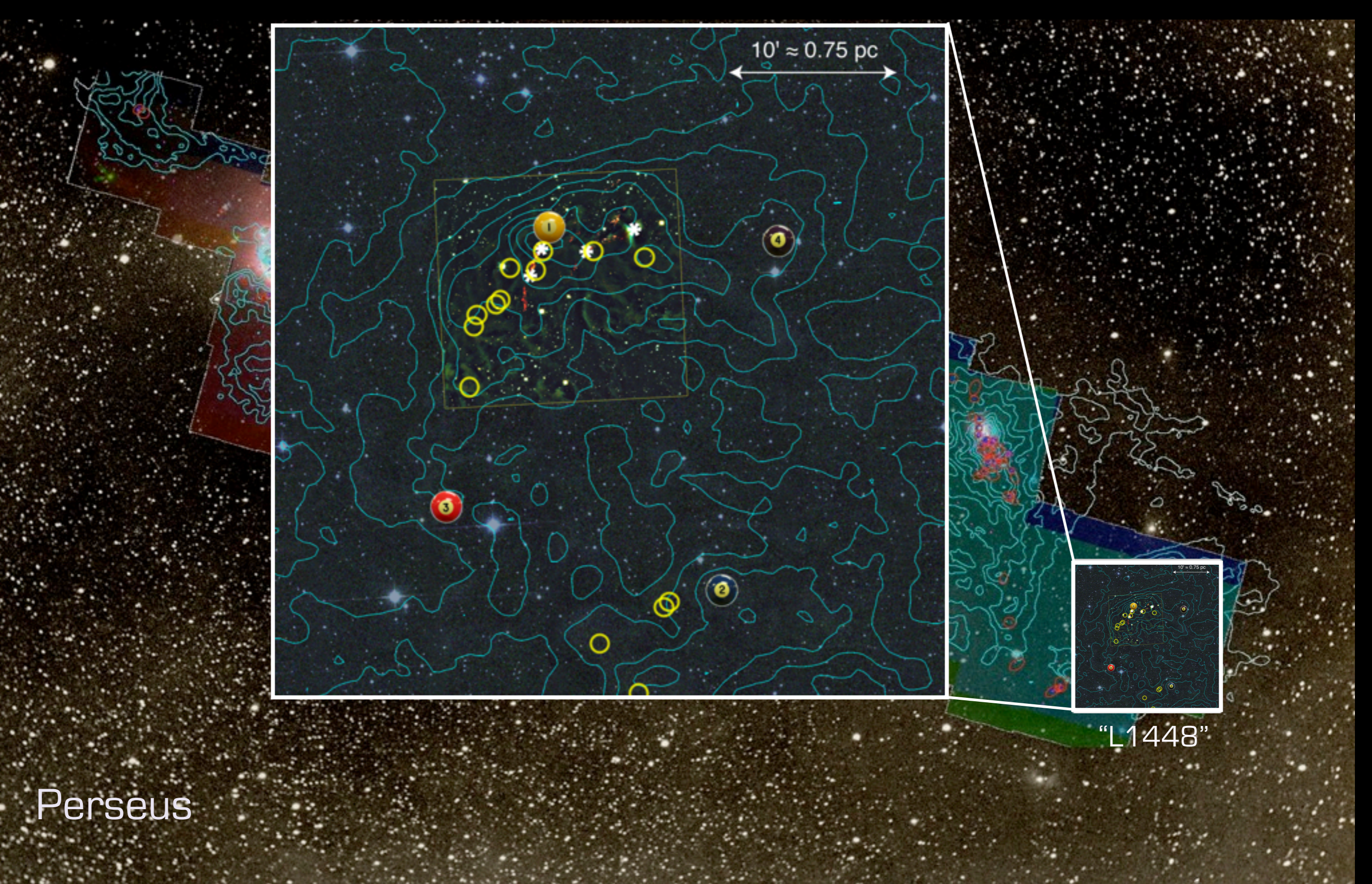


“column  
density”

“COMPLETE”

( (3) ...later)





Perseus

"L1448"



"integrated intensity"

"column density"

COMPLETE



COMPLETE Data Coverage Tool

http://www.worldwidetelescope.org/COMPLETE/WWTCoverageTool.htm#

# COMPLETE

## COMPLETE Data Available

Center on Perseus | Center on Ophiuchus | Center on Serpens

### Full-Cloud Data (Phase I, All Data Available)

Dataset	Show	Perseus	Ophiuchus	Serpens	Link
GBT: HI Data Cube	<input checked="" type="checkbox"/>	✓	✓	∅	<a href="#">Data</a>
IRAS: Av/Temp Maps	<input checked="" type="checkbox"/>	✓	✓	✓	<a href="#">Data</a>
FCRAO: 12CO	<input checked="" type="checkbox"/>	✓	✓	✓	<a href="#">Data</a>
FCRAO: 13CO	<input checked="" type="checkbox"/>	✓	✓	✓	<a href="#">Data</a>
JCMT: 850 microns	<input checked="" type="checkbox"/>	✓	✓	∅	<a href="#">Data</a>
Spitzer c2d: IRAC 1,3 (3.6,5.8 μm)	<input checked="" type="checkbox"/>	✓	✓	✓	<a href="#">Data</a>
Spitzer c2d: IRAC 2,4 (4.5,8 μm)	<input checked="" type="checkbox"/>	✓	✓	✓	<a href="#">Data</a>
CSO/Bolocam: 1.2-mm	<input checked="" type="checkbox"/>	✓	∅	∅	<a href="#">Data</a>
Spitzer MIPS: Derived Dust Map	<input checked="" type="checkbox"/>	✓	∅	∅	<a href="#">Data</a>

### Targeted Regions (Phase II, Some Data Not Yet Available)

CTIO/Calar Alto: NIR (J,H,Ks)	<input checked="" type="checkbox"/>	✓	✓	∅	<a href="#">Data</a>
IRAM 30-m: N2H+ and C18O	<input checked="" type="checkbox"/>	✓	∅	∅	<a href="#">Data</a>
IRAM 30-m: 1.1-mm continuum	<input checked="" type="checkbox"/>	✓	∅	∅	<a href="#">Data</a>
Megacam/MMT: r,i,z images	<input checked="" type="checkbox"/>	✓	∅	∅	<a href="#">Data</a>

### Catalogs & Pointed Surveys

NH3 Pointed Survey	<input type="checkbox"/>	✓	∅	∅	<a href="#">Data</a>
YSO Candidate list (c2d)	<input type="checkbox"/>	✓	✓	✓	<a href="#">Data</a>

Microsoft Research  
WorldWide Telescope

Done

To explore on your own, go to <http://www.cfa.harvard.edu/COMPLETE/>, then click on



and choose to see the Interactive Coverage Tool in either Google Sky or WorldWide Telescope.

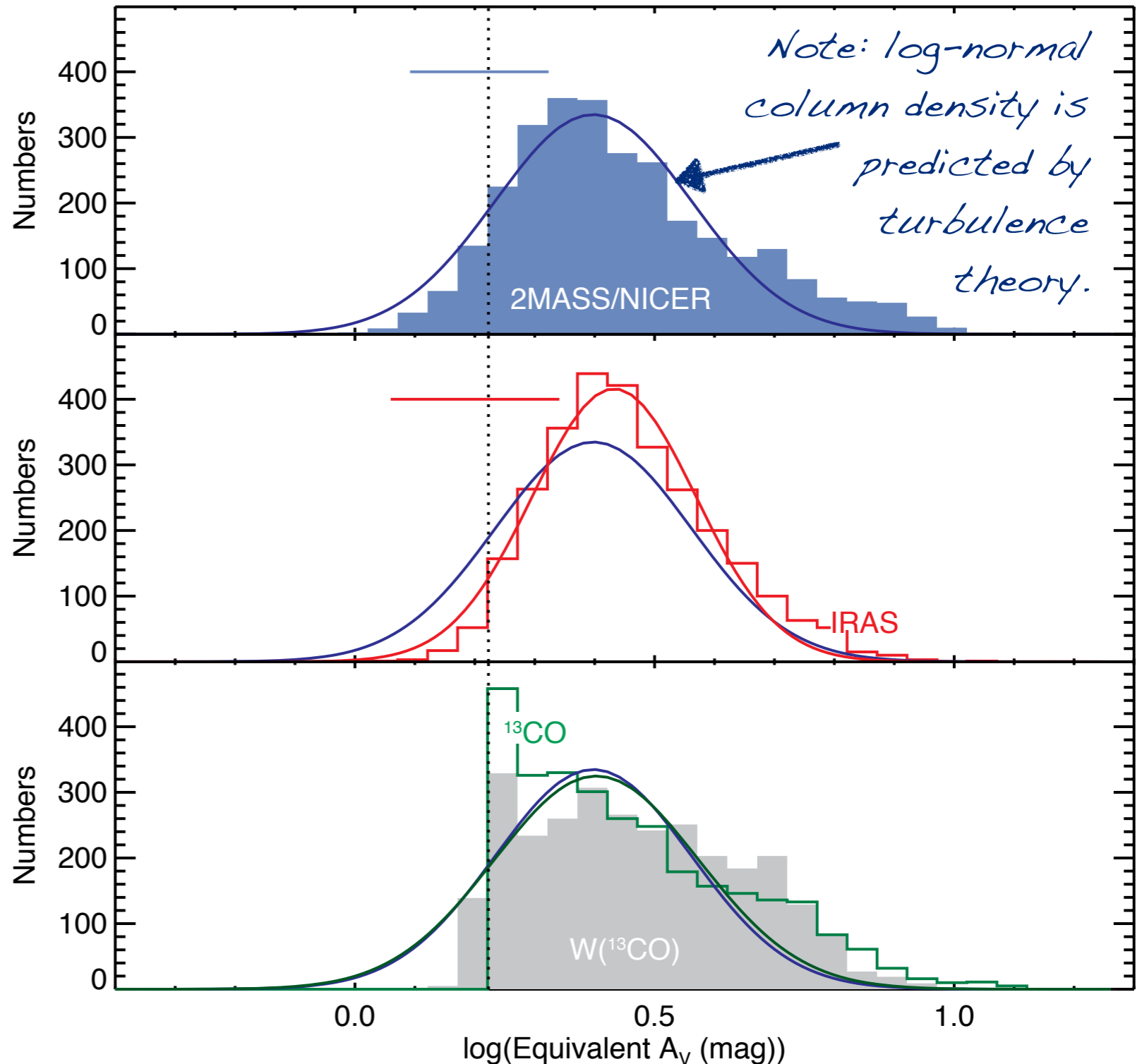
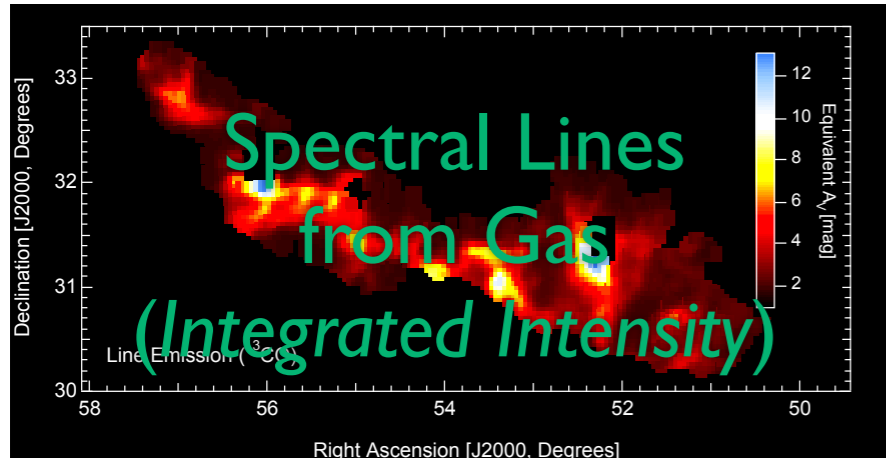
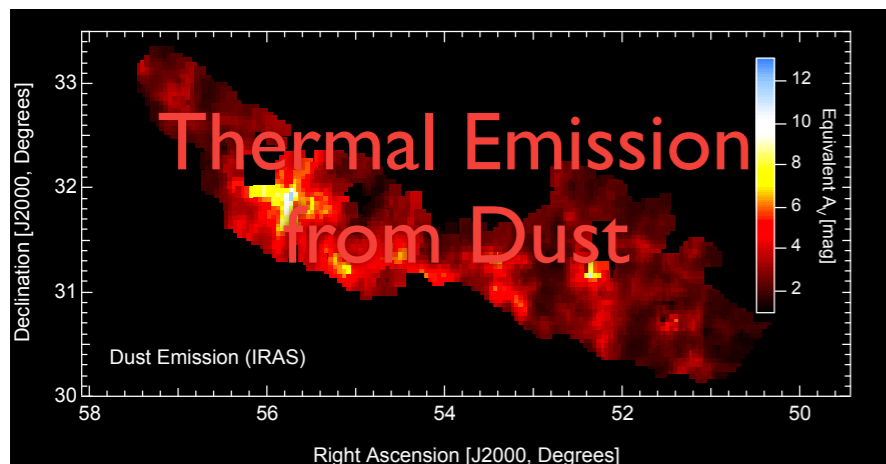
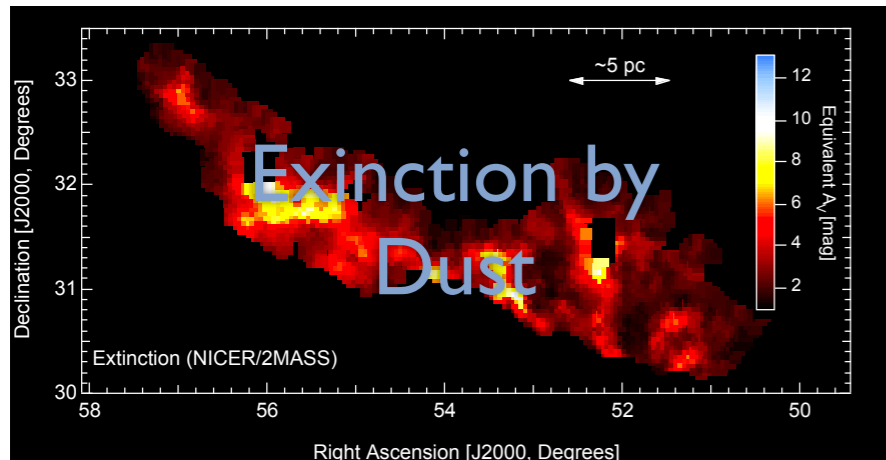
Many thanks to Jonathan Foster, Gus Muench & Jonathan Fay (MSR/WWT team) for these tools!





# Column Density in Perseus, Measured 3 Ways

TASTE  
TEST





“turbulent fragmentation”

“L1448”

“(magneto-)hydrodynamic simulation”

“Cloudshine”

“pre-stellar core”

“protostar”

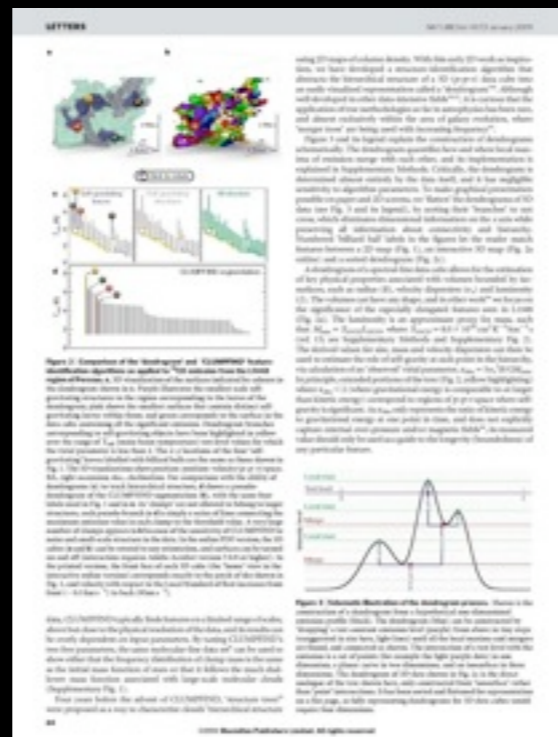
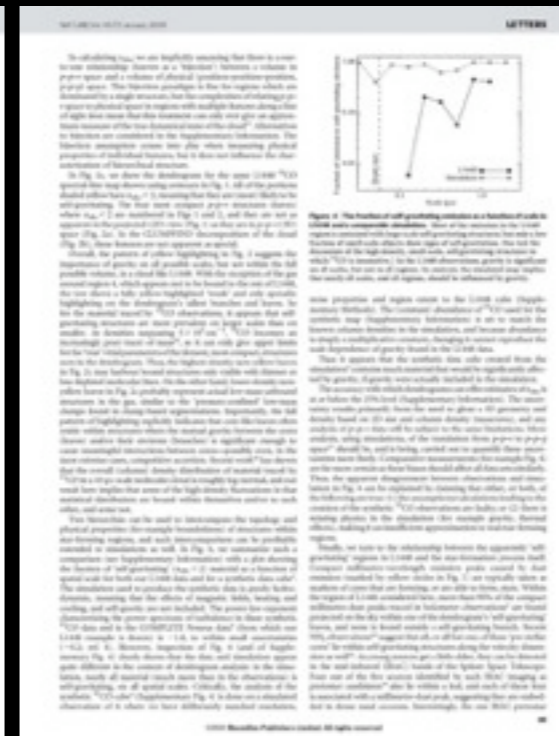
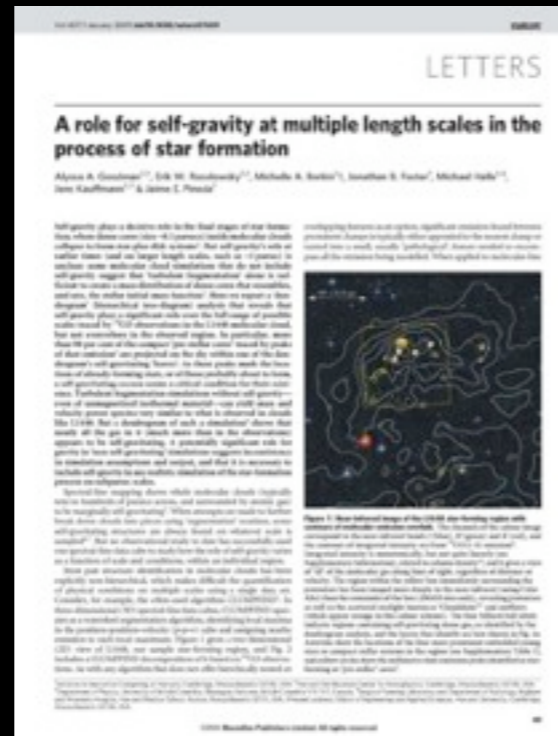
“integrated intensity\*”

“p-p-v cube”

“segmentation”

“CLUMPFIND”

“Dendrogram”



“COMPLETE”

“3D PDF”

“bi-jection”

“virial parameter”

“column density”

“turbulent power spectrum”

“synthetic observation”

“depletion, opacity”

“taste-test”

caveats

\*...more to come



“turbulent fragmentation”

“(magneto-)hydrodynamic simulation”

“bi-jection”

“virial parameter”

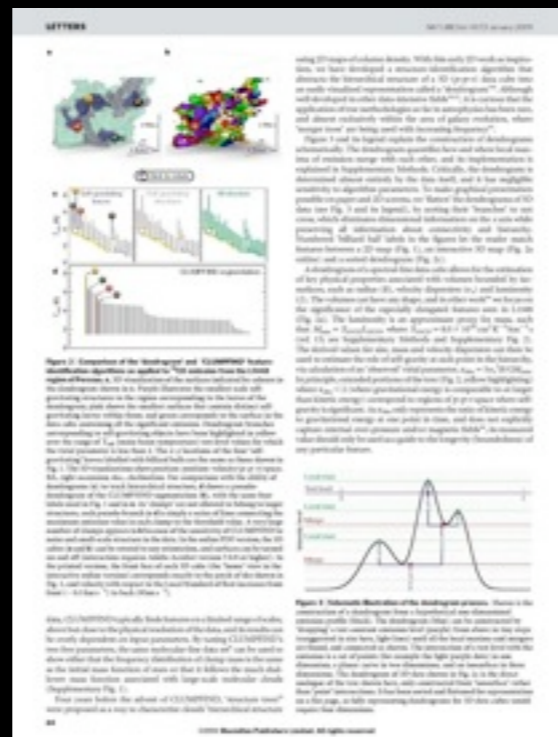
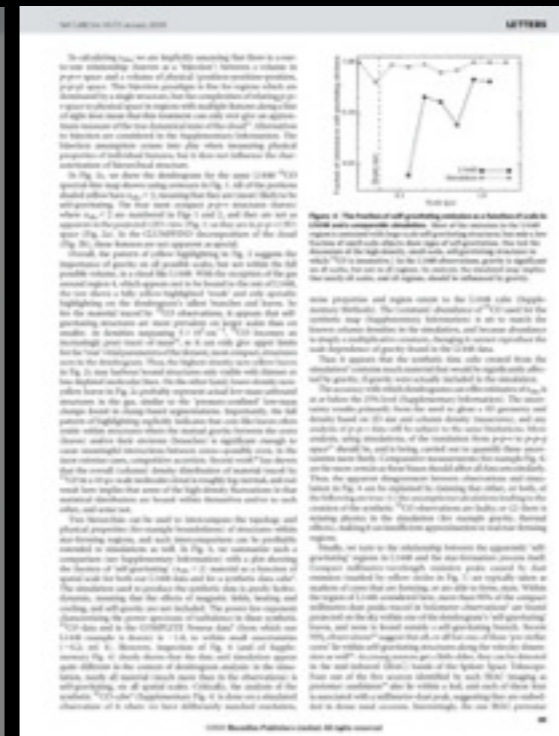
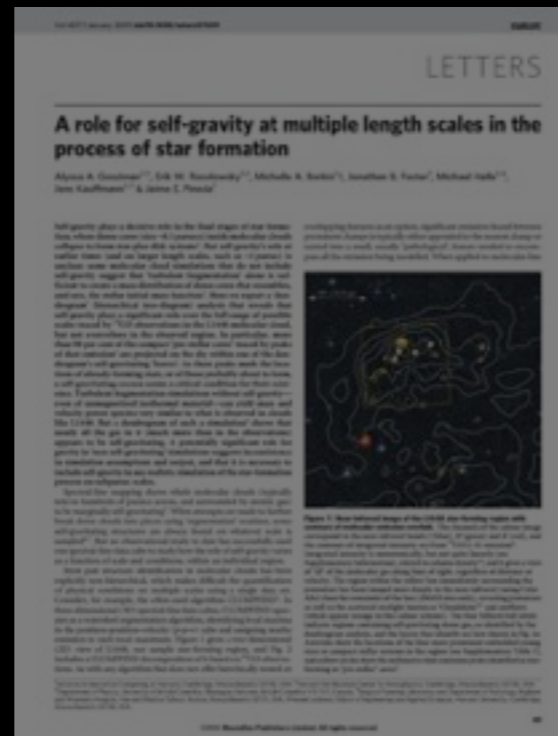
“integrated intensity\*”

“p-p-v cube”

“segmentation”

“CLUMPFIND”

“Dendrogram”



“turbulent power spectrum”

“synthetic observation”

“depletion, opacity”

“taste-test”

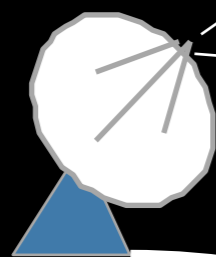
“3D PDF”

caveats

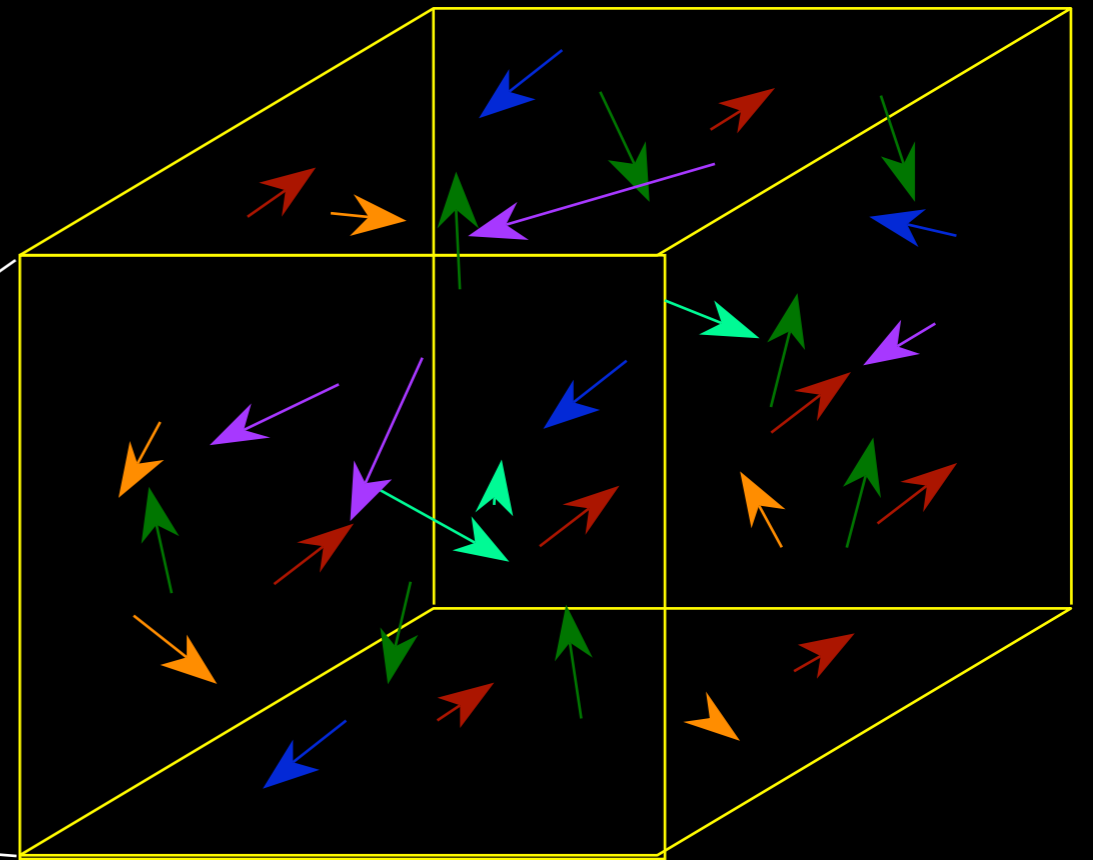
\*...more to come



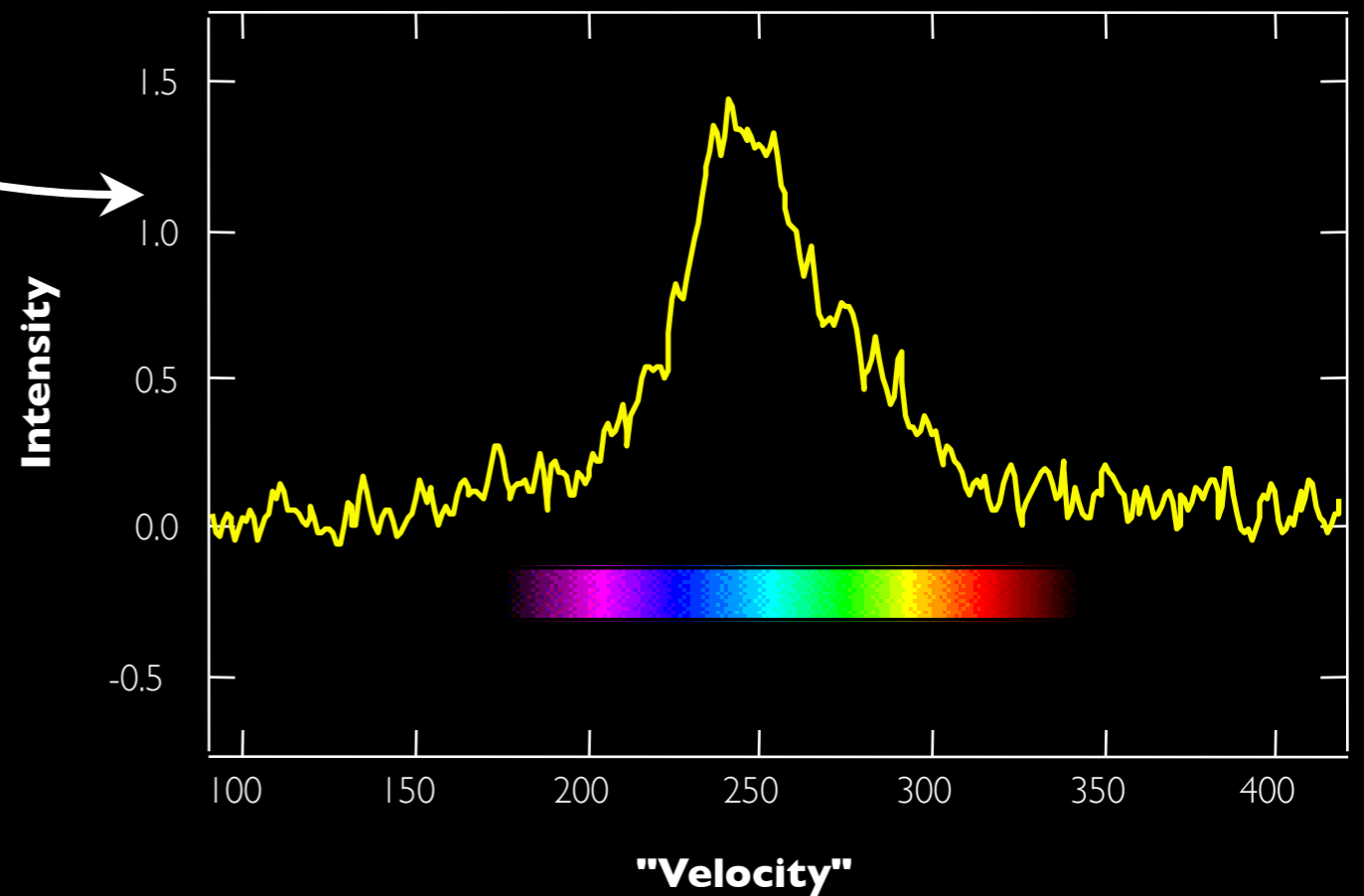
# Velocity from Spectroscopy



Telescope +  
Spectrometer



Observed Spectrum



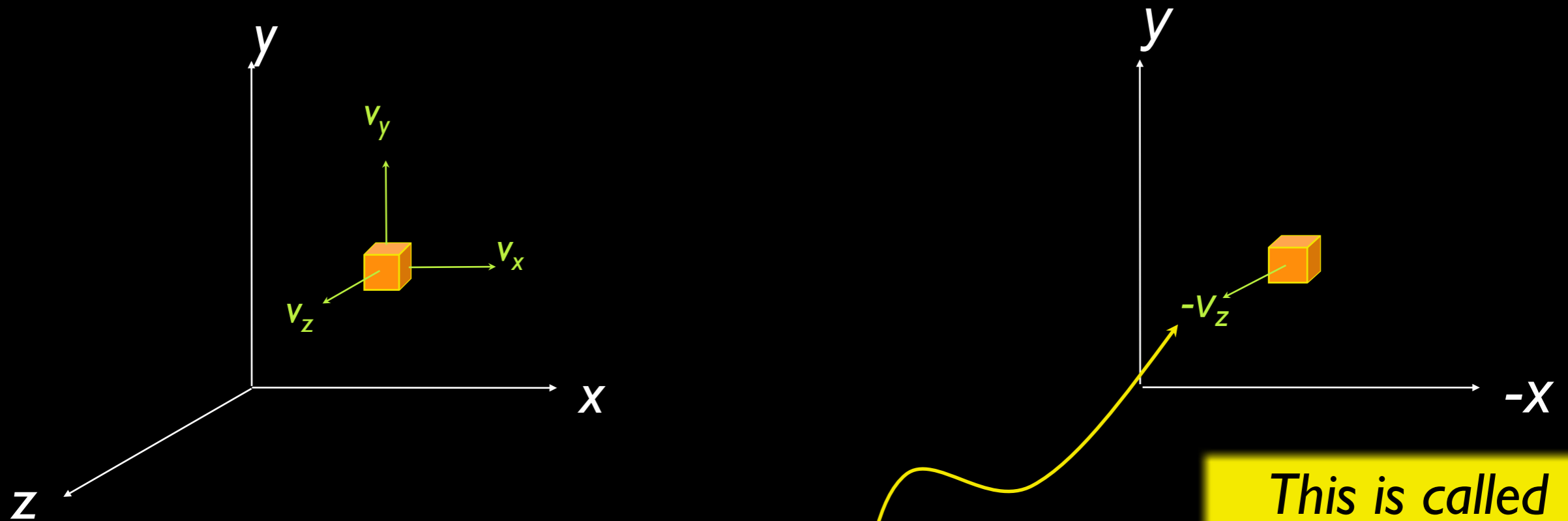
All thanks to Doppler



# “Three” Dimensions: Spectral-Line Mapping

We wish we could measure...

*But* we can measure...

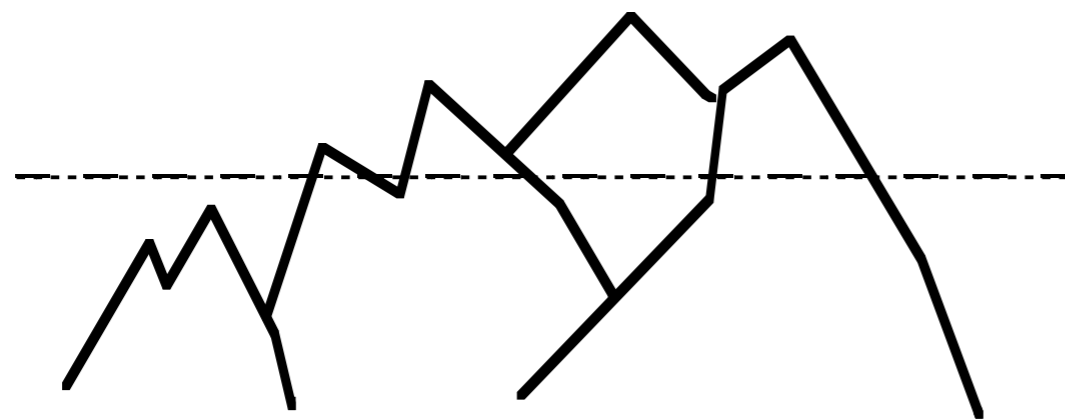
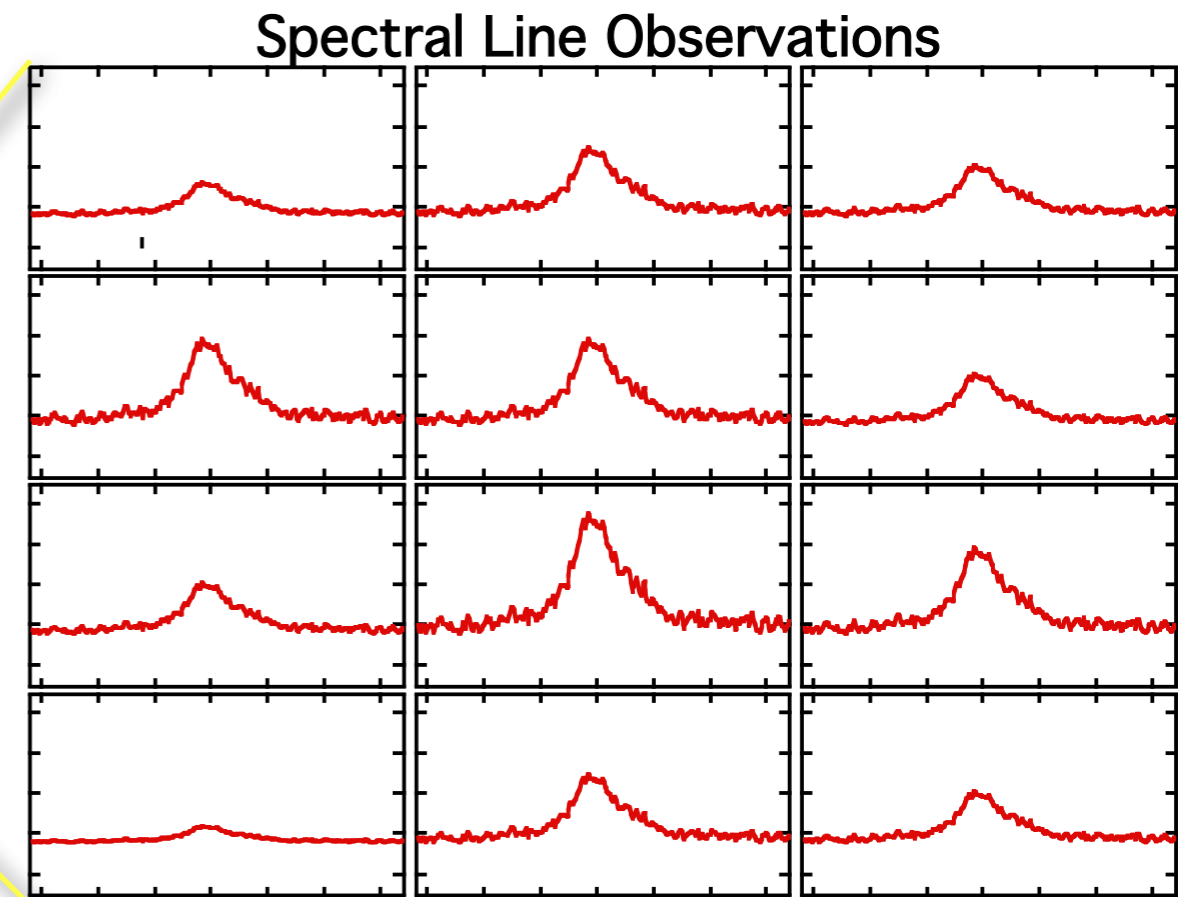
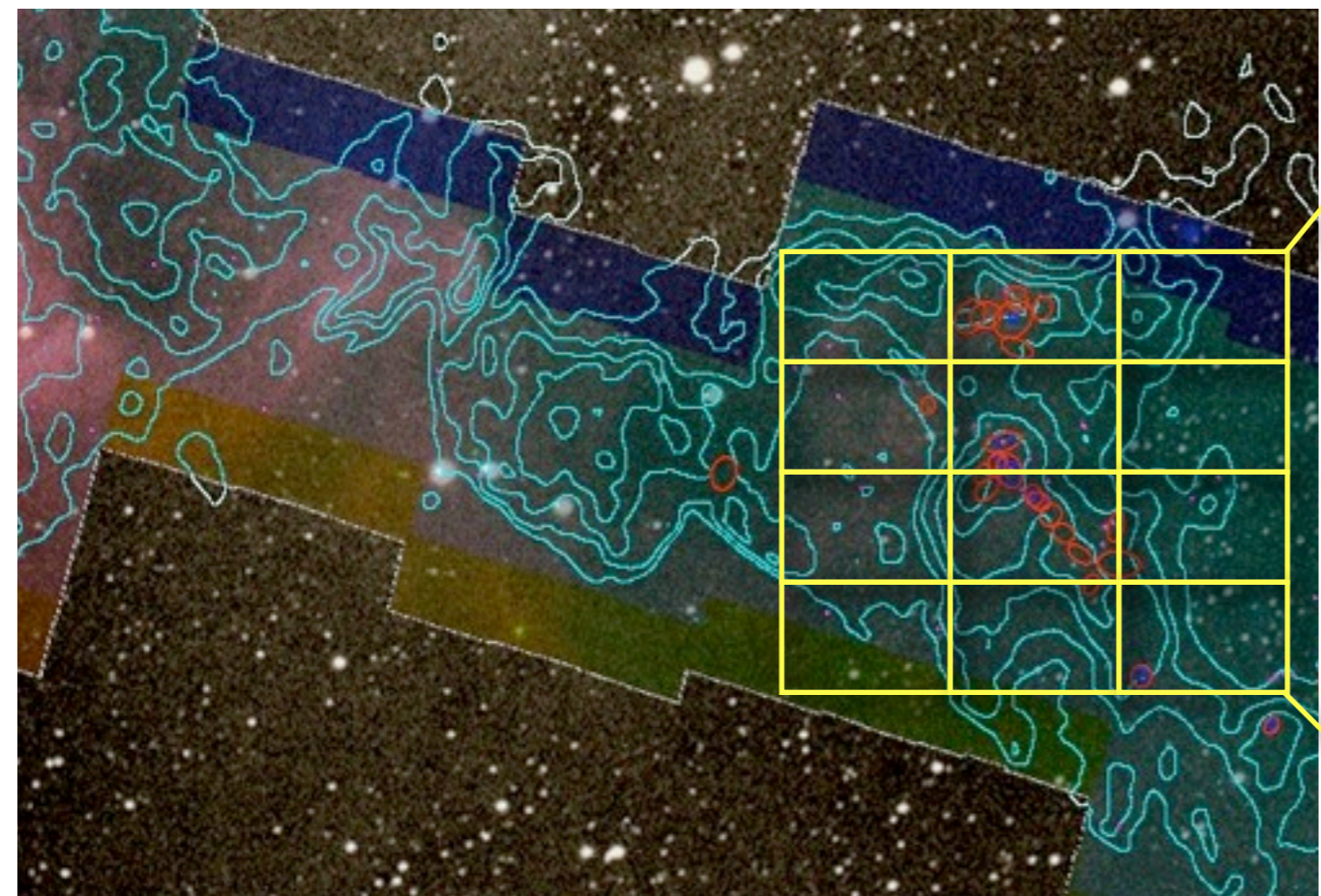


$v_z$  *only* from  
“spectral-line  
maps”

This is called  
“**p-p-v**” or  
“position-  
position-velocity”  
space.



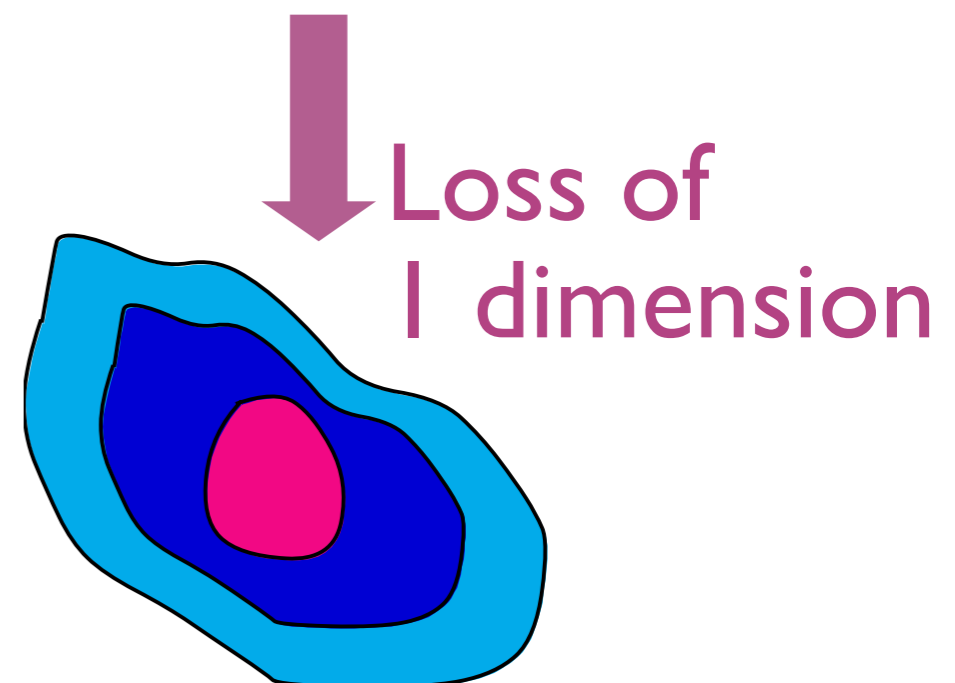
# There's much more to life than "integrated intensity"



Mountain Range



No loss of information

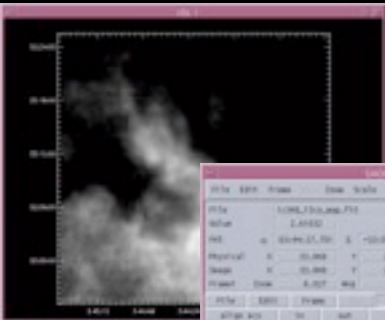


Loss of 1 dimension

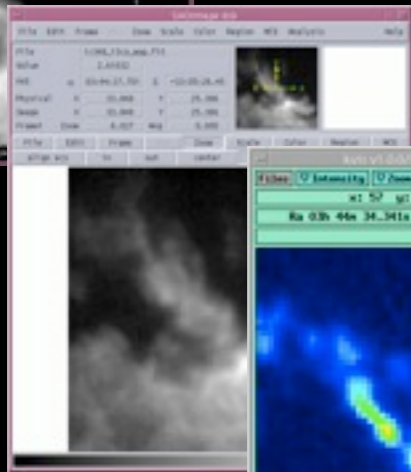


# Astronomical Visualization Tools are Traditionally 2D

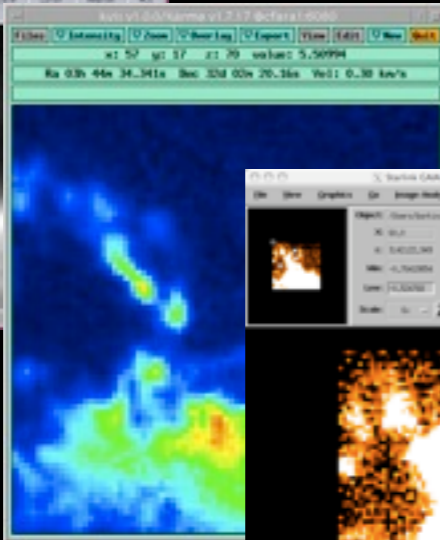
IDL



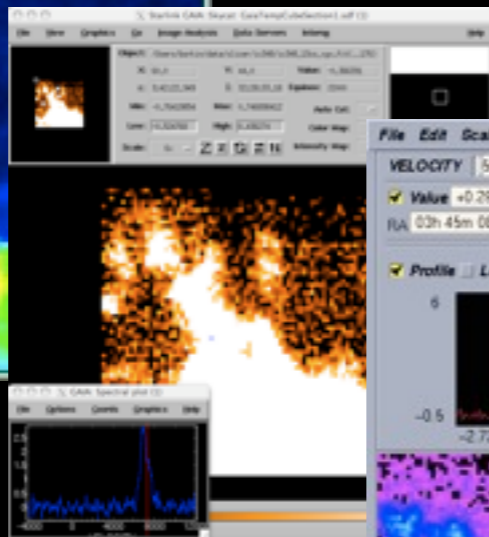
DS9



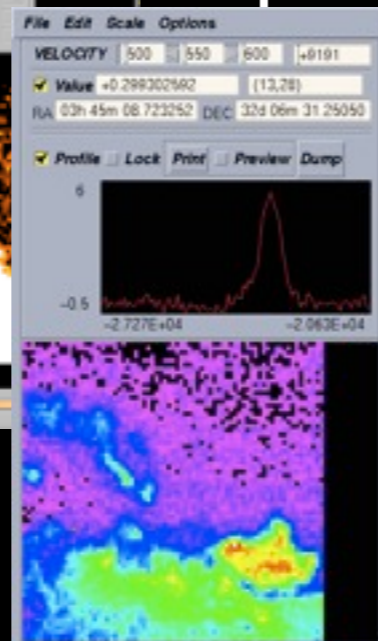
Karma\*



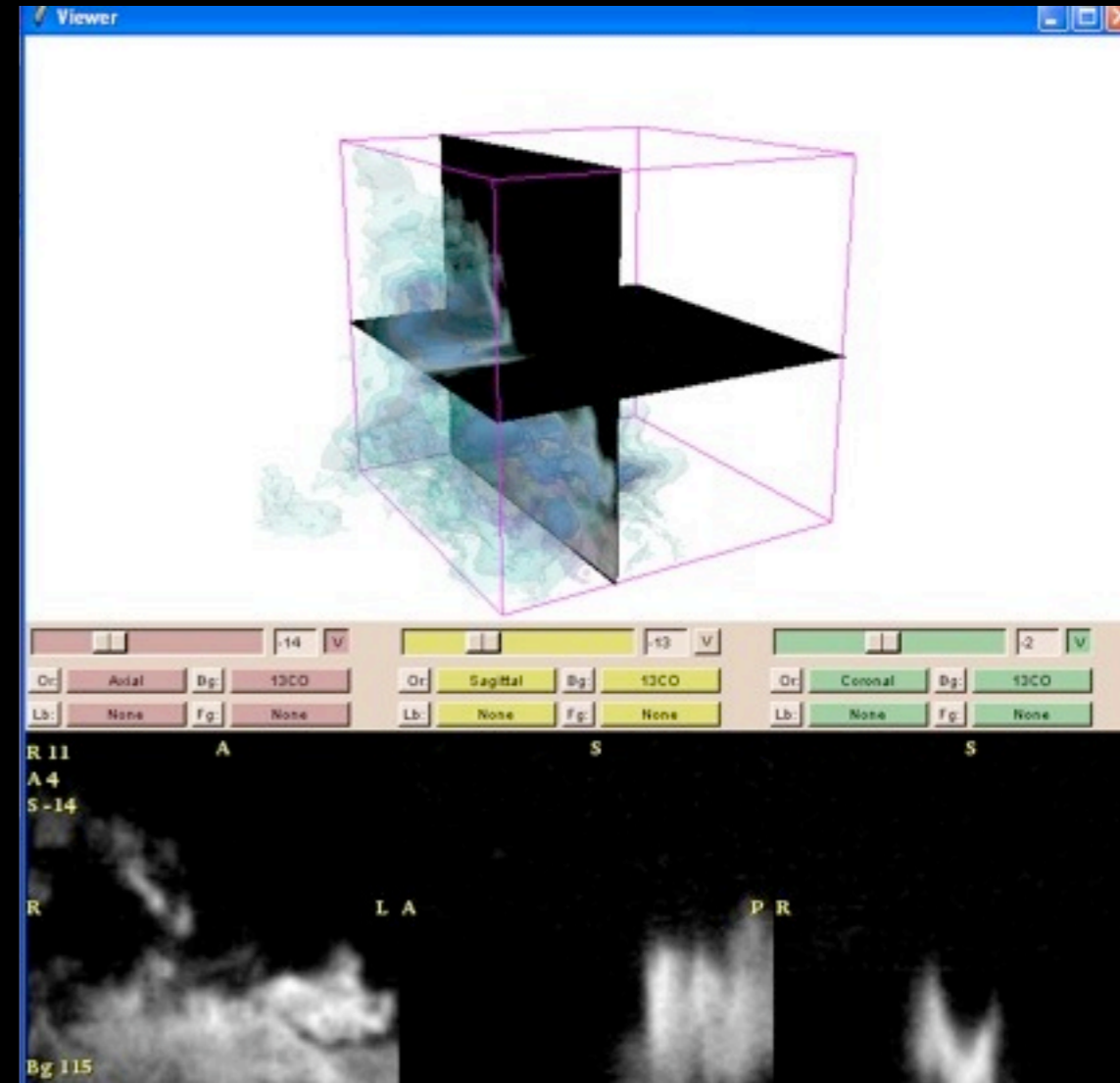
GAIA



Aipsview



3D Slicer





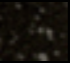


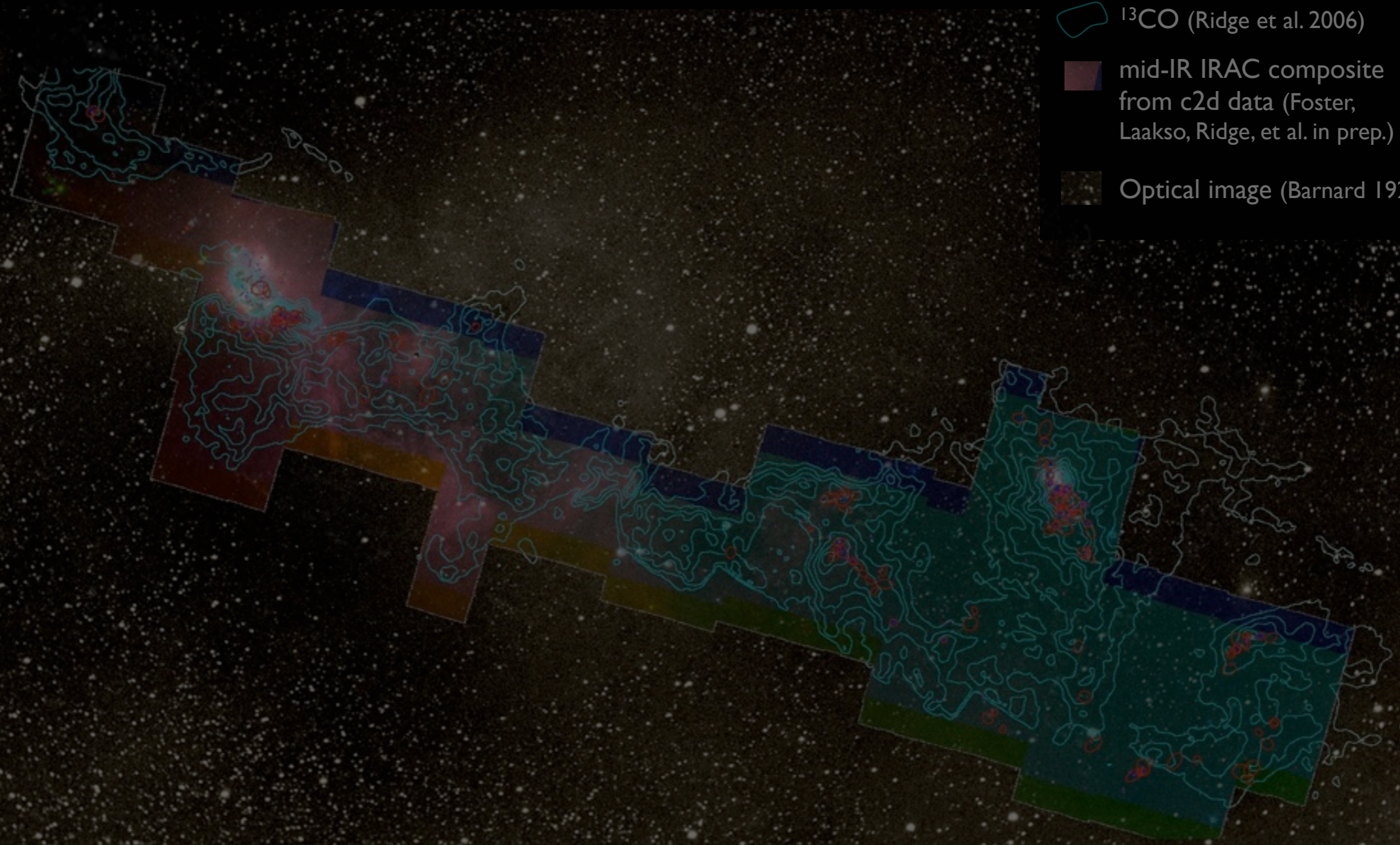
“3D”=movies



# COMPLETE Perseus

Image size: 1305 x 733  
VL: 63 WW: 127

-  mm peak (Enoch et al. 2006)
-  sub-mm peak (Hatchell et al. 2005, Kirk et al. 2006)
-   $^{13}\text{CO}$  (Ridge et al. 2006)
-  mid-IR IRAC composite from c2d data (Foster, Laakso, Ridge, et al. in prep.)
-  Optical image (Barnard 1927)

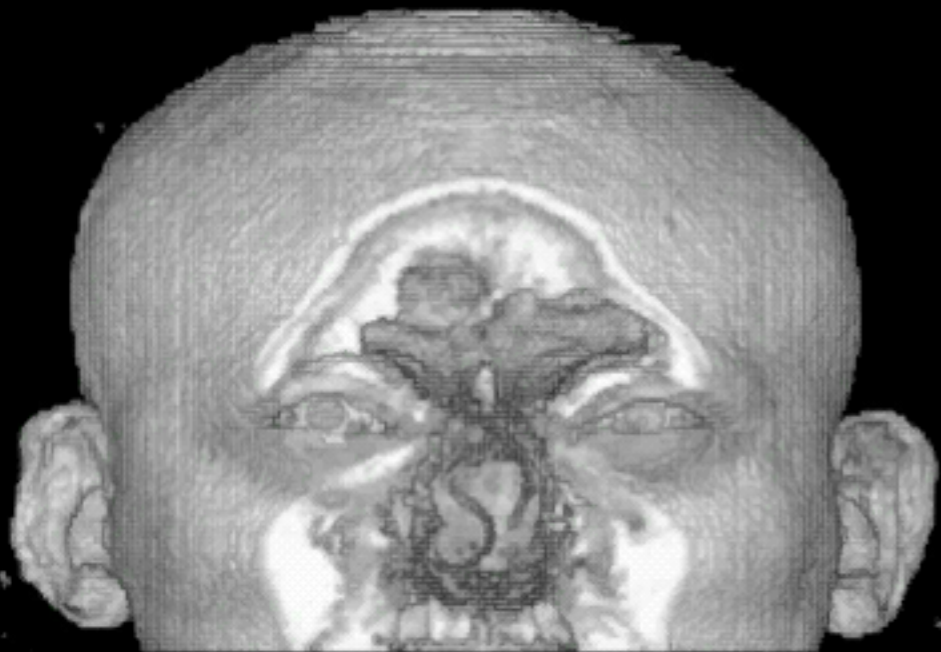


m: 1/249  
Zoom: 227% Angle: 0



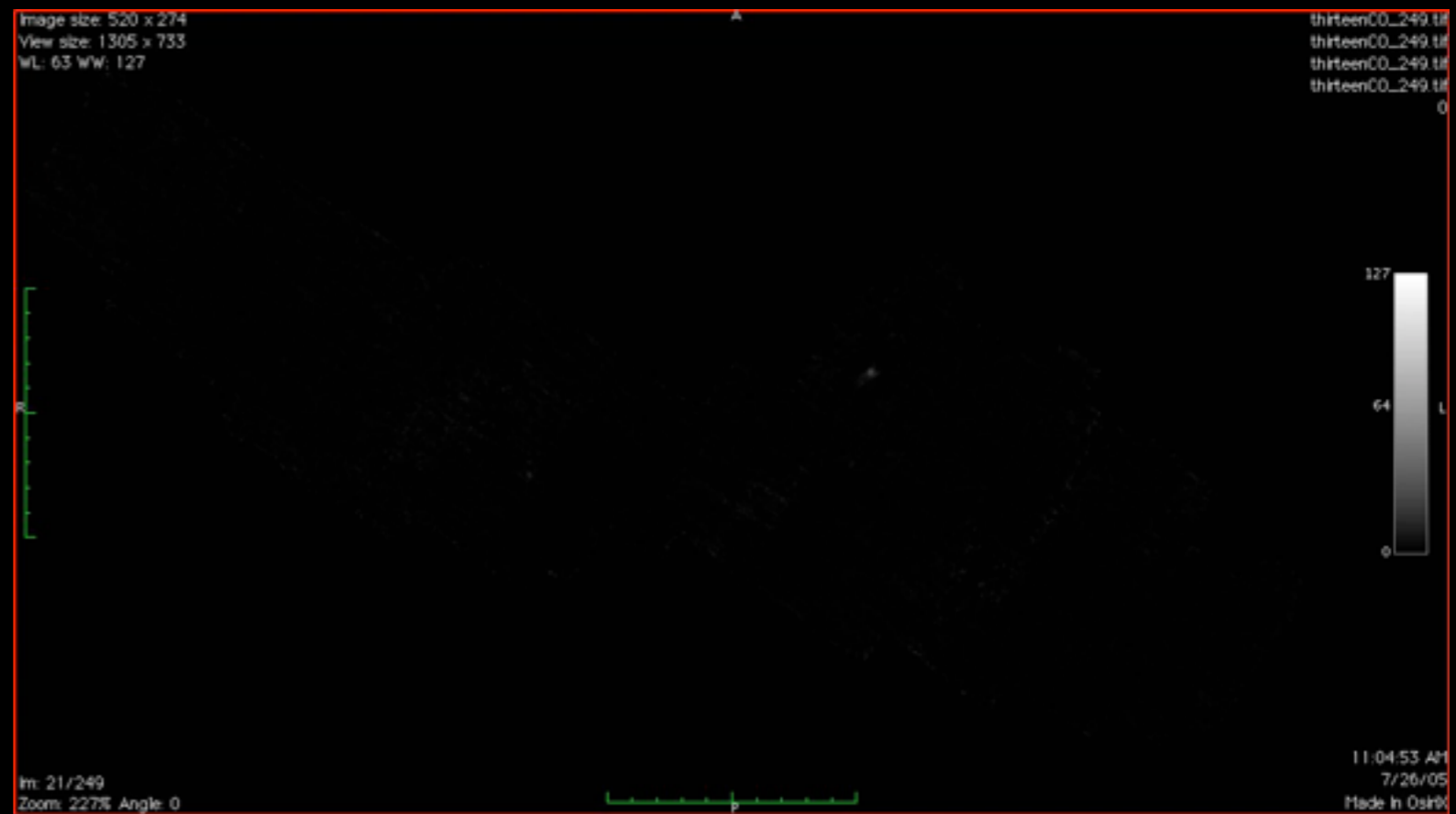
# “Astronomical Medicine”

“KEITH”



“z” is depth into head

“PERSEUS”

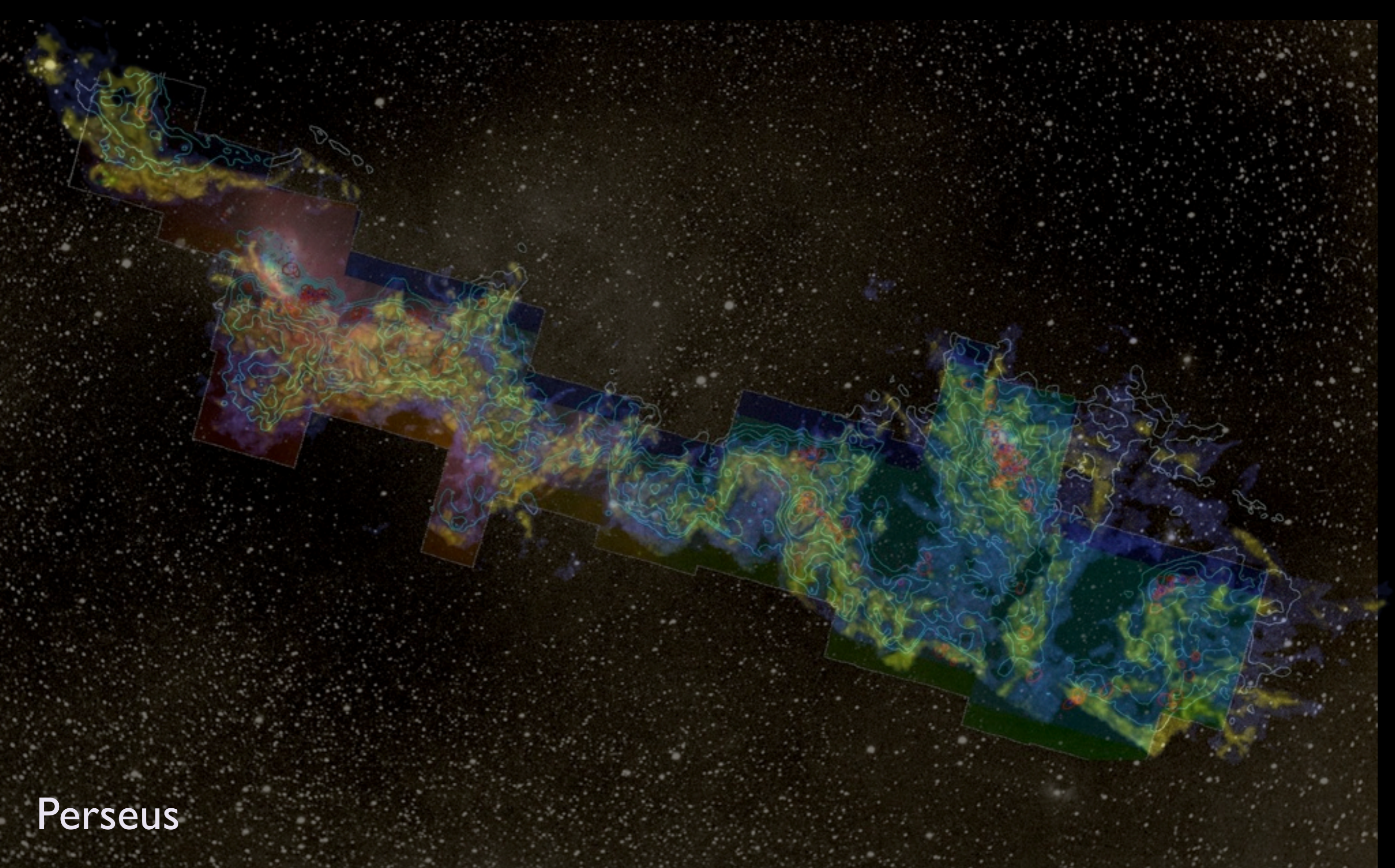


“z” is line-of-sight velocity

(This kind of “series of 2D slices view” is known in the Viz as “the grand tour”)



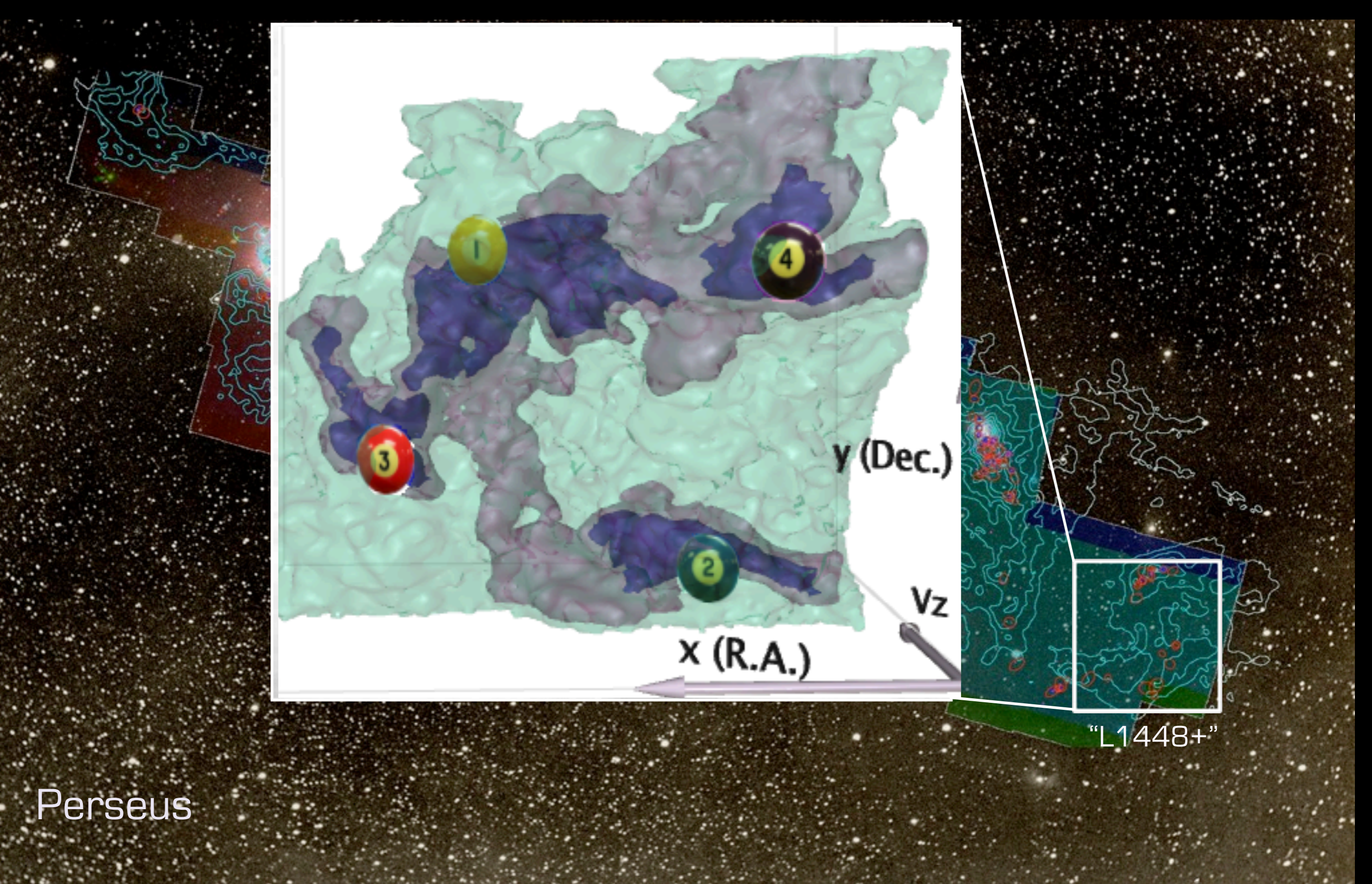




Perseus

3D Viz made with VolView





Perseus



“turbulent fragmentation”

“(magneto-)hydrodynamic simulation”

“bi-jection”

“virial parameter”

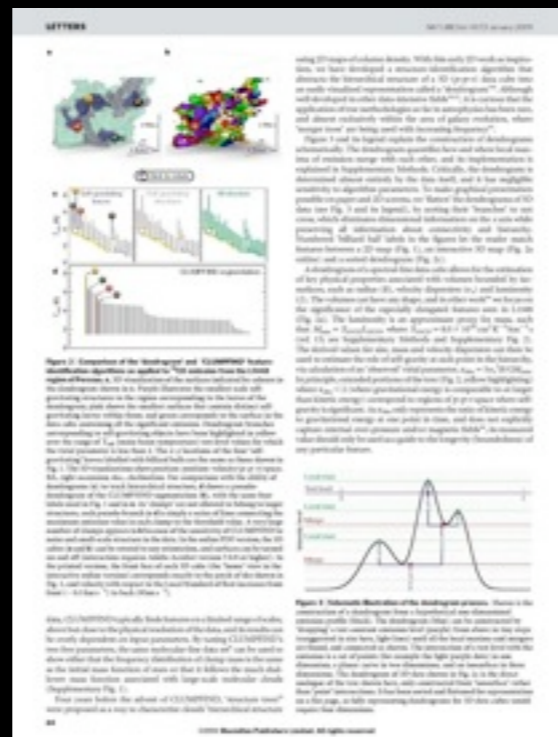
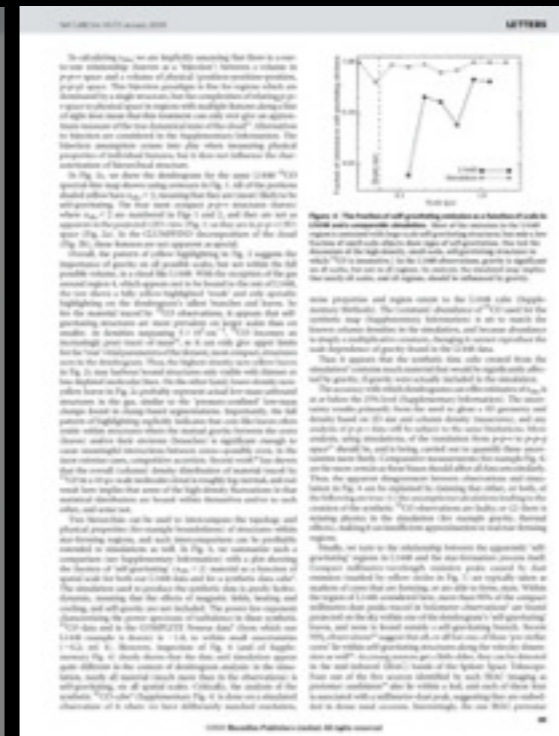
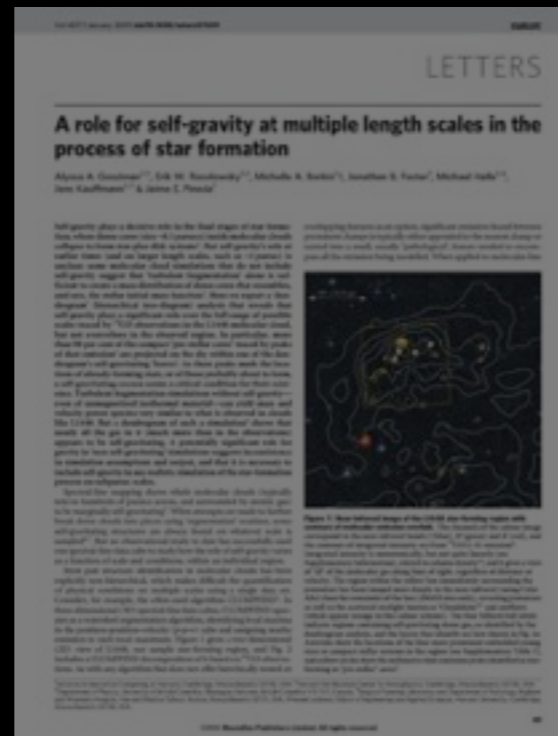
“turbulent power spectrum”

“synthetic observation”

“depletion, opacity”

“taste-test”

caveats



“3D PDF”

✓ “integrated intensity\*”

✓ “p-p-v cube”

“segmentation”

“CLUMPFIND”

“Dendrogram”



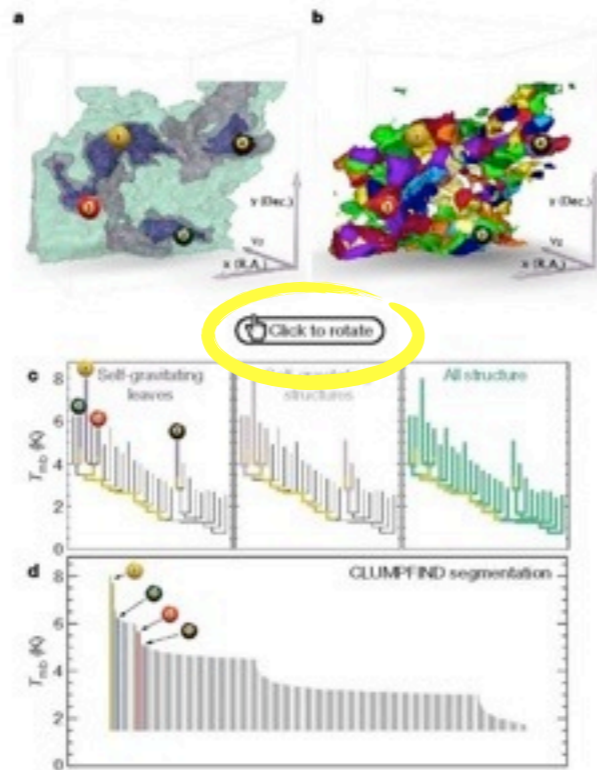


**Figure 2** | Comparison of the 'dendrogram' and 'CLUMPFIND' feature-identification algorithms as applied to  $^{13}\text{CO}$  emission from the L1448 region of Perseus. **a**, 3D visualization of the surfaces indicated by colours in the dendrogram shown in **c**. Purple illustrates the smallest scale self-gravitating structures in the region corresponding to the leaves of the dendrogram; pink shows the smallest surfaces that contain distinct self-gravitating leaves within them; and green corresponds to the surface in the data cube containing all the significant emission. Dendrogram branches corresponding to self-gravitating objects have been highlighted in yellow over the range of  $T_{\text{obs}}$  (main-beam temperature) test-level values for which the virial parameter is less than 2. The  $x$ - $y$  locations of the four 'self-gravitating' leaves labelled with billiard balls are the same as those shown in Fig. 1. The 3D visualizations show position-position-velocity ( $p$ - $p$ - $v$ ) space. RA, right ascension; dec., declination. For comparison with the ability of dendrograms (**c**) to track hierarchical structure, **d** shows a pseudo-dendrogram of the CLUMPFIND segmentation (**b**), with the same four labels used in Fig. 1 and in **a**. As 'dumps' are not allowed to belong to larger structures, each pseudo-branch in **d** is simply a series of lines connecting the maximum emission value in each clump to the threshold value. A very large number of dumps appears in **b** because of the sensitivity of CLUMPFIND to noise and small-scale structure in the data. In the online PDF version, the 3D cubes (**a** and **b**) can be rotated to any orientation, and surfaces can be turned on and off (interaction requires Adobe Acrobat version 7.0.8 or higher). In the printed version, the front face of each 3D cube (the 'home' view in the interactive online version) corresponds exactly to the patch of sky shown in Fig. 1, and velocity with respect to the Local Standard of Rest increases from front ( $-0.5 \text{ km s}^{-1}$ ) to back ( $8 \text{ km s}^{-1}$ ).

data, CLUMPFIND typically finds features on a limited range of scales, above but close to the physical resolution of the data, and its results can be overly dependent on input parameters. By tuning CLUMPFIND's two free parameters, the same molecular-line data set<sup>8</sup> can be used to show either that the frequency distribution of clump mass is the same as the initial mass function of stars or that it follows the much shallower mass function associated with large-scale molecular clouds (Supplementary Fig. 1).

Four years before the advent of CLUMPFIND, 'structure trees'<sup>9</sup> were proposed as a way to characterize clouds' hierarchical structure

using 2D maps of column density. With this early 2D work as inspiration, we have developed a structure-identification algorithm that abstracts the hierarchical structure of a 3D ( $p$ - $p$ - $v$ ) data cube into an easily visualized representation called a 'dendrogram'<sup>10</sup>. Although well developed in other data-intensive fields<sup>11,12</sup>, it is curious that the application of tree methodologies so far in astrophysics has been rare, and almost exclusively within the area of galaxy evolution, where 'merger trees' are being used with increasing frequency<sup>13</sup>.

Figure 3 and its legend explain the construction of dendrograms schematically. The dendrogram quantifies how and where local maxima of emission merge with each other, and its implementation is explained in Supplementary Methods. Critically, the dendrogram is determined almost entirely by the data itself, and it has negligible sensitivity to algorithm parameters. To make graphical presentation possible on paper and 2D screens, we 'flatten' the dendrograms of 3D data (see Fig. 3 and its legend), by sorting their 'branches' to not cross, which eliminates dimensional information on the  $x$  axis while preserving all information about connectivity and hierarchy. Numbered 'billiard ball' labels in the figures let the reader match features between a 2D map (Fig. 1), an interactive 3D map (Fig. 2a online) and a sorted dendrogram (Fig. 2c).

A dendrogram of a spectral-line data cube allows for the estimation of key physical properties associated with volumes bounded by isosurfaces, such as radius ( $R$ ), velocity dispersion ( $\sigma_v$ ) and luminosity ( $L$ ). The volumes can have any shape, and in other work<sup>14</sup> we focus on the significance of the especially elongated features seen in L1448 (Fig. 2a). The luminosity is an approximate proxy for mass, such that  $M_{\text{gas}} = X_{13\text{CO}} L_{13\text{CO}}$  where  $X_{13\text{CO}} = 8.0 \times 10^{26} \text{ cm}^2 \text{ K}^{-1} \text{ km}^{-1} \text{ s}$  (ref. 15; see Supplementary Methods and Supplementary Fig. 2). The derived values for size, mass and velocity dispersion can then be used to estimate the role of self-gravity at each point in the hierarchy, via calculation of an 'observed' virial parameter,  $\alpha_{\text{obs}} = 5\sigma_v^2 R / GM_{\text{gas}}$ . In principle, extended portions of the tree (Fig. 2, yellow highlighting) where  $\alpha_{\text{obs}} < 2$  (where gravitational energy is comparable to or larger than kinetic energy) correspond to regions of  $p$ - $p$ - $v$  space where self-gravity is significant. As  $\alpha_{\text{obs}}$  only represents the ratio of kinetic energy to gravitational energy at one point in time, and does not explicitly capture external over-pressure and/or magnetic fields<sup>16</sup>, its measured value should only be used as a guide to the longevity (boundedness) of any particular feature.

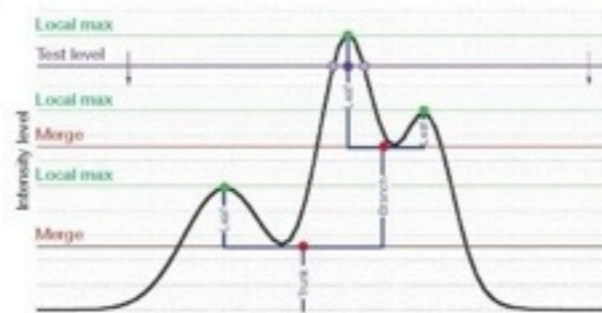


**Figure 3** | Schematic illustration of the dendrogram process. Shown is the construction of a dendrogram from a hypothetical one-dimensional emission profile (black). The dendrogram (blue) can be constructed by 'dropping' a test constant emission level (purple) from above in tiny steps (exaggerated in size here, light lines) until all the local maxima and mergers are found, and connected as shown. The intersection of a test level with the emission is a set of points (for example the light purple dots) in one dimension, a planar curve in two dimensions, and an isosurface in three dimensions. The dendrogram of 3D data shown in Fig. 2c is the direct analogue of the tree shown here, only constructed from 'isosurface' rather than 'point' intersections. It has been sorted and flattened for representation on a flat page, as fully representing dendrograms for 3D data cubes would require four dimensions.



“turbulent fragmentation”

“(magneto-)hydrodynamic simulation”

“bi-jection”

“virial parameter”

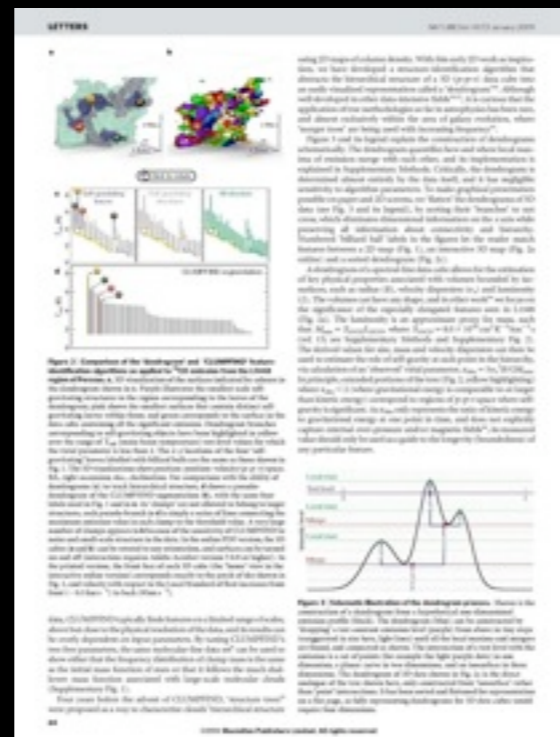
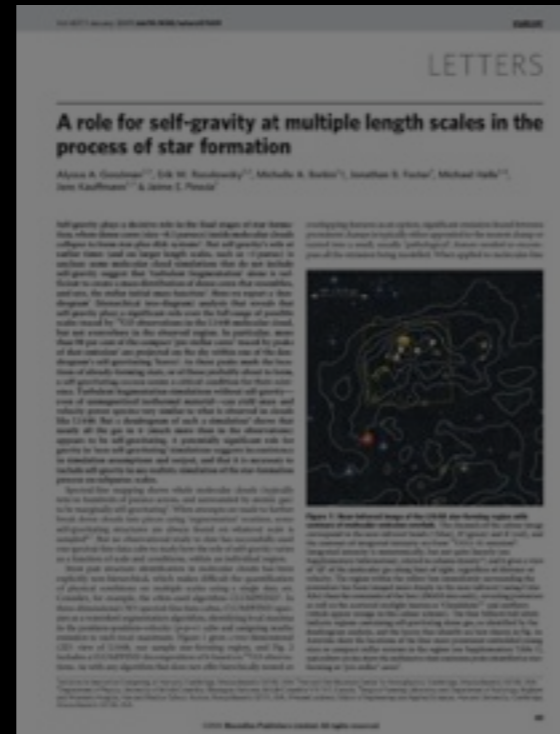
“turbulent power spectrum”

“synthetic observation”

“depletion, opacity”

“taste-test”

caveats



✓ “integrated intensity\*”

✓ “p-p-v cube”

“segmentation”

“CLUMPFIND”

“Dendrogram”

✓ “3D PDF”



“turbulent fragmentation”

“(magneto-)hydrodynamic simulation”

“bi-jection”

“virial parameter”

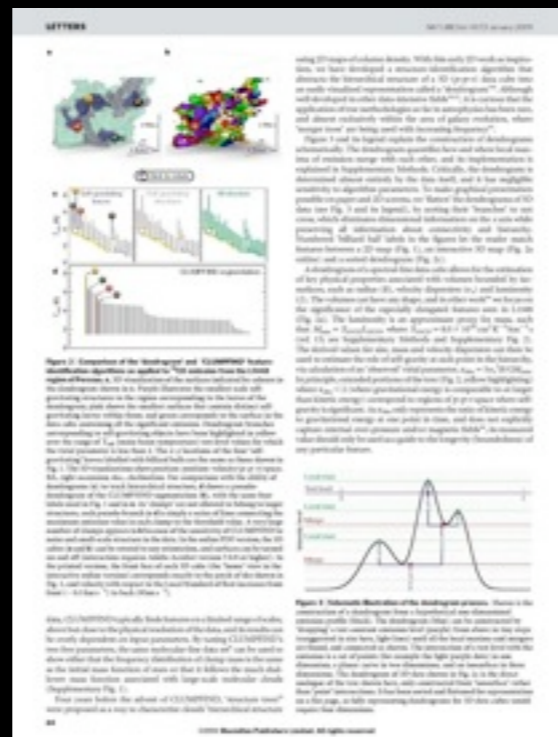
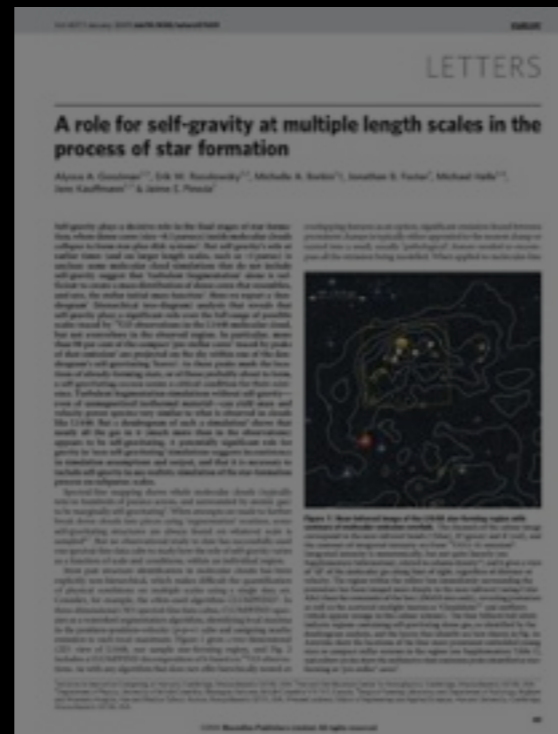
“turbulent power spectrum”

“synthetic observation”

“depletion, opacity”

“taste-test”

caveats



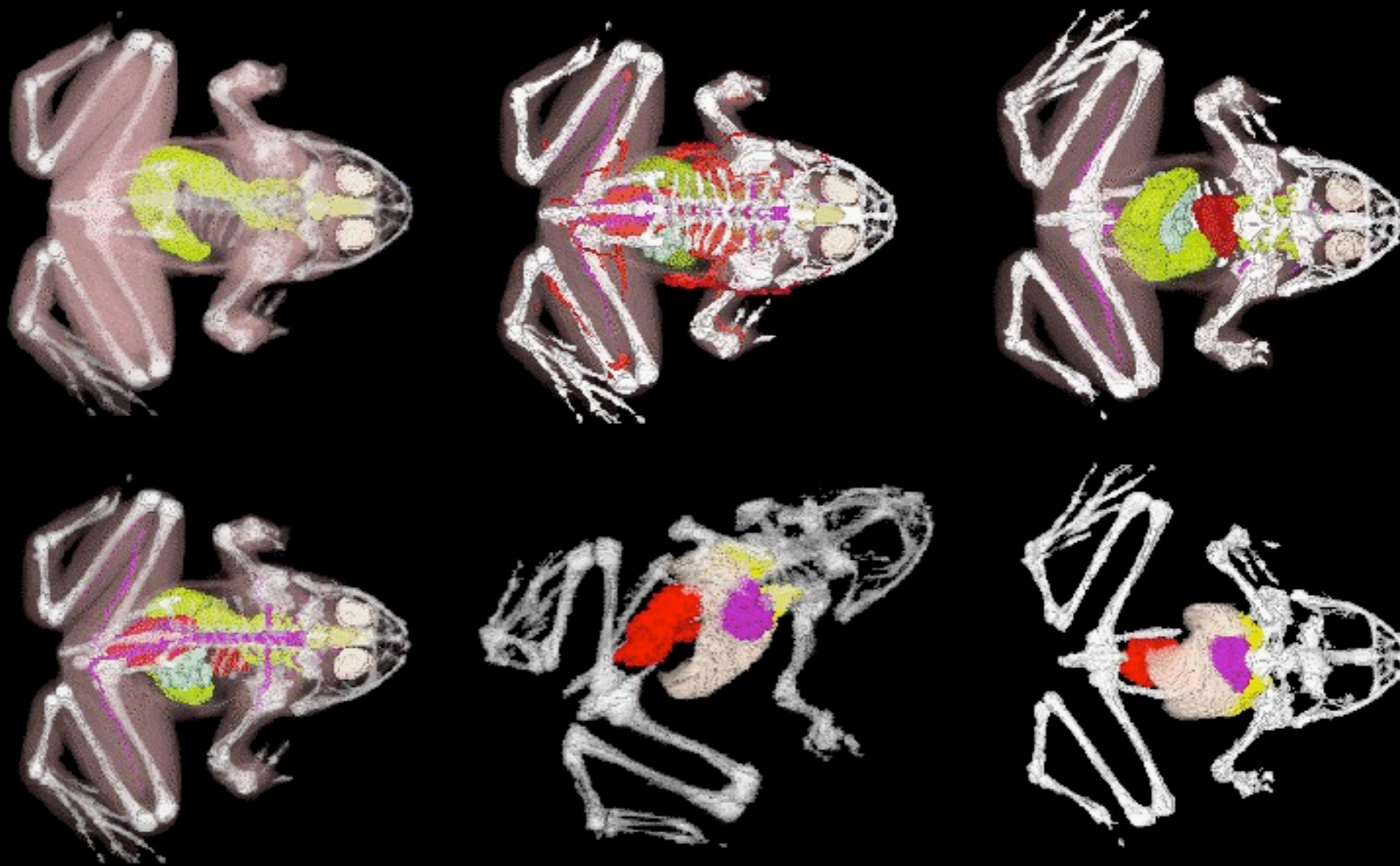
“segmentation”

“CLUMPFIND”

“Dendrogram”

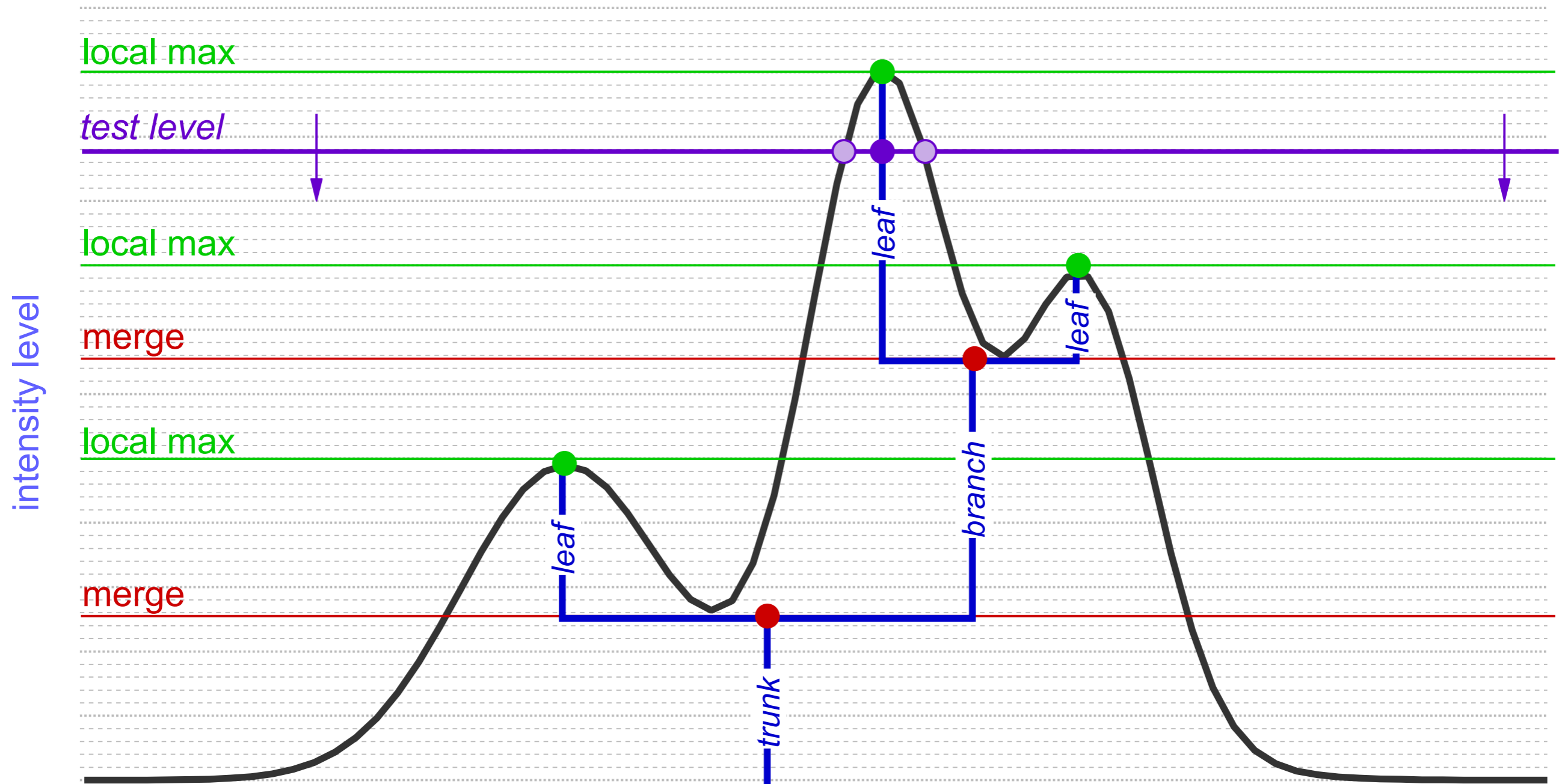


# “Segmentation”





# Dendrograms

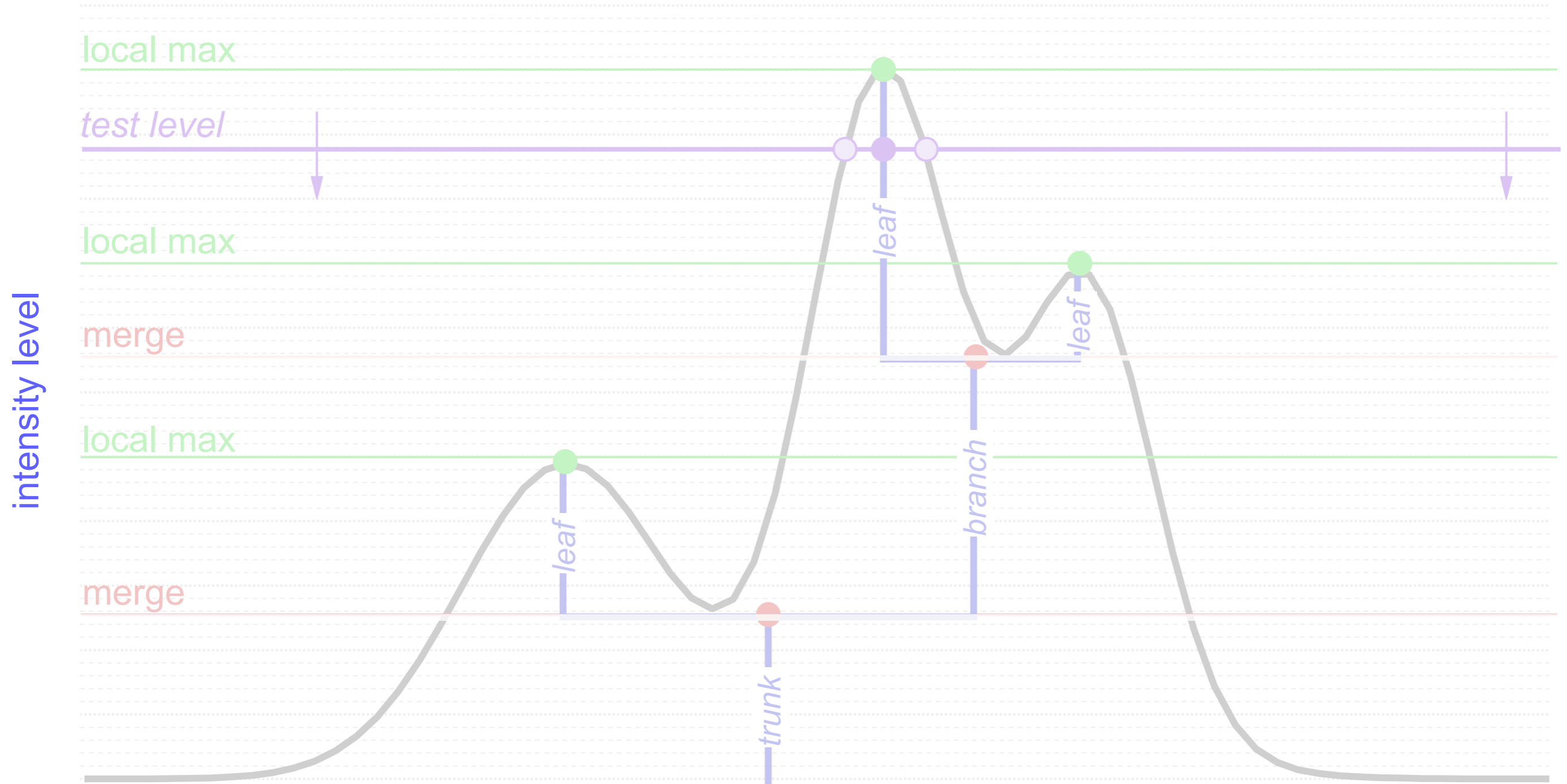


## Hierarchical "Segmentation"

*Rosolowsky, Pineda, Kauffmann & Goodman 2008*



# Dendrograms



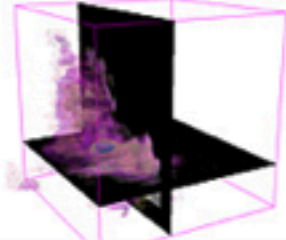

1-D: points; 2-D closed curves (contours); 3-D surfaces enclosing volumes  
see 2D demo at <http://am.iic.harvard.edu/index.cgi/DendroStar/applet>



DendroStar/applet - IIC/AstroMed

http://am.iic.harvard.edu/index.cgi/DendroStar/applet

astronomical medicine

The Astronomical Medicine Project

Initiative In Innovative Computing at Harvard

### The DendroStar Applet for L1448: Try me!

**Harvard IIC Home**

**AM Project**  
 overview  
 what's new?  
 press  
 about us  
 contact us

**Research**  
 background  
 projects  
 papers  
 images  
 movies

**Software**  
 overview  
 Slicer: getting started  
 Slicer 3  
 fits2itk  
 OsiriX  
 DendroStar

**Links**  
 Center for Astrophysics  
 COMPLETE Survey  
 Surgical Planning Lab  
 3D Slicer  
 related projects

**User**  
 Login


**Search**

Tint:

Suppress tint:

Reset:

Applet DendroStar started

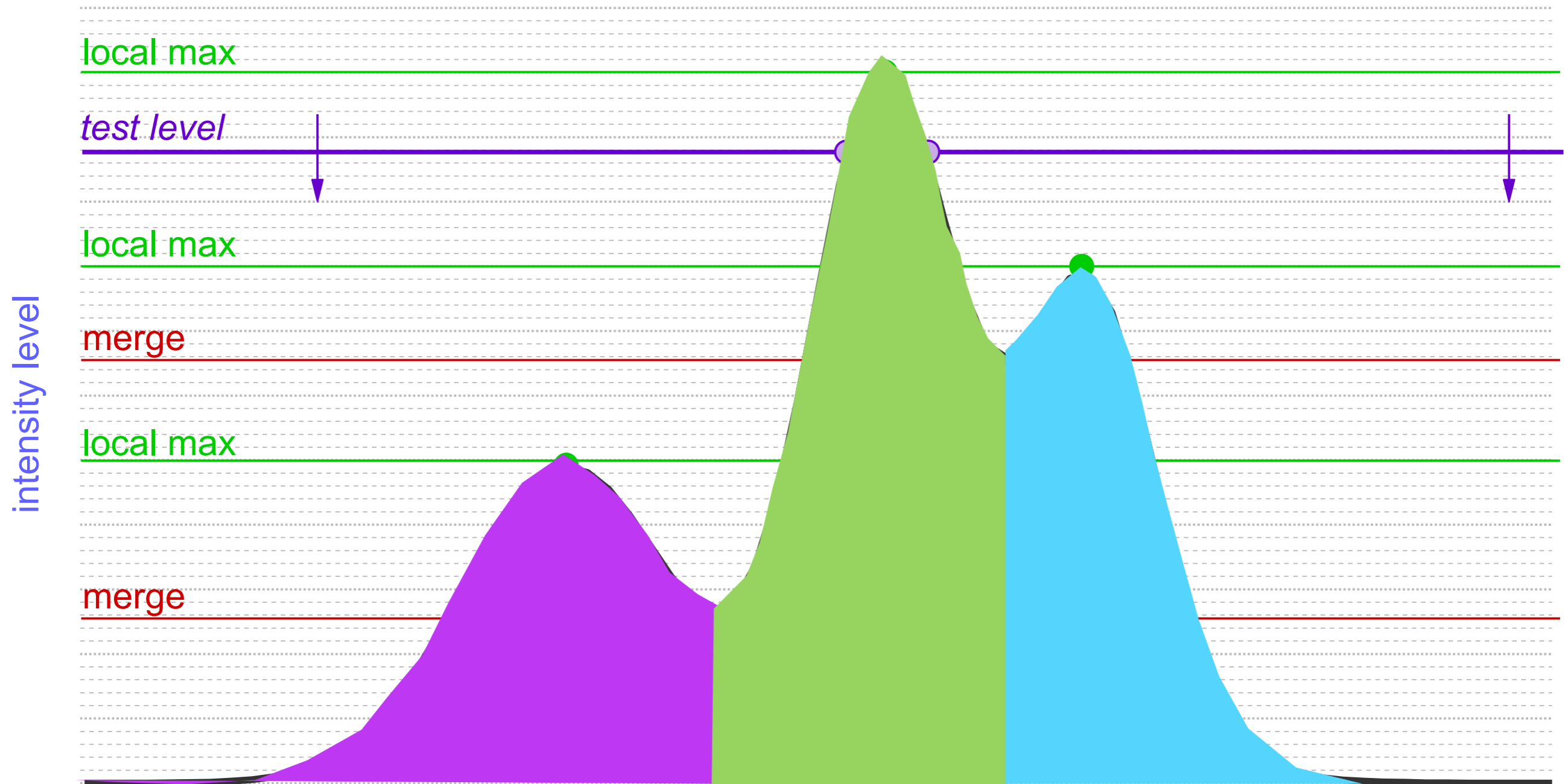


<http://am.iic.harvard.edu/index.cgi/DendroStar/applet>  
 Dendrogram Algorithm by Erik Rosolwosky; Applet by Douglas Alan

3D, see PDF...



# What would *CLUMPFIND* do?



No hierarchy is allowed, all clumps go to the baseline.  
(Williams, De Geus & Blitz 1994)



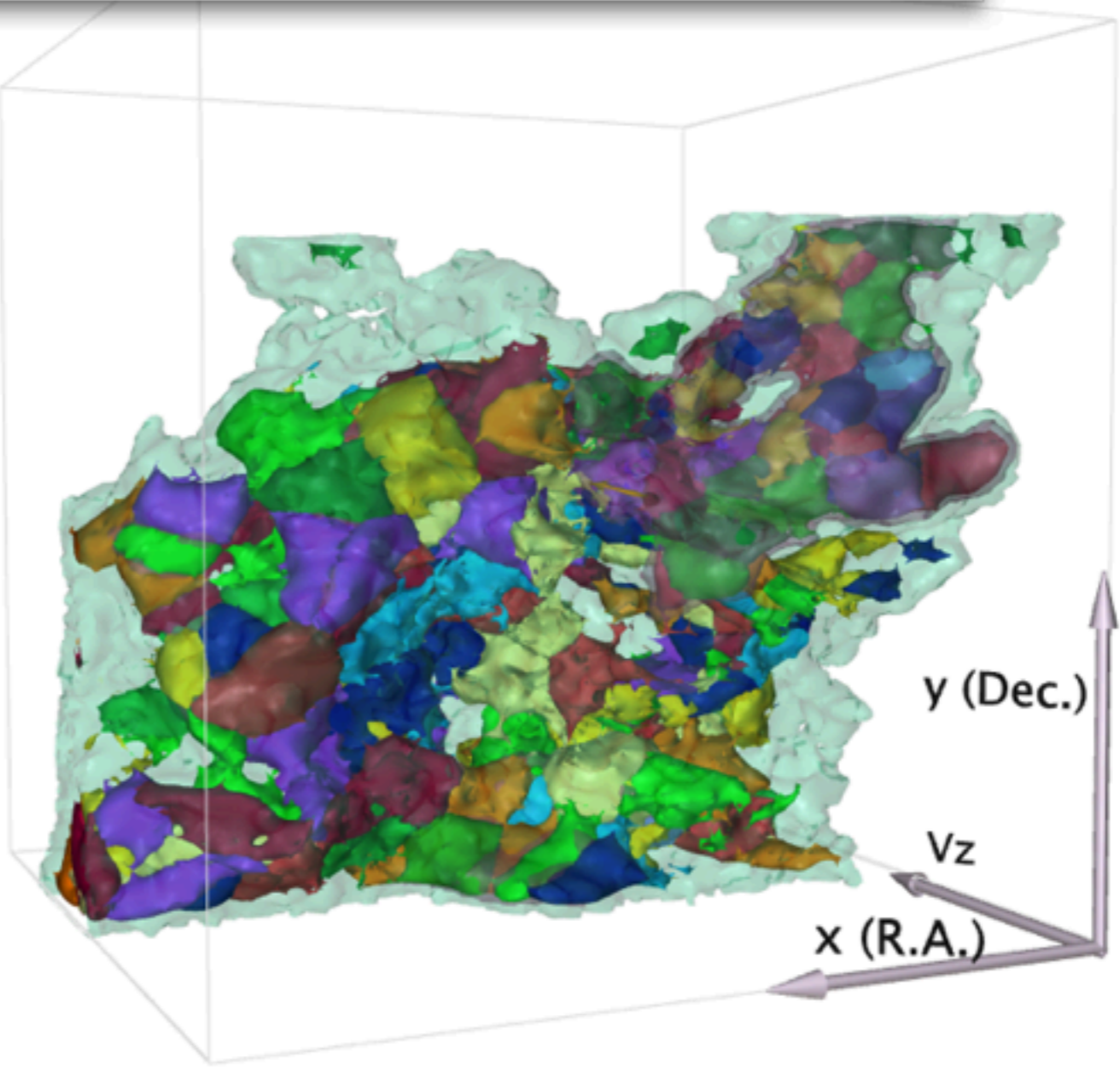


Model Tree

- Highlight Color
- model
  - Dendrogram decomposition
    - self-gravitating leaves
    - self-gravitating structures
    - all structure
  - CLUMPFIND decomposition
    - peaks within leaves
    - other clumps
  - billiard markers
  - axes

Options

- CLUMPFIND: peaks within leaves
- CLUMPFIND: R.A.-Dec.
- CLUMPFIND: R.A.-Vz
- CLUMPFIND: Vz-Dec.
- Combined: all structure
- Combined: self-grav. and peaks within leaves
- Combined: all structure



This interactive 3D figure shows the result of the dendrogram hierarchical feature-identification algorithm applied to a data cube of <sup>13</sup>CO emission of the L1448 region of Perseus. Purple areas are the smallest scale self-gravitating structures in the region, pink shows the smallest regions that contain distinct self-gravitating sub-regions, and green depicts all regions with significant emission. Different views of the data cube can be selected from the Views menu. In addition, results of the alternative

<http://iic.harvard.edu/sites/all/files/interactive.pdf>  
with many thanks to Mike Halle, Michelle Borkin, Jens Kauffmann & Douglas Alan



“Crowded” 3D data  
(very dangerous)

“Sparse” 2D data  
(OK)

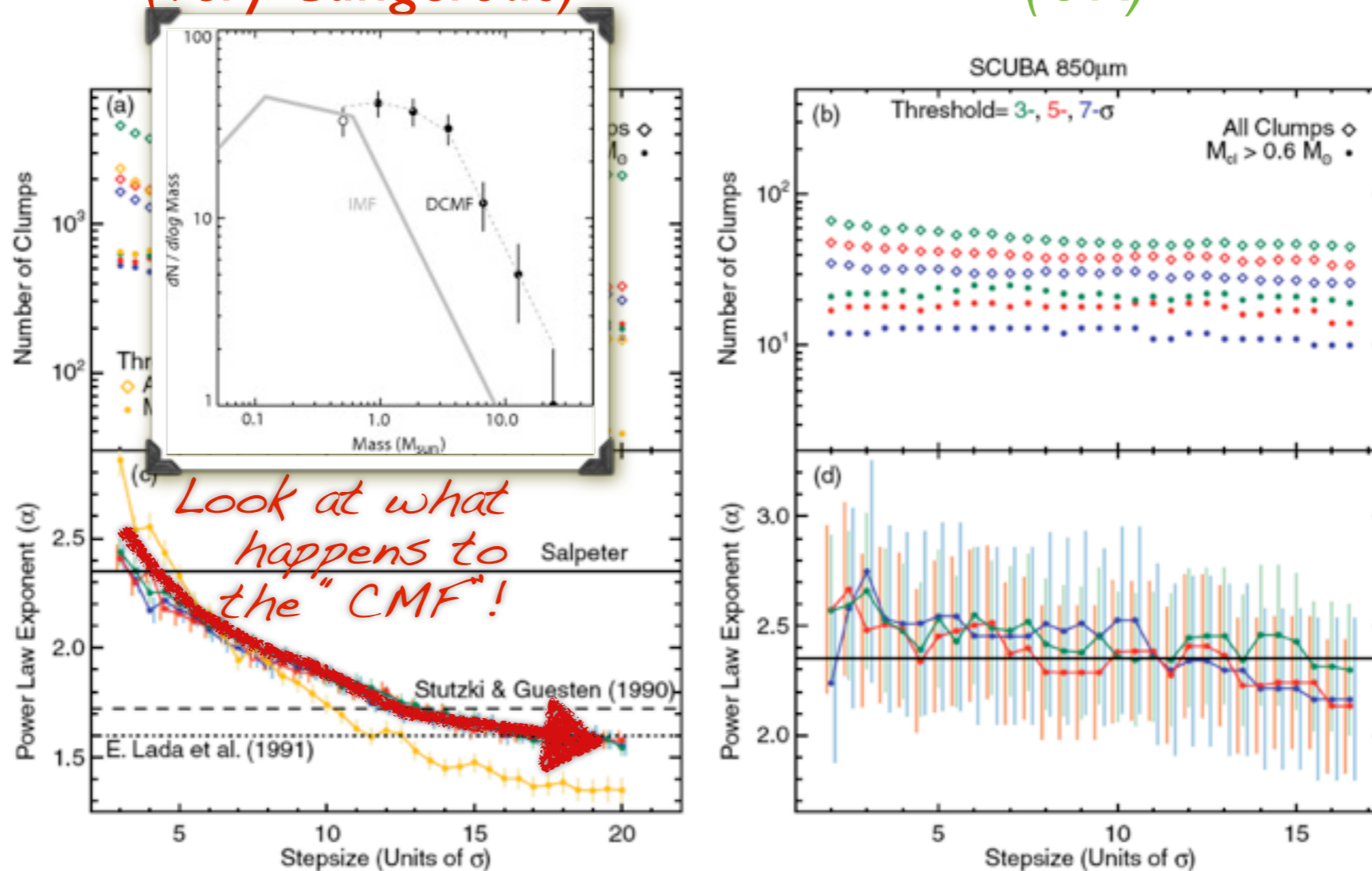


**Figure 2.** Summary of all Clumpfind runs as a function of stepsize. Color represent different thresholds: blue, red, and green for  $3\sigma$ ,  $5\sigma$ , and  $7\sigma$ , respectively; we also show in orange results with a threshold of  $5\sigma$  for  $^{13}\text{CO}$  data with added noise. Left and right columns show results for  $^{13}\text{CO}$  and SCUBA data, respectively. Panels (a) and (b) show the number of clumps under a given category per model. Total number of clumps found, and total number of clumps with mass larger than the completeness limit are shown in open diamonds and filled circles, respectively. Panels (c) and (d) show the exponent of the fitted mass spectrum of clumps above the completeness limit,  $dN/dM \propto M^{-\alpha}$ , with error bars estimated from Equation (6). Horizontal black lines show some fiducial exponents for comparison. Average noise in  $^{13}\text{CO}$ ,  $^{13}\text{CO}$  with added noise, and SCUBA data is  $0.1 \text{ K}$ ,  $0.2 \text{ K}$ , and  $0.06 \text{ Jy beam}^{-1}$ , respectively. Completeness limit is estimated to be  $4 M_{\odot}$ ,  $3 M_{\odot}$ , and  $0.6 M_{\odot}$  for  $^{13}\text{CO}$ ,  $^{13}\text{CO}$  with added noise, and SCUBA data. Panel (c) also shows that for different noise level in the data, if a threshold of  $\sim 2 \text{ K}$  ( $20\sigma$  and  $10\sigma$  for original and noise-added data, respectively) is used, then the fitted power-law exponents are closer to previous works.

from “**The Perils of CLUMPFIND**” by Pineda, Rosolowsky & Goodman 2009



“turbulent fragmentation”

“(magneto-)hydrodynamic simulation”

“bi-jection”

“virial parameter”

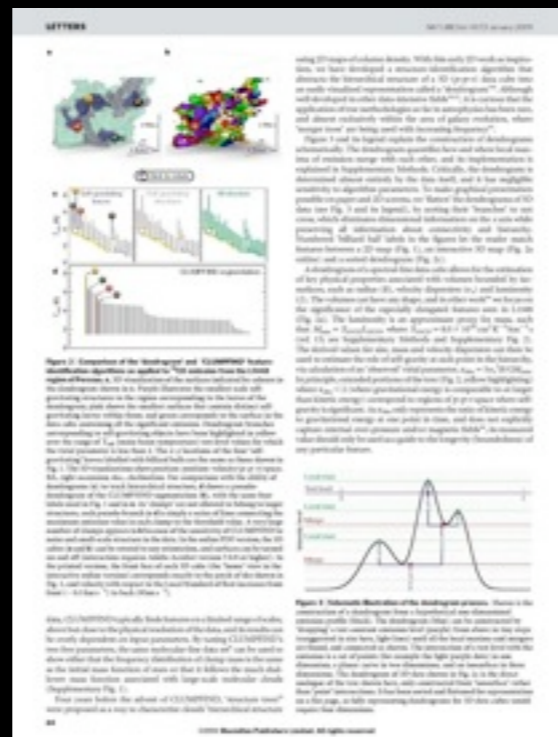
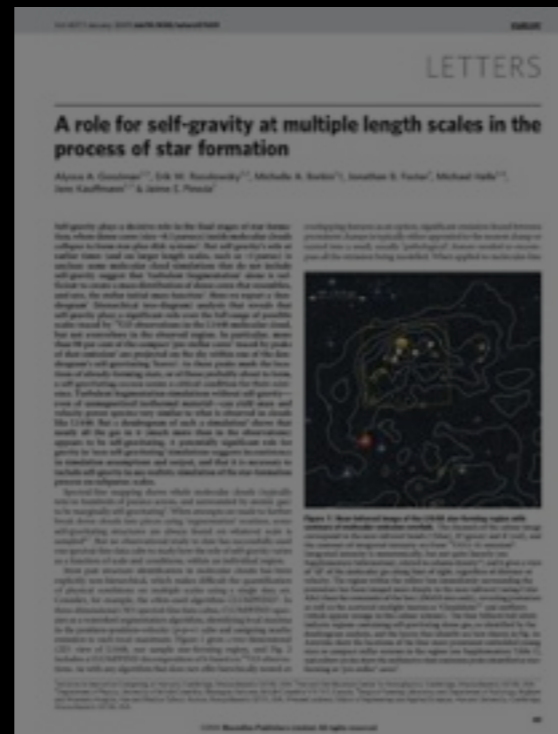
“turbulent power spectrum”

“synthetic observation”

“depletion, opacity”

“taste-test”

caveats



✓ “segmentation”

✓ “CLUMPFIND”

✓ “Dendrogram”



“turbulent fragmentation”

“(magneto-)hydrodynamic simulation”

“bi-jection”

“virial parameter”

“turbulent power spectrum”

“synthetic observation”

“depletion, opacity”

“taste-test”

caveats

LETTERS

**A role for self-gravity at multiple length scales in the process of star formation**

Alexis A. Goodman<sup>1,2</sup>, Erik W. Rosolowsky<sup>1,2</sup>, Michelle R. Borker<sup>1</sup>, Jonathan S. Foster<sup>1</sup>, Michael Hebb<sup>1</sup>, Steve Kaufman<sup>1</sup>, & James I. Proser<sup>1</sup>

Self-gravity plays a decisive role in the final stages of star formation, where dense cores evolve to compact protostellar structures. However, the role of self-gravity is less clear at larger length scales, such as the formation of molecular cloud filaments. We use a bijective mapping to show that self-gravity plays a role in the fragmentation of molecular clouds, and that this role is more significant at larger length scales than previously thought. We use a bijective mapping to show that self-gravity plays a role in the fragmentation of molecular clouds, and that this role is more significant at larger length scales than previously thought. We use a bijective mapping to show that self-gravity plays a role in the fragmentation of molecular clouds, and that this role is more significant at larger length scales than previously thought.




Figure 1 shows a 3D visualization of a molecular cloud structure, showing a complex, filamentary network of gas and dust. The structure is rendered in a dark, translucent style, highlighting the intricate, interconnected nature of the cloud's internal structure.

LETTERS

**The formation of self-gravitating structures in a turbulent medium**

Figure 2 shows a plot of the virial parameter  $\alpha_{\text{vir}}$  versus the turbulent Mach number  $\mathcal{M}_{\text{turb}}$ . The x-axis ranges from 0 to 1.5, and the y-axis ranges from 0 to 1.5. The data points show a clear trend where  $\alpha_{\text{vir}}$  increases with  $\mathcal{M}_{\text{turb}}$ , indicating that self-gravity becomes more important as the turbulence becomes stronger.

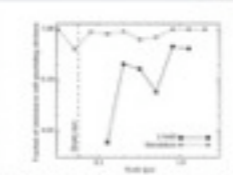


Figure 2 shows a plot of the virial parameter  $\alpha_{\text{vir}}$  versus the turbulent Mach number  $\mathcal{M}_{\text{turb}}$ . The x-axis ranges from 0 to 1.5, and the y-axis ranges from 0 to 1.5. The data points show a clear trend where  $\alpha_{\text{vir}}$  increases with  $\mathcal{M}_{\text{turb}}$ , indicating that self-gravity becomes more important as the turbulence becomes stronger.

LETTERS

**Comparison of the bijective and COINTEGRATED bijective algorithms as applied to COINTEGRATED bijective**

Figure 3 shows a comparison of the bijective and COINTEGRATED bijective algorithms. The top panel shows a 3D visualization of a molecular cloud structure. The middle panel shows a plot of the virial parameter  $\alpha_{\text{vir}}$  versus the turbulent Mach number  $\mathcal{M}_{\text{turb}}$ . The bottom panel shows a plot of the turbulent power spectrum.

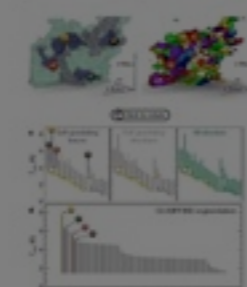


Figure 3 shows a comparison of the bijective and COINTEGRATED bijective algorithms. The top panel shows a 3D visualization of a molecular cloud structure. The middle panel shows a plot of the virial parameter  $\alpha_{\text{vir}}$  versus the turbulent Mach number  $\mathcal{M}_{\text{turb}}$ . The bottom panel shows a plot of the turbulent power spectrum.

LETTERS

**Substrate structure of the bijective algorithm**

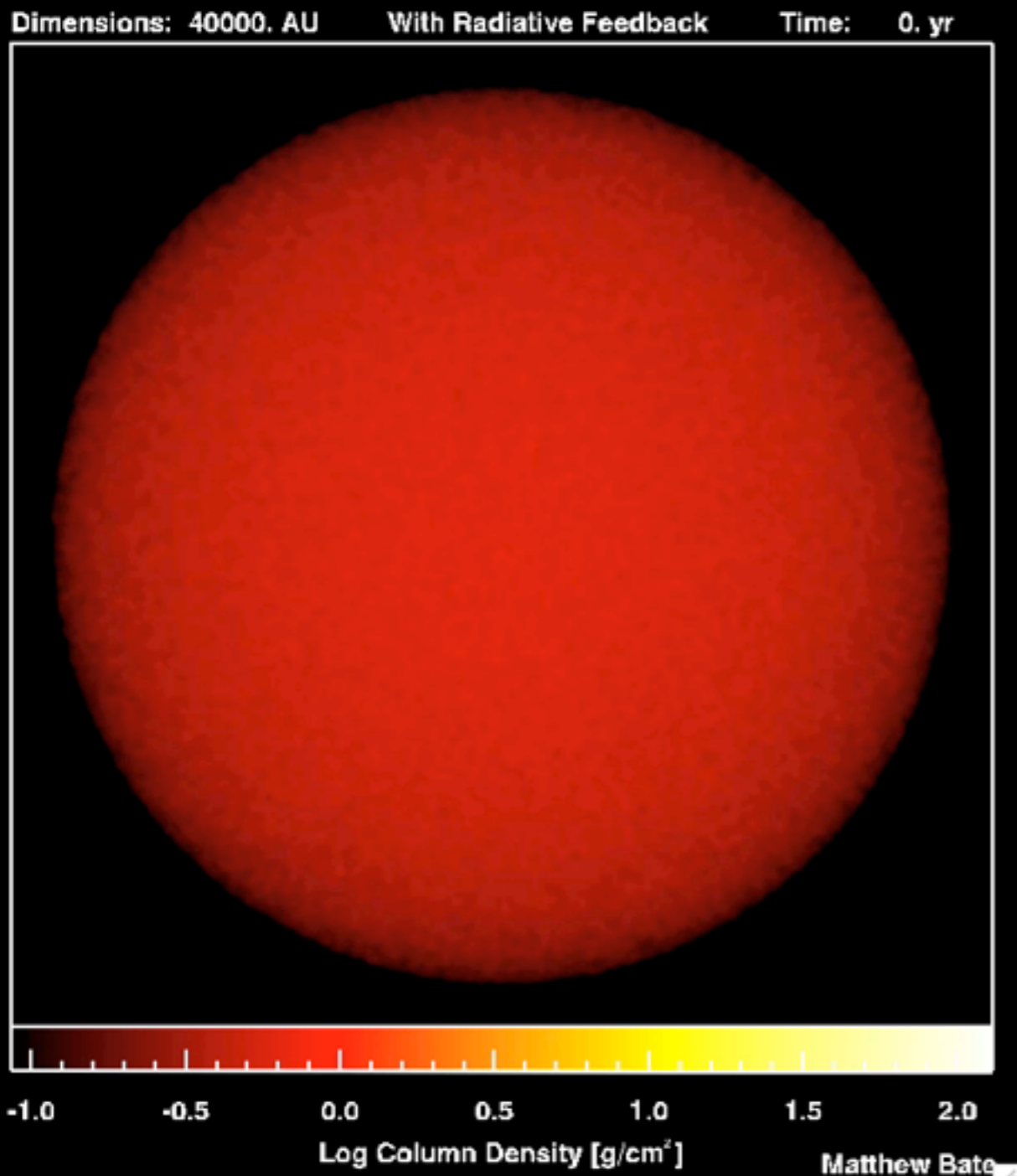
Figure 4 shows a plot of the substrate structure of the bijective algorithm. The x-axis represents the turbulent Mach number  $\mathcal{M}_{\text{turb}}$  and the y-axis represents the virial parameter  $\alpha_{\text{vir}}$ . The plot shows a clear trend where  $\alpha_{\text{vir}}$  increases with  $\mathcal{M}_{\text{turb}}$ , indicating that self-gravity becomes more important as the turbulence becomes stronger.



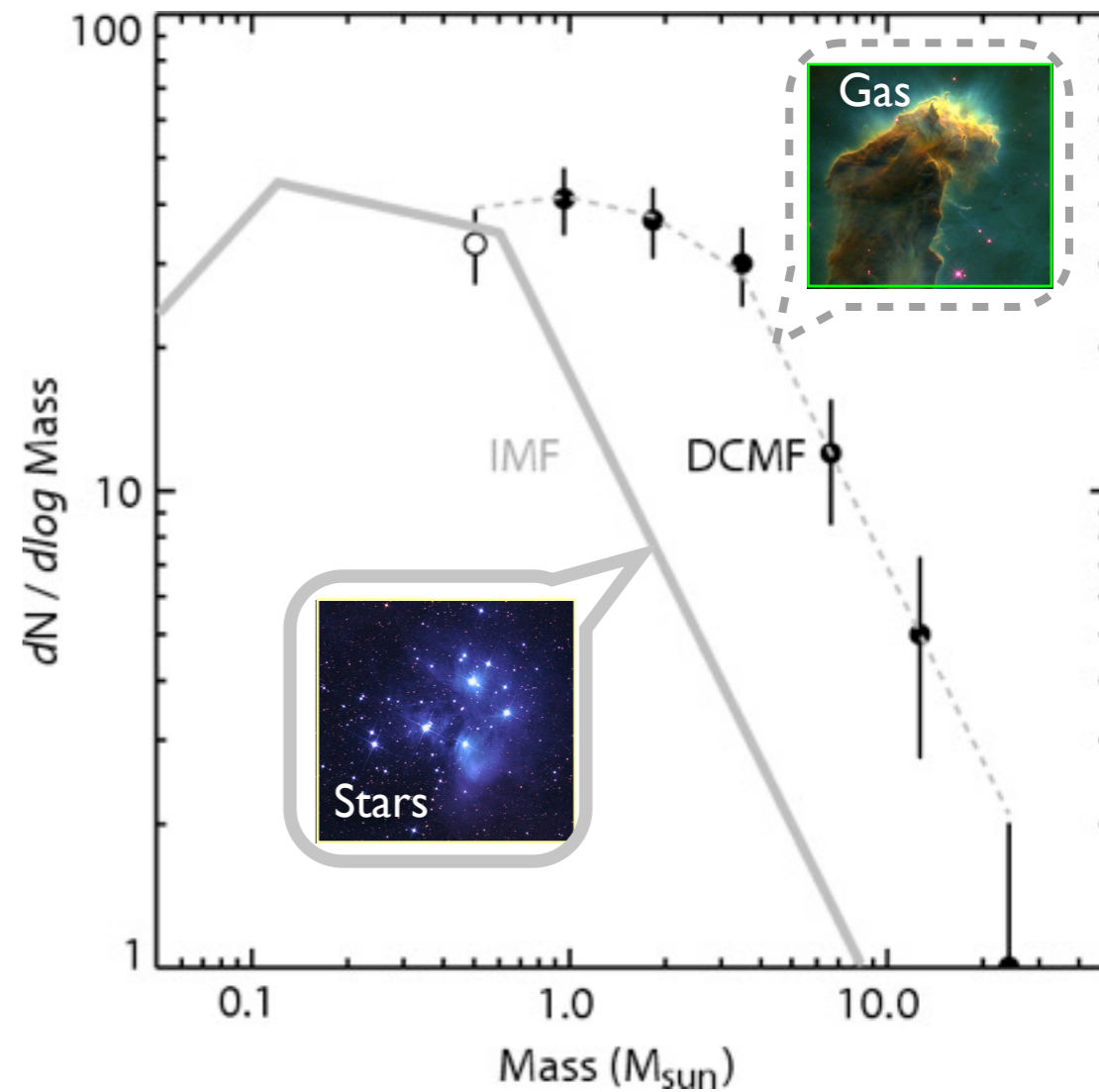
Figure 4 shows a plot of the substrate structure of the bijective algorithm. The x-axis represents the turbulent Mach number  $\mathcal{M}_{\text{turb}}$  and the y-axis represents the virial parameter  $\alpha_{\text{vir}}$ . The plot shows a clear trend where  $\alpha_{\text{vir}}$  increases with  $\mathcal{M}_{\text{turb}}$ , indicating that self-gravity becomes more important as the turbulence becomes stronger.



# (MHD) Simulations, Turbulent Fragmentation



*cf. Padoan & Nordlund 2002*



*Alves, Lombardi & Lada 2007*



✓ “turbulent fragmentation”

✓ “(magneto-)hydrodynamic simulation”

“bi-jection”

“virial parameter”

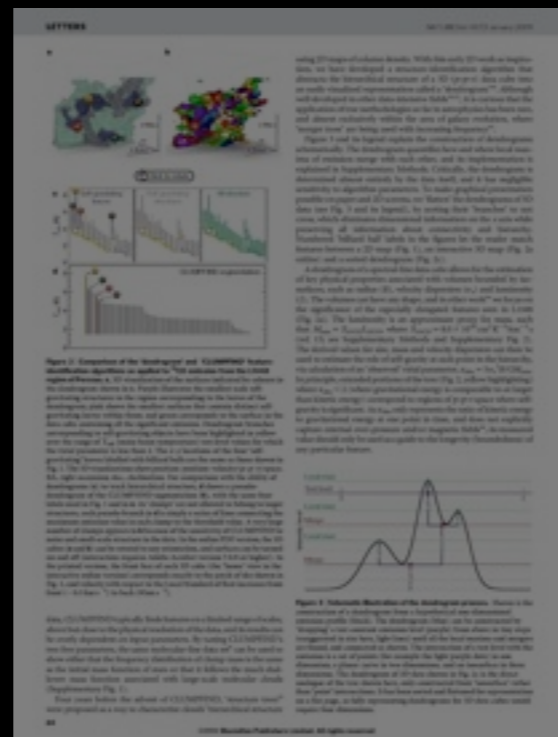
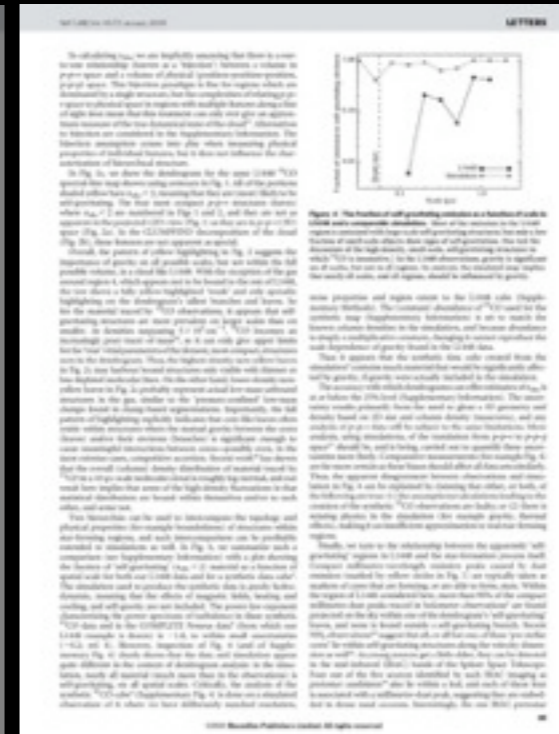
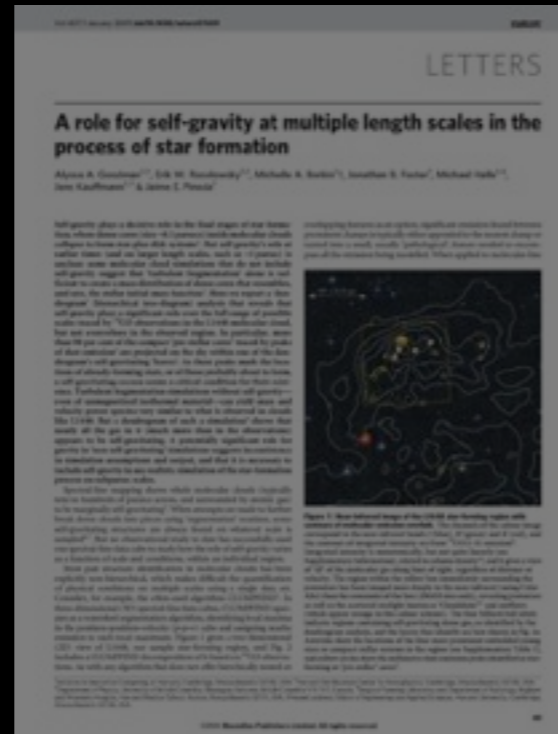
“turbulent power spectrum”

“synthetic observation”

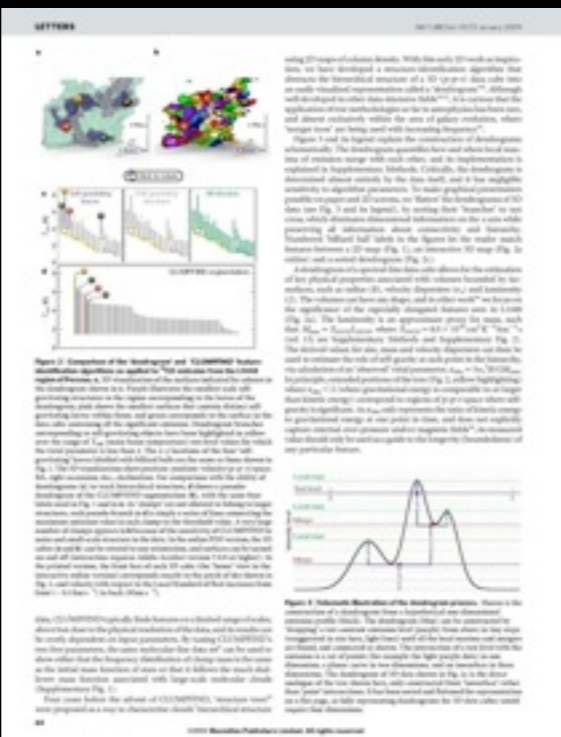
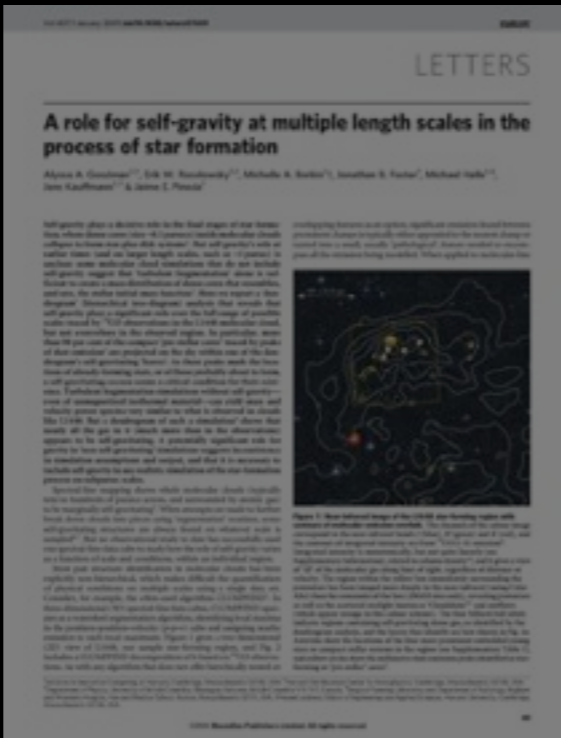
“depletion, opacity”

“taste-test”

caveats







“bi-jection”

“virial parameter”

“turbulent power spectrum”

“synthetic observation”

“depletion, opacity”

“taste-test”

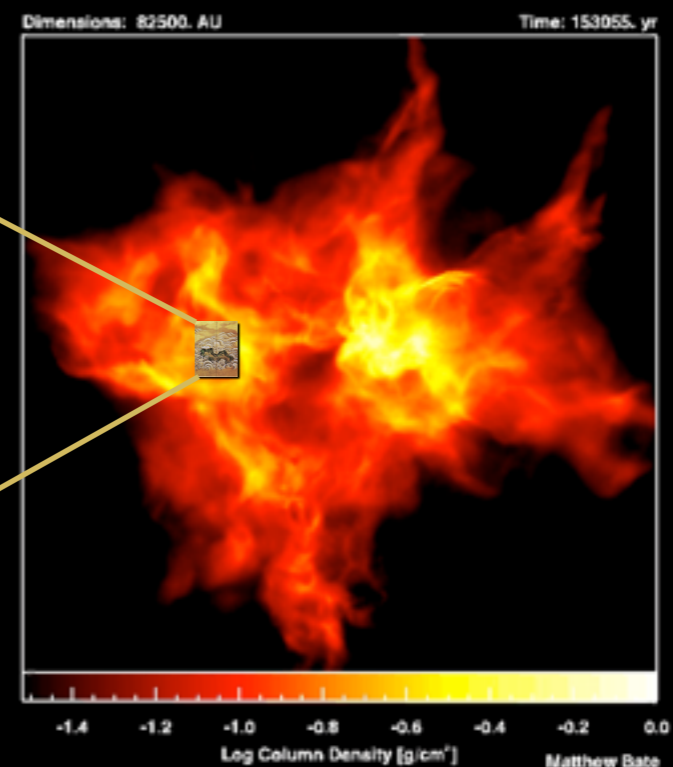
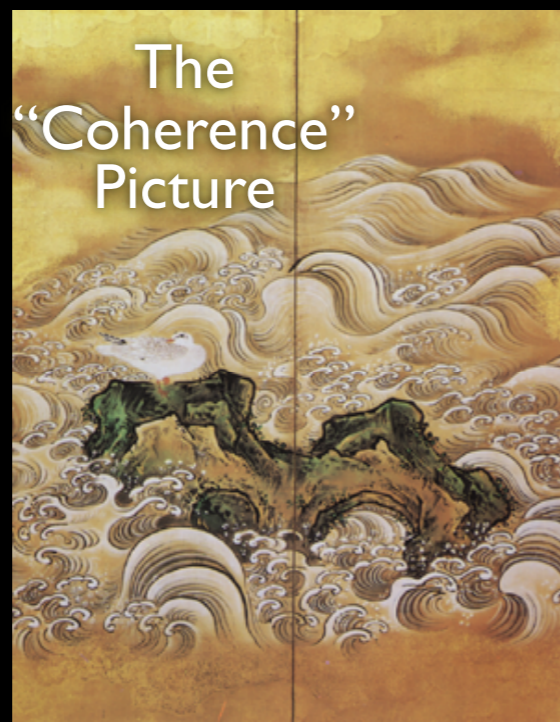
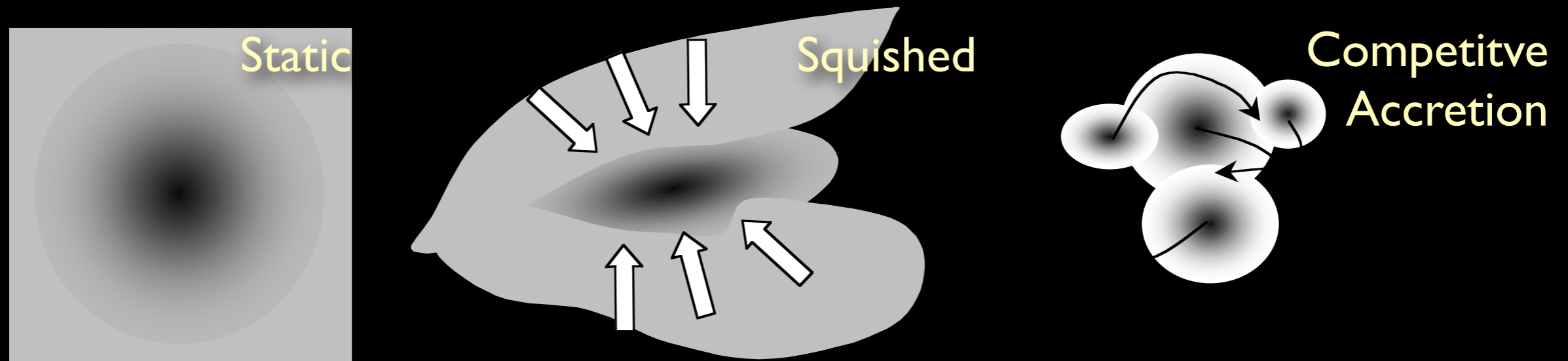
caveats



# How calm, and how long-lasting are cores?

(relevant motions/forces & the “virial parameter”)

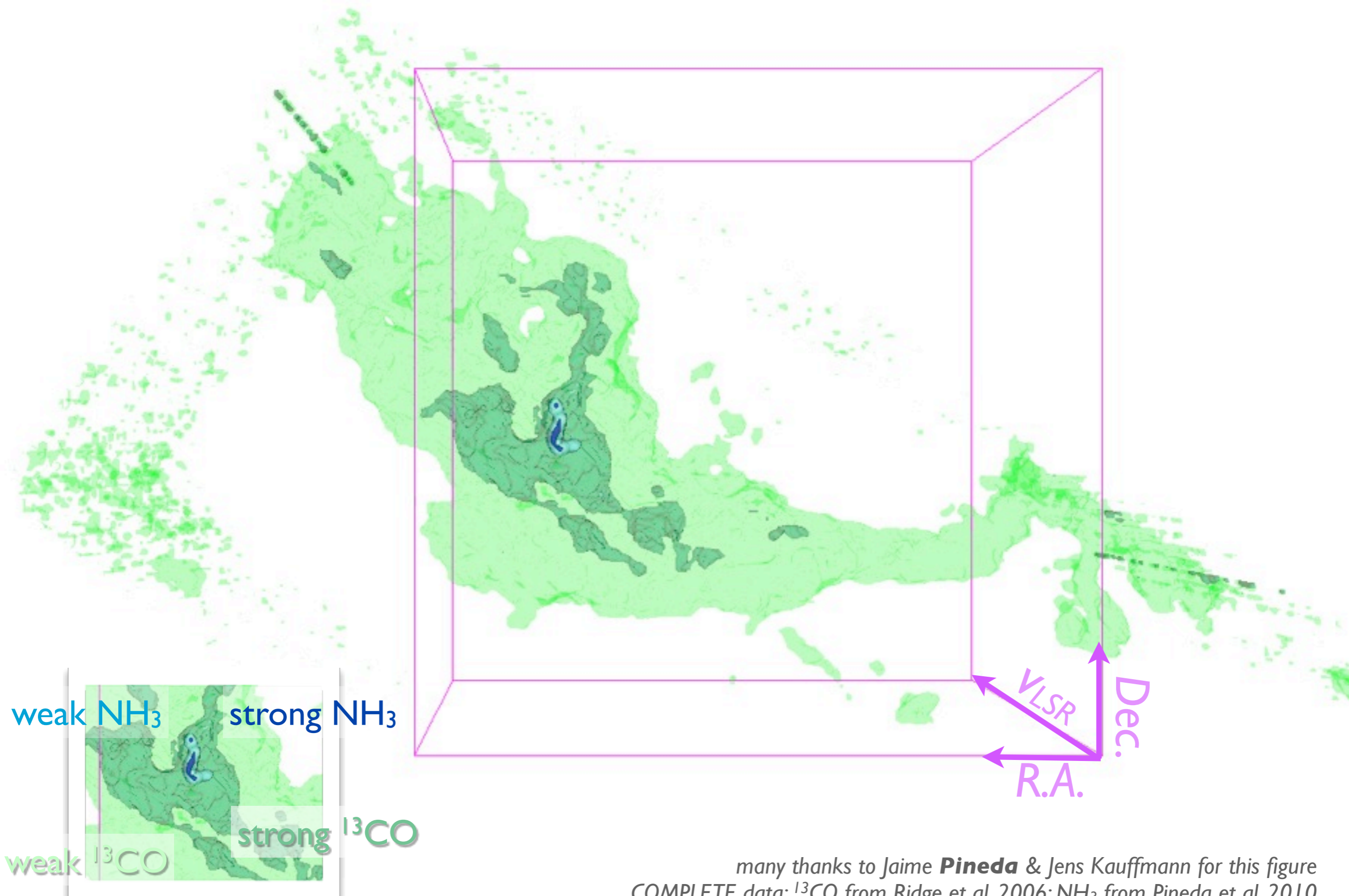
Three main views at present...



The “*bijection*” problem...  
this is  $p-p-p$ ,  
but we have only  $p-p-v$ ...



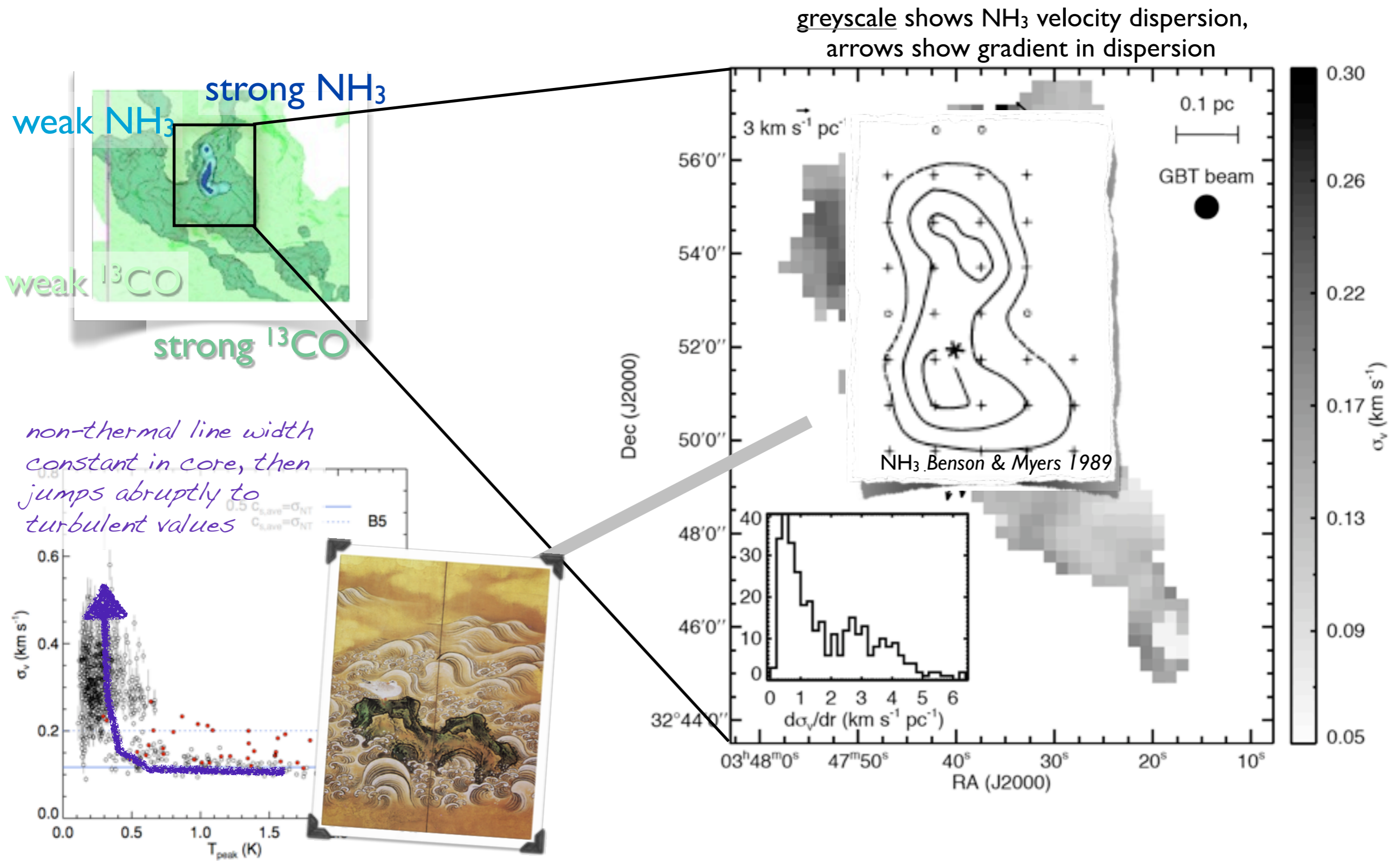
# $p$ - $p$ - $v$ structure of the B5 region in Perseus



many thanks to Jaime **Pineda** & Jens Kauffmann for this figure  
COMPLETE data:  $^{13}\text{CO}$  from Ridge et al. 2006;  $\text{NH}_3$  from Pineda et al. 2010



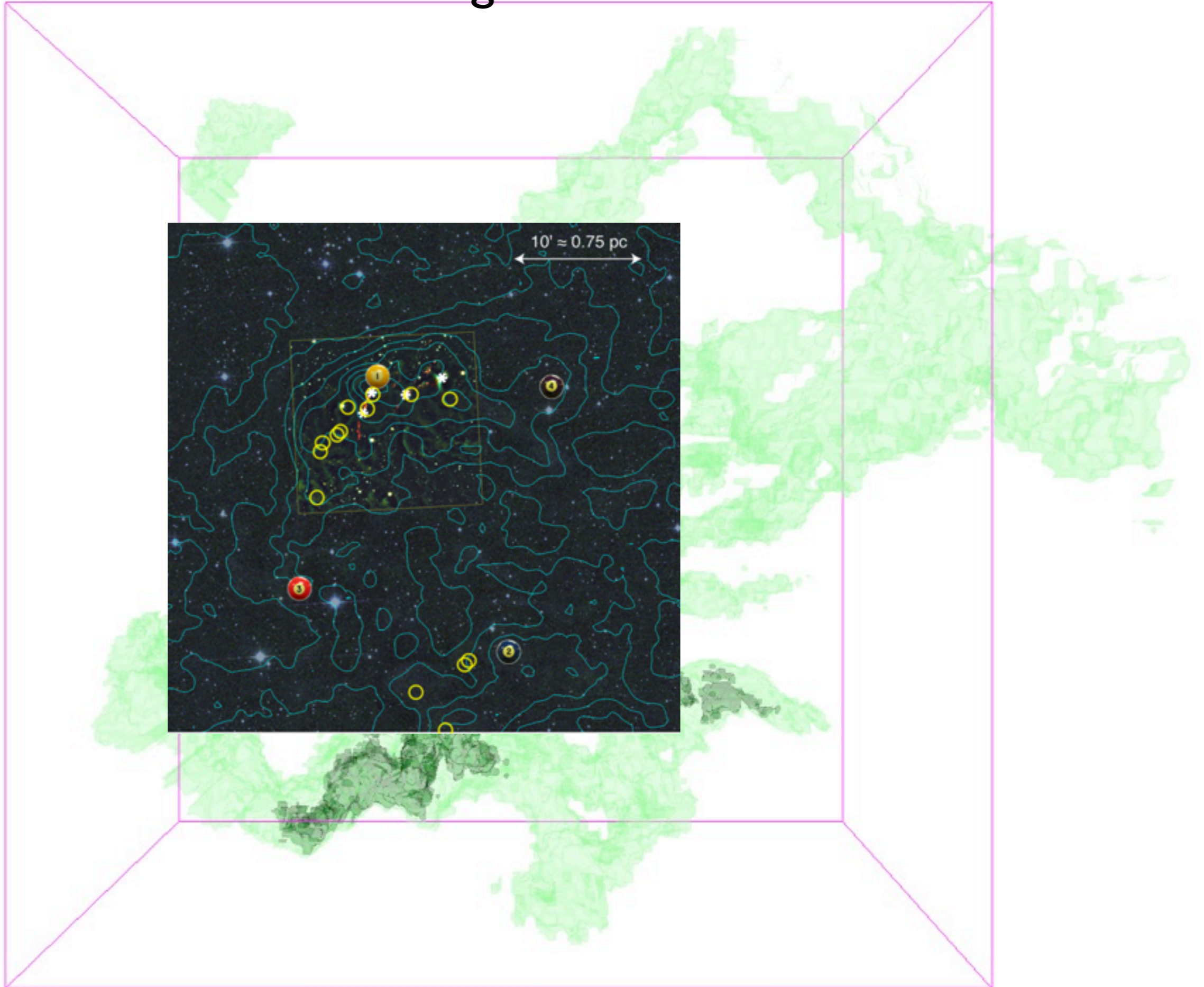
# STRONG Evidence for Coherence in Dense Cores



GBT  $\text{NH}_3$  observations of the B5 core, **Pineda et al. 2010 ApJL**;  
more cores show same behavior, Pineda et al. 2010 ApJ paper

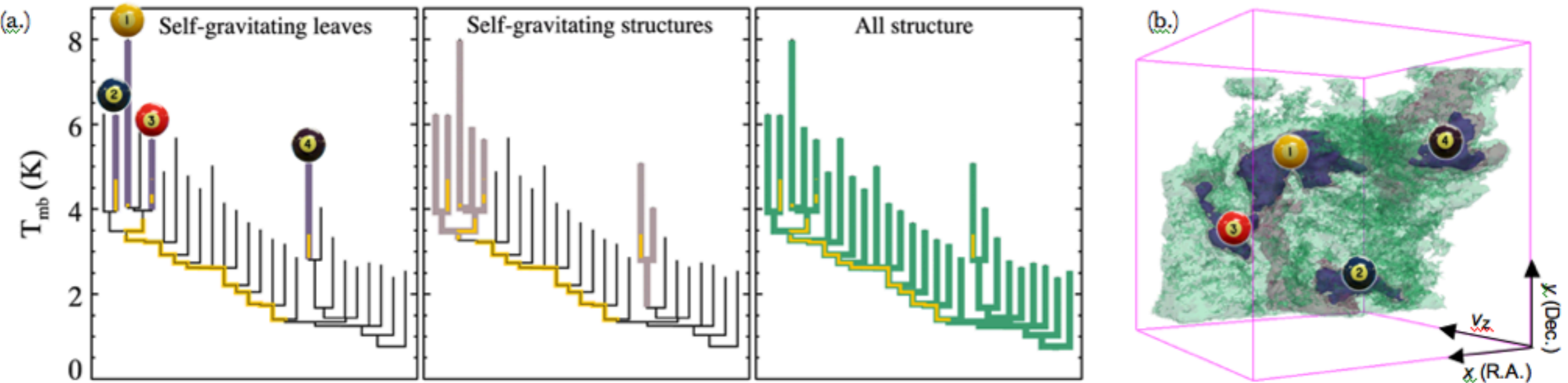


# Returning to *L1448*..





# Dendrograms & “Self-Gravity”



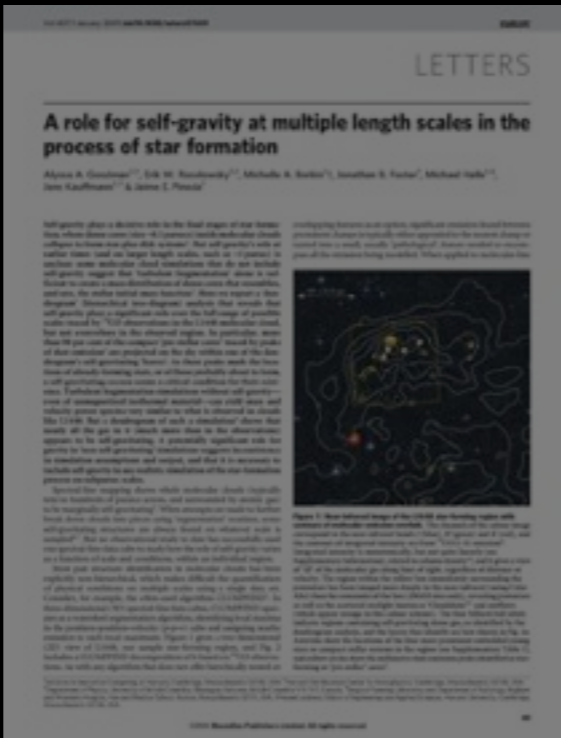
**Yellow** highlighting= “self-gravitating”

“Self-gravitating” here just means  $\alpha_{vir}$  ( $=5\sigma_v^2 R/GM_{lum}$ )  $< 2$   
(à la Bertoldi & McKee 1992)

*Rosolowsky et al. 2008 (ApJ) &  
Goodman et al. 2009 (Nature)*

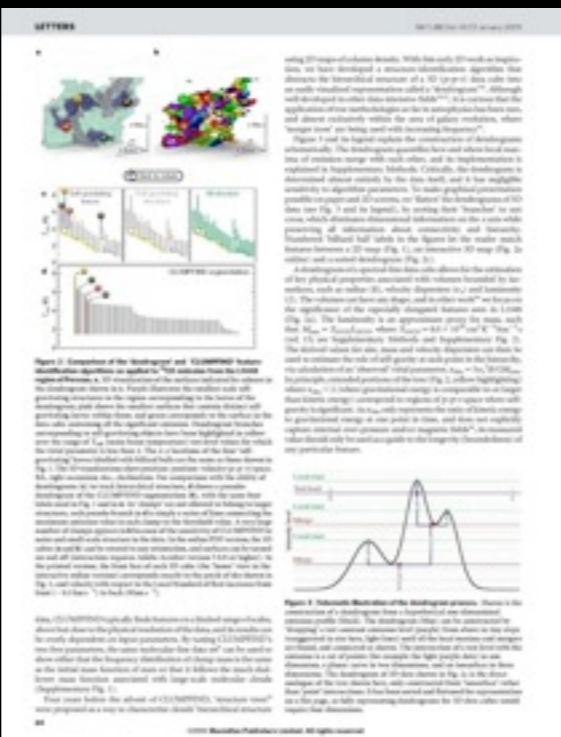
see PDF...





✓ “bi-jection”

✓ “virial parameter”



“turbulent power spectrum”

“synthetic observation”

“depletion, opacity”

“taste-test”

caveats



LETTERS

### A role for self-gravity at multiple length scales in the process of star formation

Alexis B. Goodman<sup>1,2</sup>, Erik W. Rosolowsky<sup>1</sup>, Michelle R. Borker<sup>1</sup>, Jonathan S. Foster<sup>1</sup>, Michael Heule<sup>1</sup>, Steve Kaufman<sup>1</sup>, & James I. Proser<sup>1</sup>

Self-gravity plays a decisive role in the final stages of star formation, where dense cores evolve to compact protostellar structures. However, the process of self-gravity is not understood at all scales. We use the COINTEGRATED (COIN) survey to study the evolution of protostellar cores at multiple length scales, from the initial collapse to the formation of protostellar disks. We find that self-gravity is important at all scales, from the initial collapse to the formation of protostellar disks. We find that self-gravity is important at all scales, from the initial collapse to the formation of protostellar disks. We find that self-gravity is important at all scales, from the initial collapse to the formation of protostellar disks.

Figure 1: A 3D visualization of a protostellar core showing density and temperature. The core is shown as a complex, multi-colored structure with a central protostar and surrounding protostellar disk. The colors represent different physical properties like density and temperature.

LETTERS

### The formation of self-gravitating structures in a turbulent medium

Figure 2: A plot showing the evolution of a self-gravitating structure over time. The x-axis is labeled 'Time (Myr)' and the y-axis is labeled 'Density (g/cm³)'. The plot shows a series of peaks and troughs, indicating the growth and fragmentation of the structure. The density starts at approximately 10<sup>-10</sup> g/cm³ and increases to about 10<sup>-7</sup> g/cm³ over time.

LETTERS

### Comparison of the COINTEGRATED and COINTEGRATED feature identification algorithms as applied to CO observations of the COINTEGRATED survey

Figure 3: A comparison of the COINTEGRATED and COINTEGRATED feature identification algorithms. The figure shows two panels: the left panel shows the COINTEGRATED algorithm results, and the right panel shows the COINTEGRATED algorithm results. Both panels show maps of the COINTEGRATED survey region with identified features. The COINTEGRATED algorithm identifies more features than the COINTEGRATED algorithm.

LETTERS

### Observation of the COINTEGRATED survey

Figure 4: A plot showing the observation of the COINTEGRATED survey. The x-axis is labeled 'Time (Myr)' and the y-axis is labeled 'Density (g/cm³)'. The plot shows a series of peaks and troughs, indicating the growth and fragmentation of the structure. The density starts at approximately 10<sup>-10</sup> g/cm³ and increases to about 10<sup>-7</sup> g/cm³ over time.

“turbulent power spectrum”

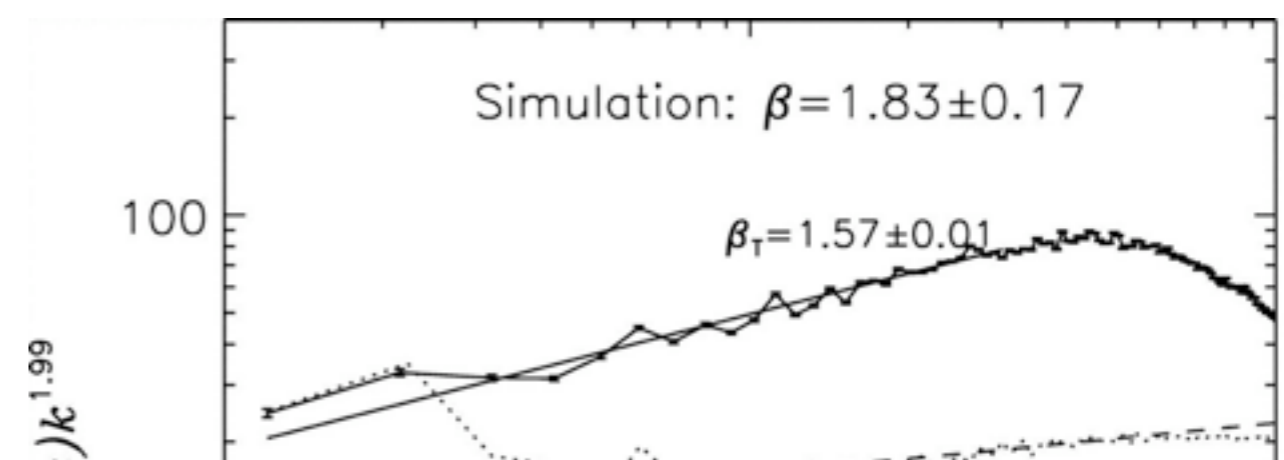
“synthetic observation”

“depletion, opacity”

“taste-test”

caveats





## THE POWER SPECTRUM OF SUPERSONIC TURBULENCE IN PERSEUS

PAOLO PADOAN,<sup>1</sup> MIKA JUVELA,<sup>2</sup> ALEXEI KRITSUK,<sup>1</sup> AND MICHAEL L. NORMAN<sup>1</sup>

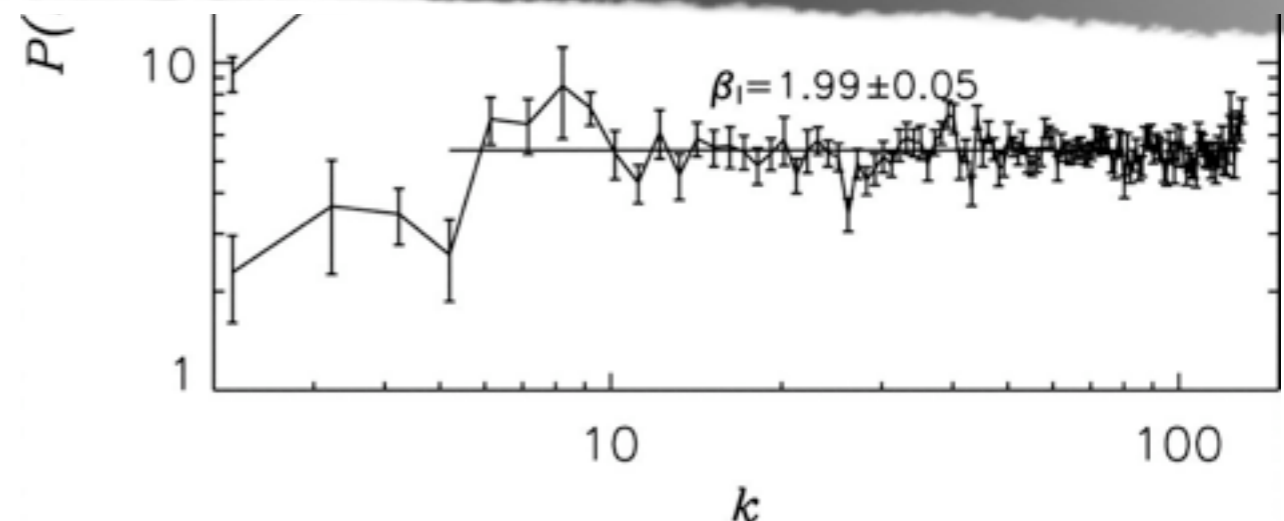
*Received 2006 August 29; accepted 2006 November 6; published 2006 November 30*

### ABSTRACT

We test a method of estimating the power spectrum of turbulence in molecular clouds based on the comparison of power spectra of integrated intensity maps and single-velocity-channel maps, suggested by A. Lazarian and D. Pogosyan. We use synthetic <sup>13</sup>CO data from non-LTE radiative transfer calculations based on density and velocity fields of a simulation of supersonic hydrodynamic turbulence. We find that the method yields the correct power spectrum with good accuracy. We then apply the method to the Five College Radio Astronomy Observatory <sup>13</sup>CO map of the Perseus region, from the COMPLETE Web site. We find a power-law power spectrum with slope  $\beta = 1.81 \pm 0.10$ . The values of  $\beta$  as a function of velocity resolution are also confirmed using the lower resolution map of the same region obtained with the AT&T Bell Laboratories antenna. Because of its small uncertainty, this result provides a useful constraint for numerical codes used to simulate molecular cloud turbulence.

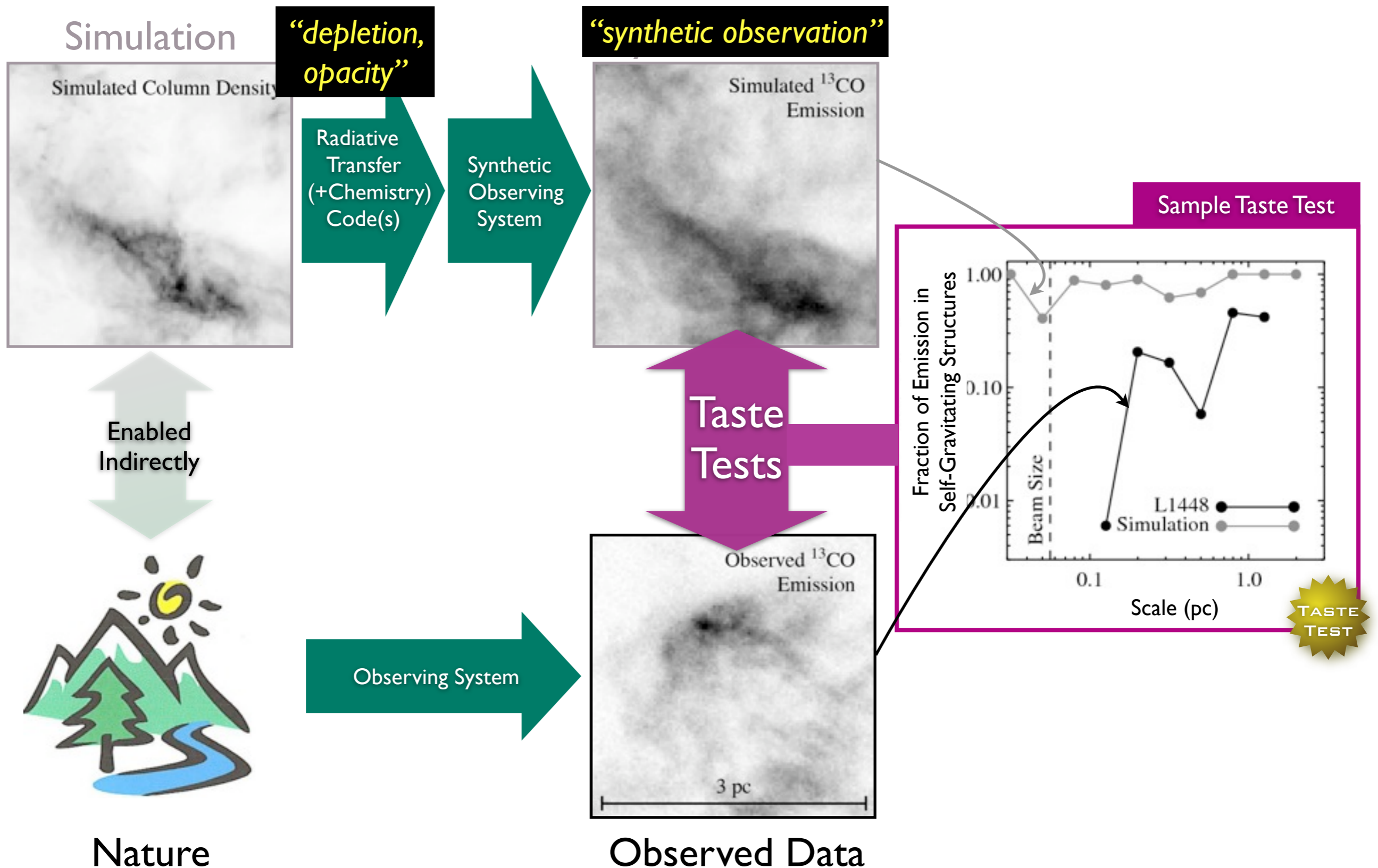
*Subject headings:* ISM: clouds — ISM: kinematics and dynamics — ISM: structure

Note: This simulation does NOT include gravity, magnetic fields, radiative effects, or explicit heating & cooling—it is pure hydrodynamics.



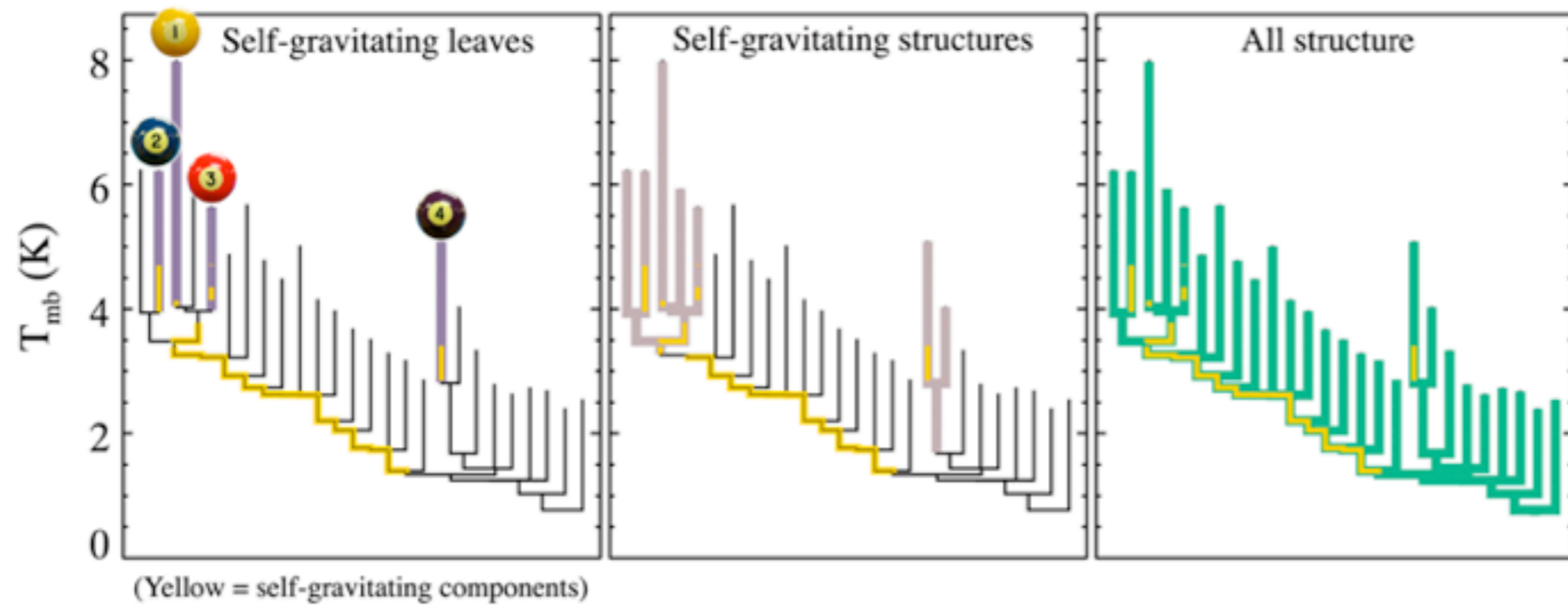


# The Taste-Testing Process

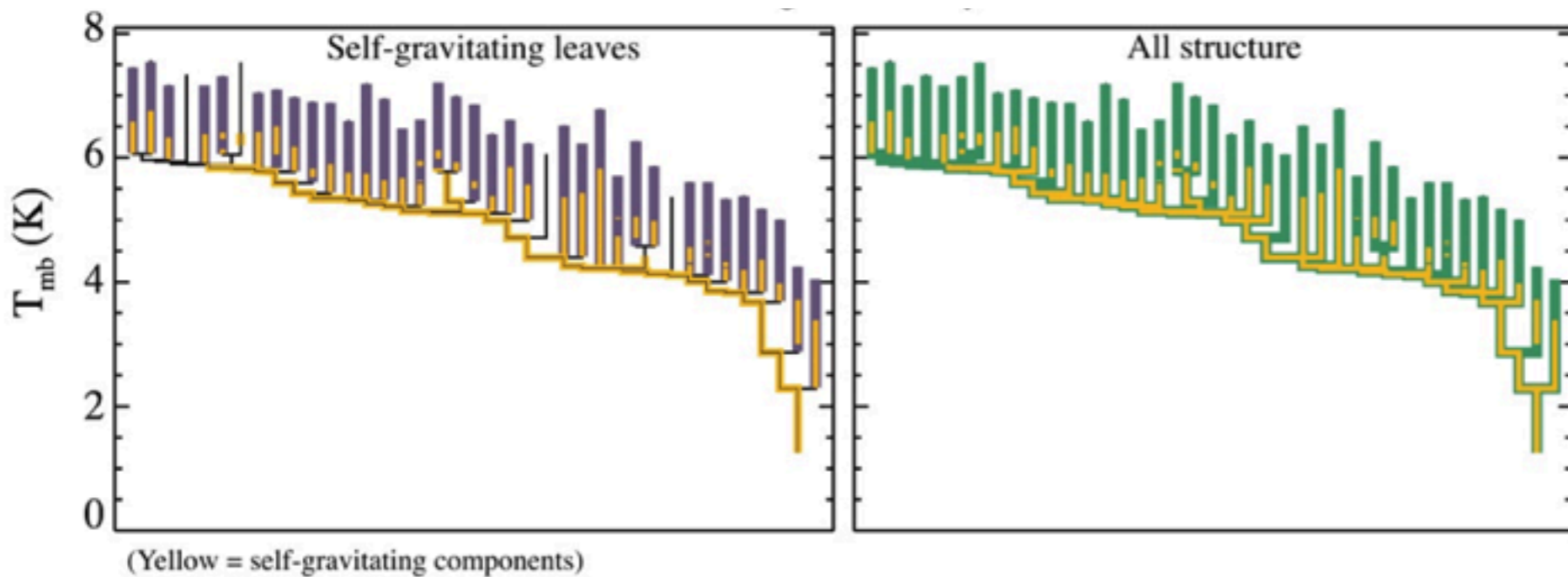
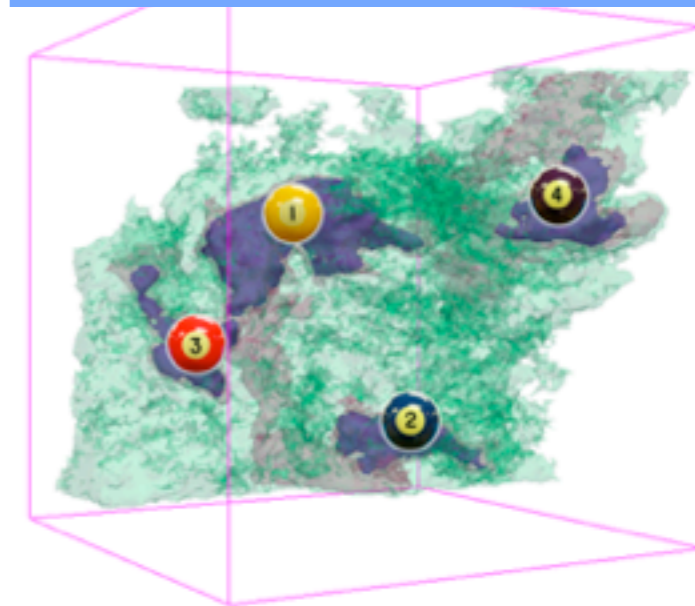




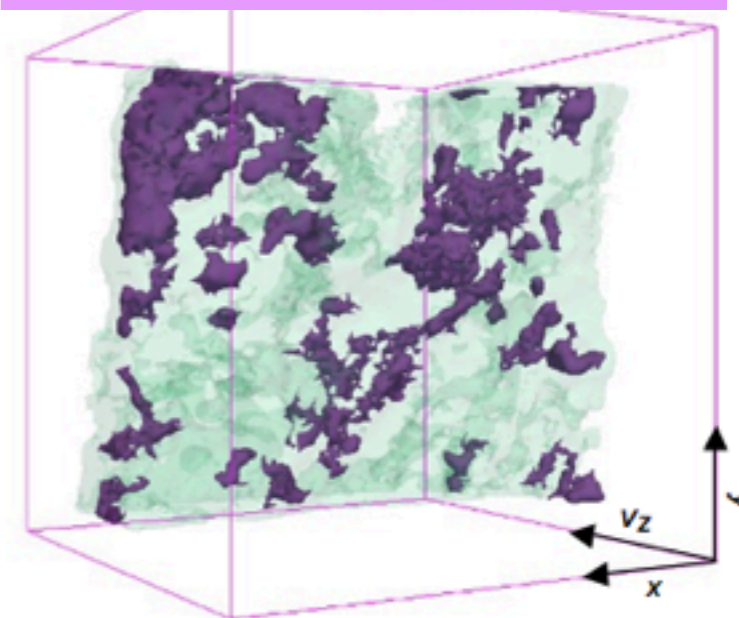
# Real vs. Simulated $^{13}\text{CO}$



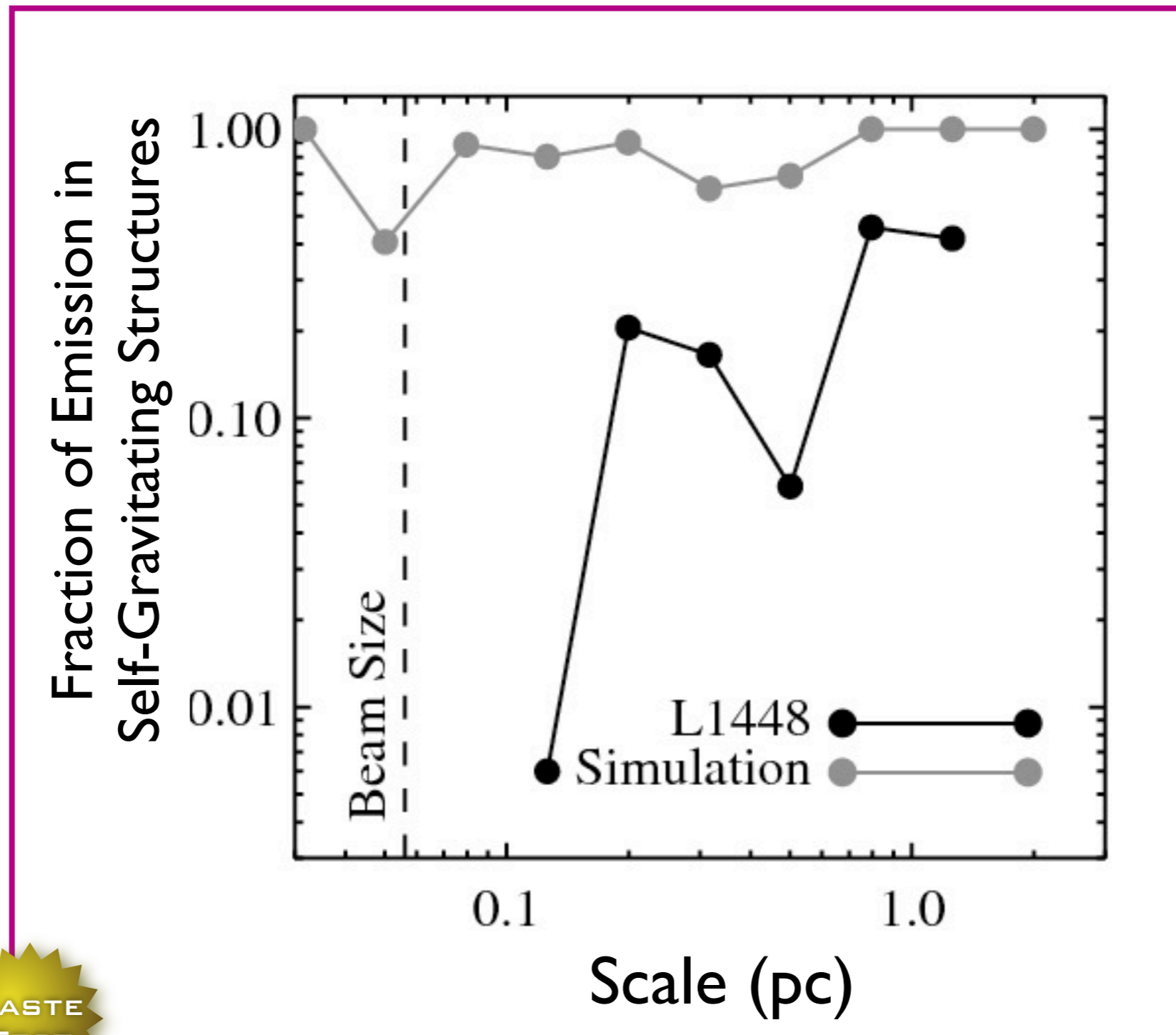
Real



Simulated



# Taste-Testing Gravity



Gravity-free HD Simulations from Padoan et al. 2006;  
L1448 analysis from Rosolowsky et al. 2008  
both lines derived from  $^{13}\text{CO}$  “observations”





### A role for self-gravity at multiple length scales in the process of star formation

Alexis B. Goodman<sup>1,2</sup>, Erik W. Rosolowsky<sup>1</sup>, Michelle R. Baker<sup>1</sup>, Jonathan S. Foster<sup>1</sup>, Michael Healy<sup>1</sup>, Sara Kaufman<sup>1</sup>, & James I. Proser<sup>1</sup>

Self-gravity plays a decisive role in the final stages of star formation, where dense cores evolve to compact protostellar protoplanets. However, the role of self-gravity in the earlier stages of star formation is less clear. We use a novel method to measure the self-gravity of protoplanets at multiple length scales, and find that self-gravity is important in the formation of protoplanets at multiple length scales. We use a novel method to measure the self-gravity of protoplanets at multiple length scales, and find that self-gravity is important in the formation of protoplanets at multiple length scales. We use a novel method to measure the self-gravity of protoplanets at multiple length scales, and find that self-gravity is important in the formation of protoplanets at multiple length scales.

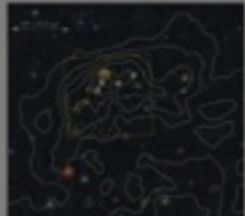


Figure 1: A 3D visualization of a protoplanetary disk showing density and self-gravity contours. The disk is shown in a perspective view, with a central protostar and a surrounding disk of gas and dust. Contours represent density and self-gravity, showing how they vary across the disk and towards the center.

The self-gravity of protoplanets is a key factor in the final stages of star formation. We use a novel method to measure the self-gravity of protoplanets at multiple length scales, and find that self-gravity is important in the formation of protoplanets at multiple length scales. We use a novel method to measure the self-gravity of protoplanets at multiple length scales, and find that self-gravity is important in the formation of protoplanets at multiple length scales.

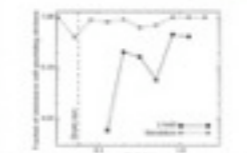


Figure 2: A line graph showing the relationship between self-gravity and protoplanet mass. The x-axis represents protoplanet mass, and the y-axis represents self-gravity. The graph shows a series of data points connected by lines, illustrating how self-gravity changes as the mass of the protoplanet increases.

Our results show that self-gravity is a key factor in the final stages of star formation. We use a novel method to measure the self-gravity of protoplanets at multiple length scales, and find that self-gravity is important in the formation of protoplanets at multiple length scales. We use a novel method to measure the self-gravity of protoplanets at multiple length scales, and find that self-gravity is important in the formation of protoplanets at multiple length scales.

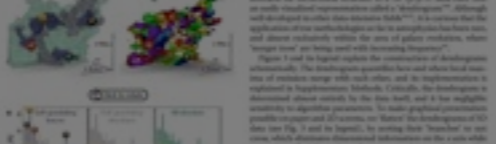


Figure 3: A 3D visualization of a protoplanetary disk showing density and self-gravity contours. The disk is shown in a perspective view, with a central protostar and a surrounding disk of gas and dust. Contours represent density and self-gravity, showing how they vary across the disk and towards the center.

Our results show that self-gravity is a key factor in the final stages of star formation. We use a novel method to measure the self-gravity of protoplanets at multiple length scales, and find that self-gravity is important in the formation of protoplanets at multiple length scales. We use a novel method to measure the self-gravity of protoplanets at multiple length scales, and find that self-gravity is important in the formation of protoplanets at multiple length scales.

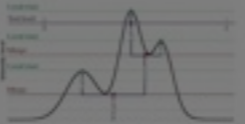


Figure 4: A line graph showing the relationship between self-gravity and protoplanet mass. The x-axis represents protoplanet mass, and the y-axis represents self-gravity. The graph shows a series of data points connected by lines, illustrating how self-gravity changes as the mass of the protoplanet increases.

The self-gravity of protoplanets is a key factor in the final stages of star formation. We use a novel method to measure the self-gravity of protoplanets at multiple length scales, and find that self-gravity is important in the formation of protoplanets at multiple length scales. We use a novel method to measure the self-gravity of protoplanets at multiple length scales, and find that self-gravity is important in the formation of protoplanets at multiple length scales.



Figure 5: A line graph showing the relationship between self-gravity and protoplanet mass. The x-axis represents protoplanet mass, and the y-axis represents self-gravity. The graph shows a series of data points connected by lines, illustrating how self-gravity changes as the mass of the protoplanet increases.

Our results show that self-gravity is a key factor in the final stages of star formation. We use a novel method to measure the self-gravity of protoplanets at multiple length scales, and find that self-gravity is important in the formation of protoplanets at multiple length scales. We use a novel method to measure the self-gravity of protoplanets at multiple length scales, and find that self-gravity is important in the formation of protoplanets at multiple length scales.

conclusion is that self-gravity is a key factor in the final stages of star formation. We use a novel method to measure the self-gravity of protoplanets at multiple length scales, and find that self-gravity is important in the formation of protoplanets at multiple length scales. We use a novel method to measure the self-gravity of protoplanets at multiple length scales, and find that self-gravity is important in the formation of protoplanets at multiple length scales.

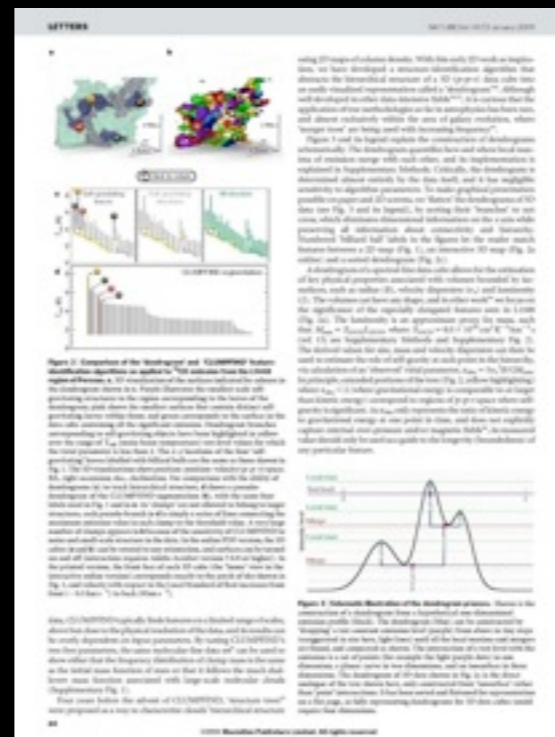


conclusions & caveats

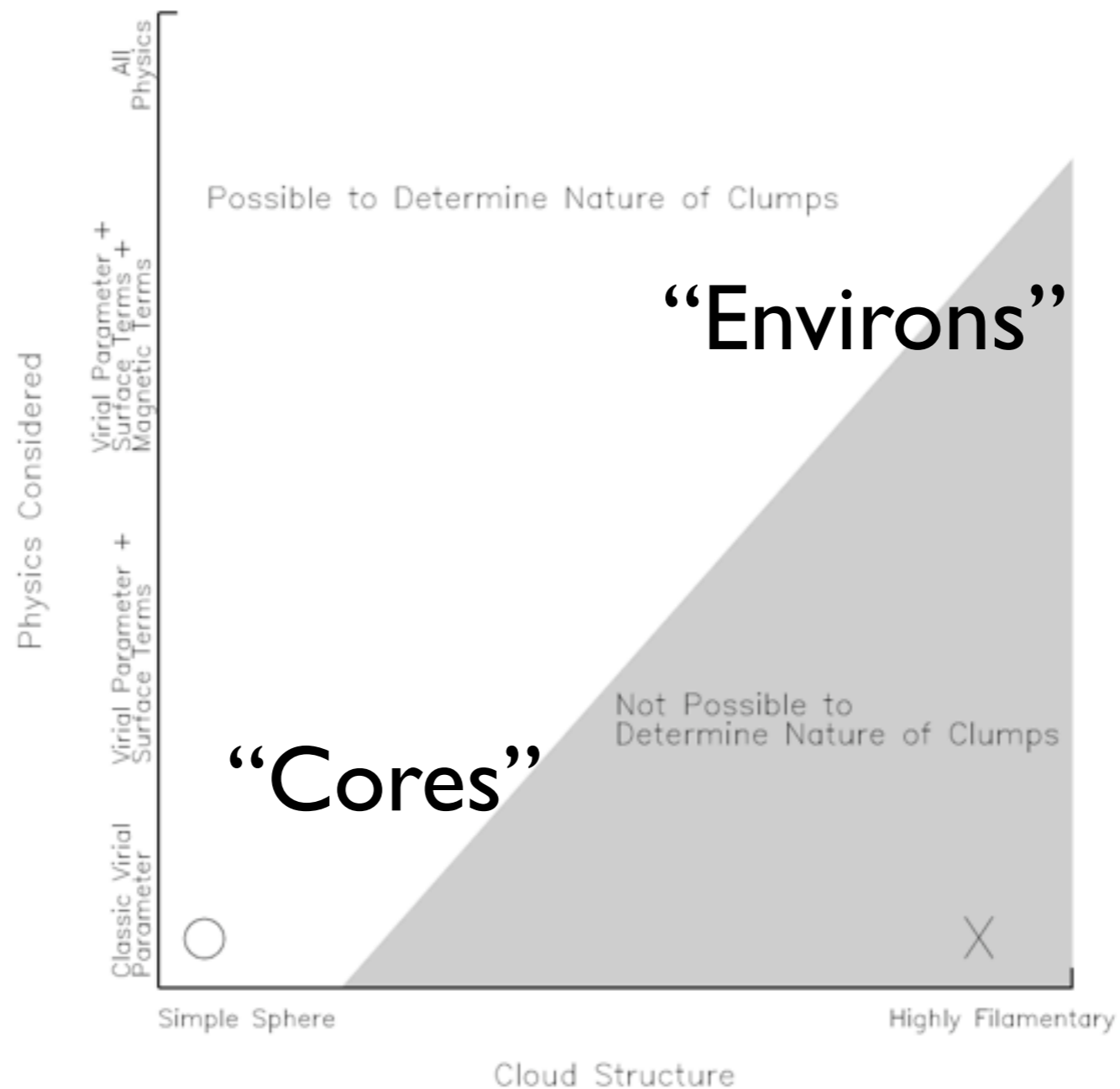




Star formation takes place in self-gravitating “coccoons,” and some of those coccoons are bound to each other.



# Caveats/Worries about $p$ - $p$ - $v$ (bijection) ... and the virial parameter



from **Shetty**, Collins, Kauffmann, Goodman, Rosolowsky 2010;  
see also recent work of Dib et al., Ostriker et al., Ballesteros-Paredes et al., Myers, and Smith, Clark & Bonnell



# What (else) keeps me up at night now...

“Bi-jection” or “ $p-p-p$  to/from  $p-p-v$ ” & the impact  
of missing terms in **virial analysis** in each space  
[Shetty, Collins, et al.]

**Projection** effects in analyzing **spatial & velocity  
offsets**  
[Kirk, Pineda, Offner, et al.]

When/how can we best **measure YSO velocities**  
& what should they be?  
[Covey, Offner, et al.]

How much excess column is there **beyond “log-  
normal”**?  
[Foster, Offner, et al.]

Effects of **Cloudshine** on **Deep NIR Point Source  
Photometry** (e.g. **JWST**) [Foster!]

Can we **differentiate** simulations **with** known &  
simple new “**taste tests**”  
[Rosolowsky, Shetty, et al.]  
...for example, how do **cores connect to** their  
**environment**?  
[Kauffmann, Myers, Pineda, Alves, Foster,  
Rosolowsky, Offner, et al.]?

Can we do better than **Kennicutt-Schmidt**,  
really?  
[Cox, Narayanan, Shetty, Rosolowsky et al.]

Effects of **B-Star Winds** on Cloud Evolution  
[Covey, Sharma, **Valverde**, Borkin, **Arce** et al.]

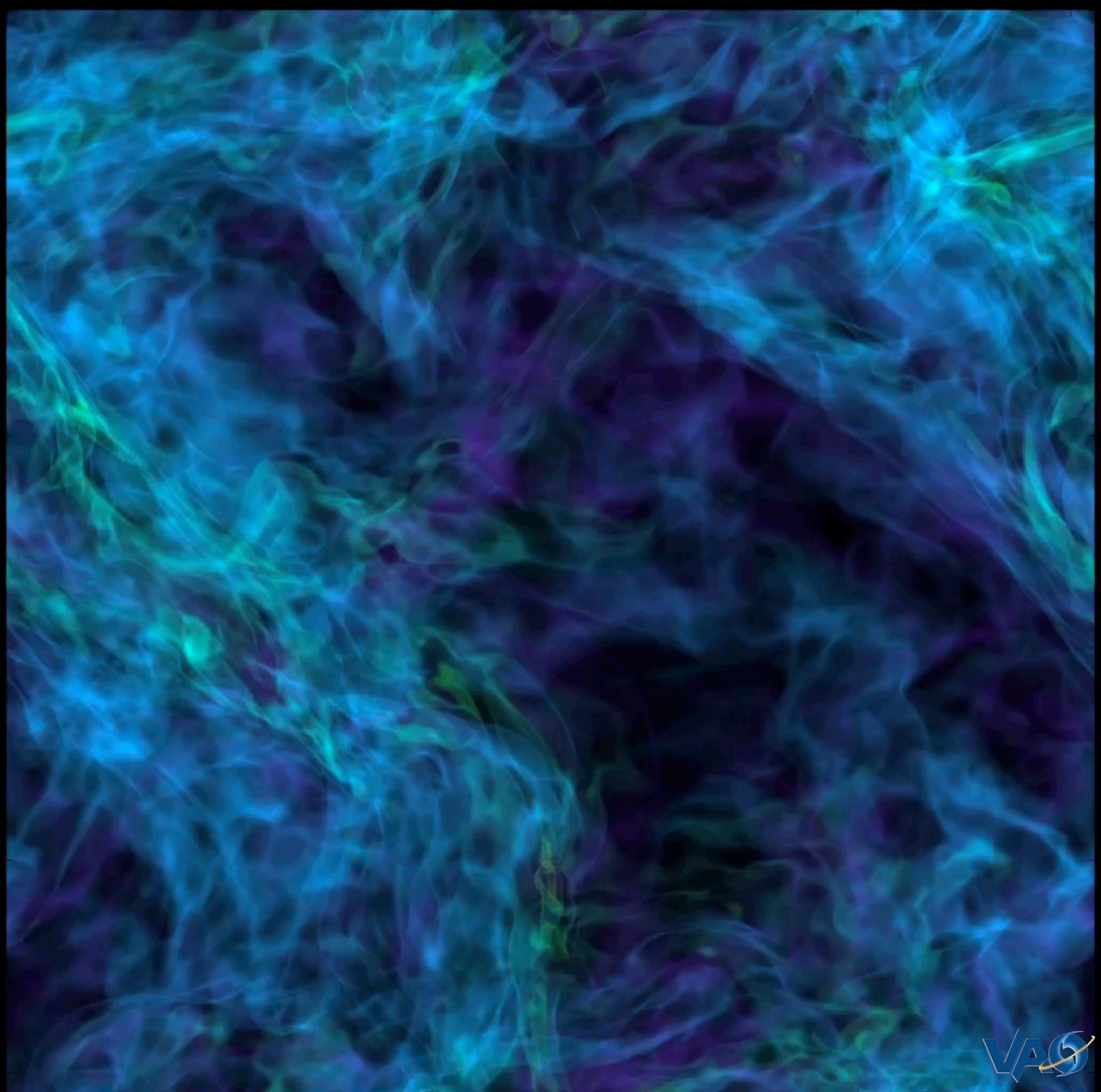
Do **dendrograms** give a different **CMF**?  
[Alves, Rosolowsky, Pineda et al.]

And, what about **magnetic fields**?!  
[Li et al. 2009...]

...and WWT, IIC, 3D Data Desk, WGBH, VAO...and my family.

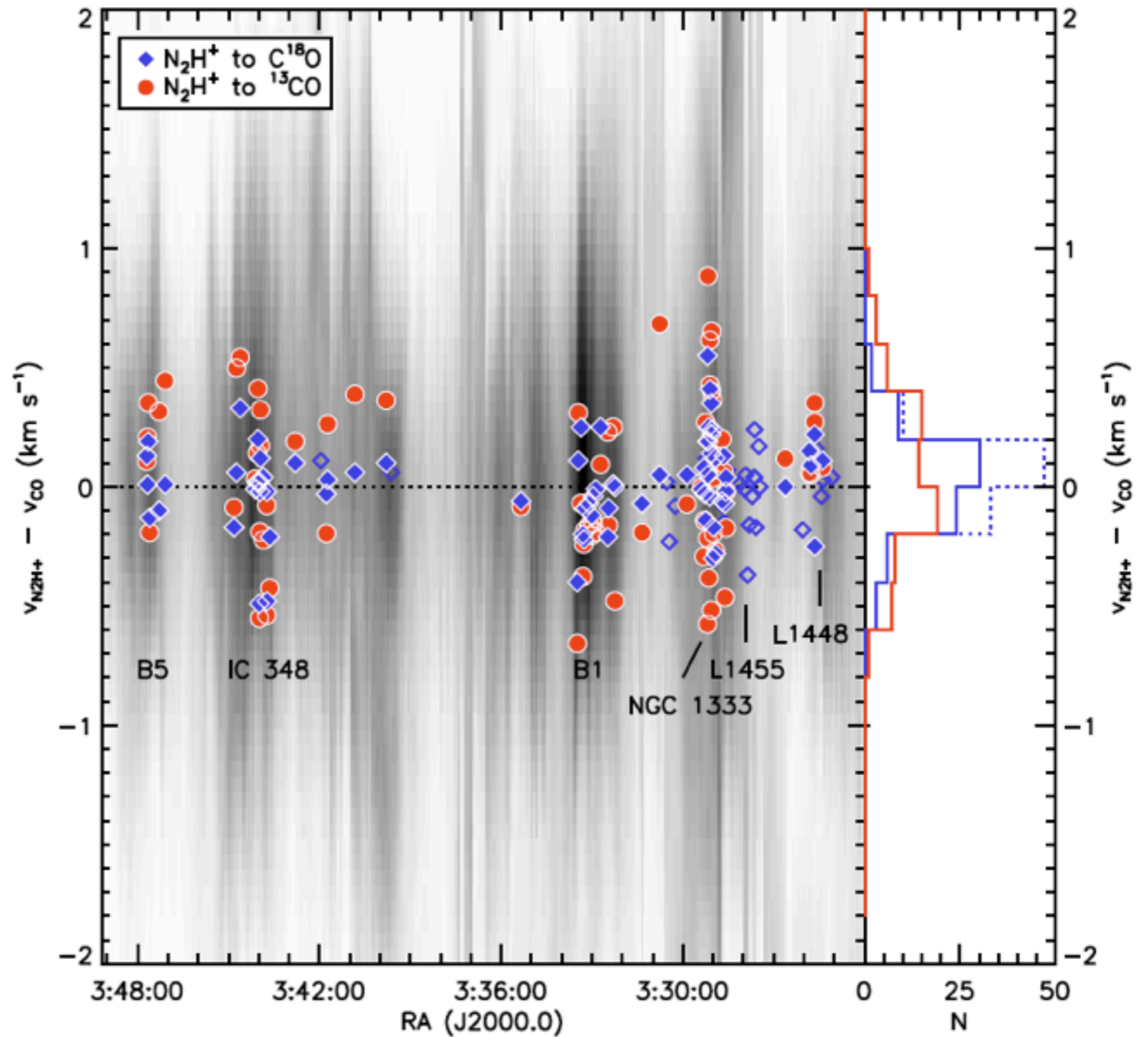
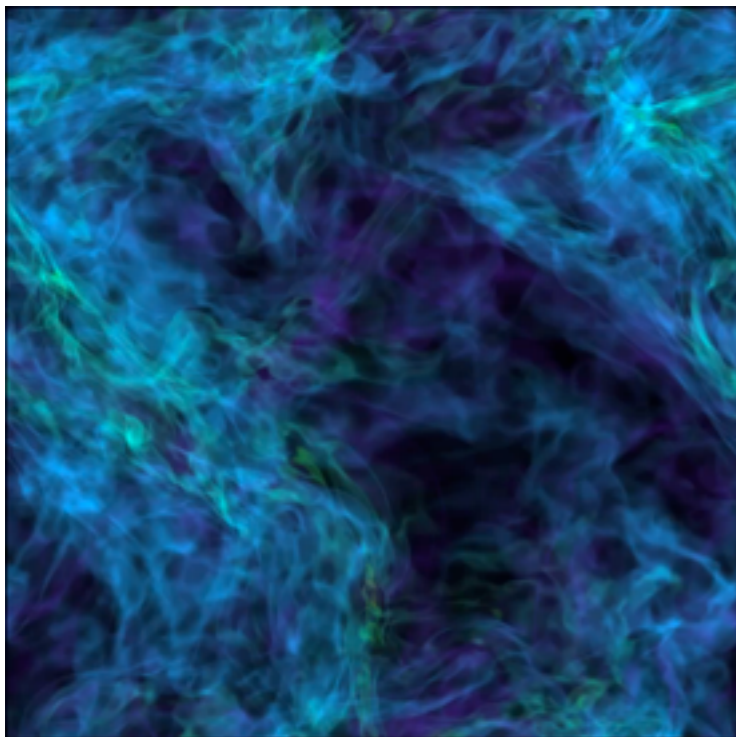


*Molecular cloud gas densities from an AMR simulation with radiation feedback (**Offner et al. 2009**). The movie is 0.65 pc on a side and covers about 0.15 Myr.*





# Why so still?



Kirk, Pineda, Johnstone & Goodman 2010



“turbulent fragmentation”

“L1448”

“(magneto-)hydrodynamic simulation”

“Cloudshine”

“pre-stellar core”

“protostar”

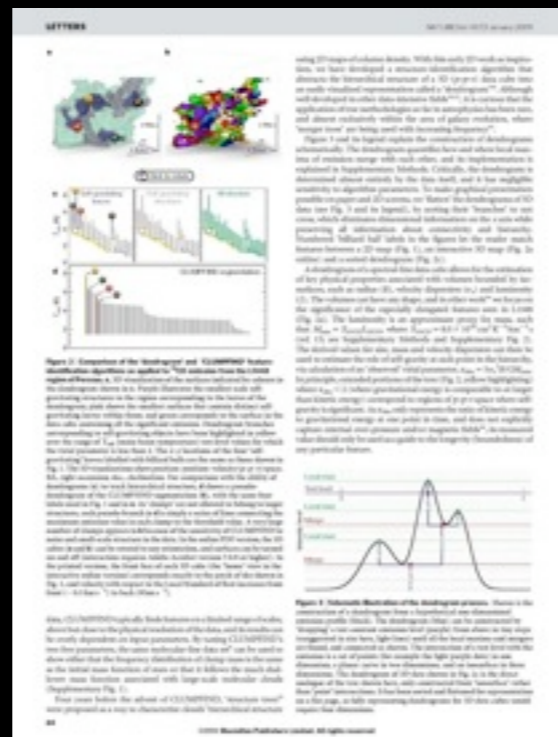
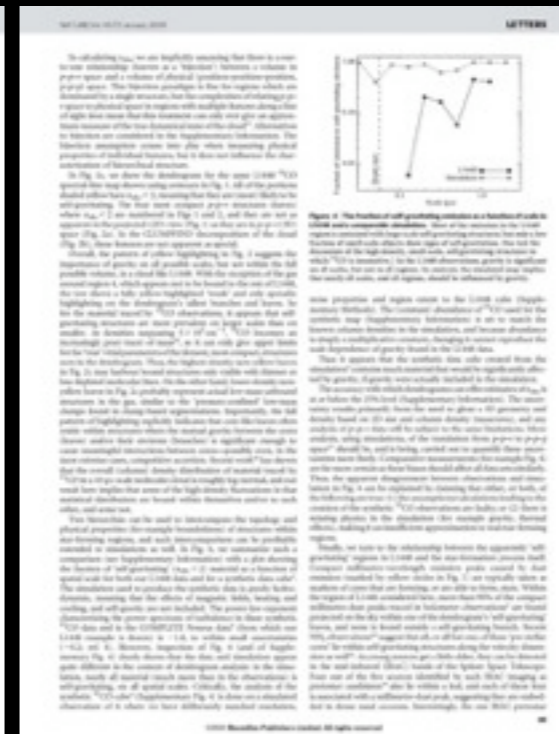
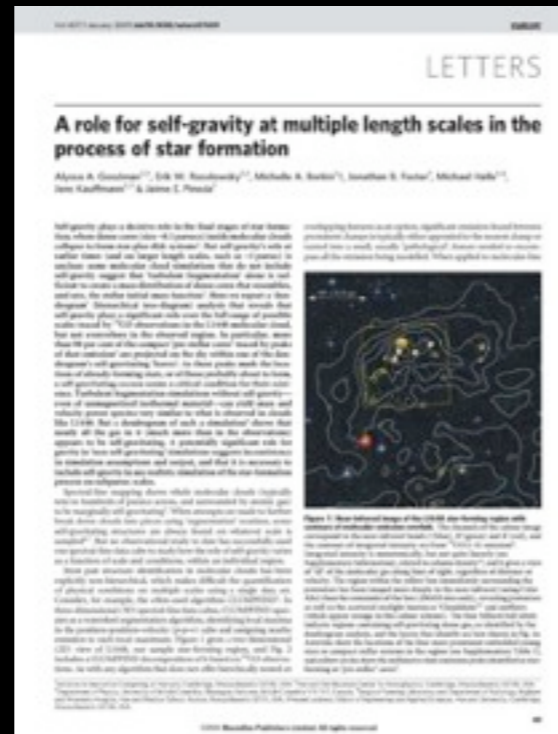
“integrated intensity”

“p-p-v cube”

“segmentation”

“CLUMPFIND”

“Dendrogram”



“COMPLETE”

“3D PDF”

“bi-jection”

“virial parameter”

“column density”

“turbulent power spectrum”

“synthetic observation”

“depletion, opacity”

“taste-test”

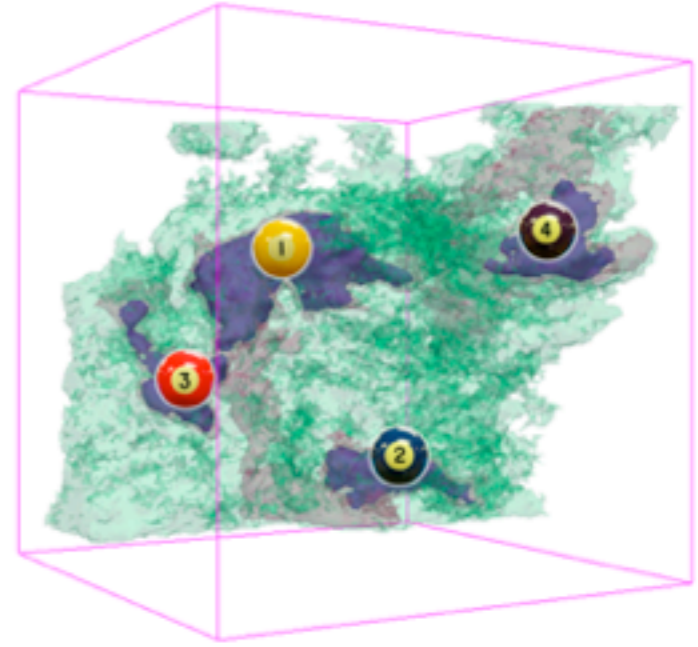
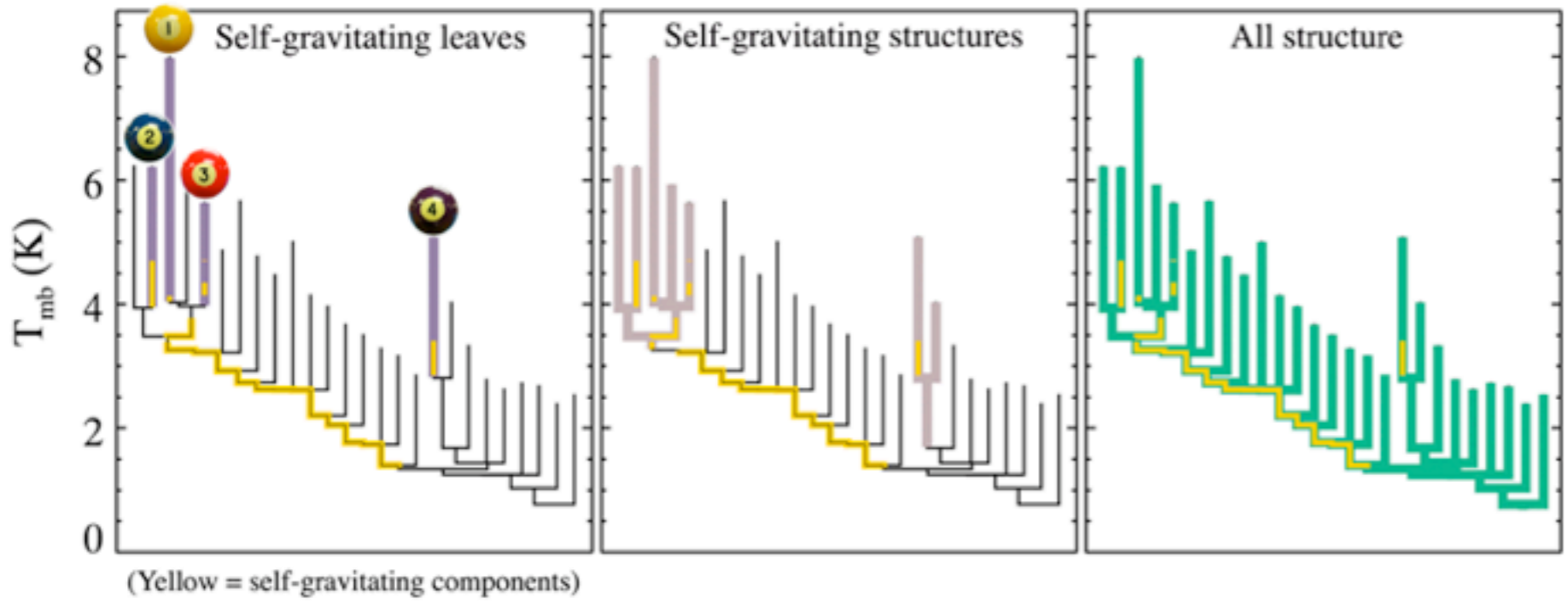
caveats





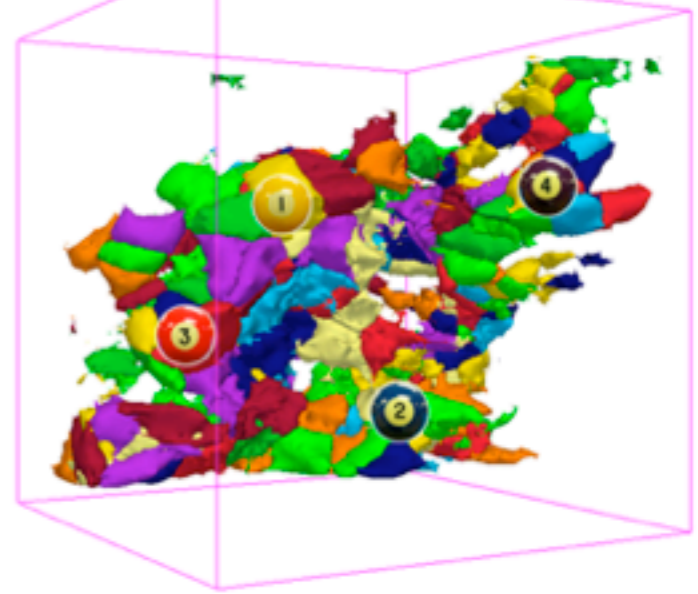
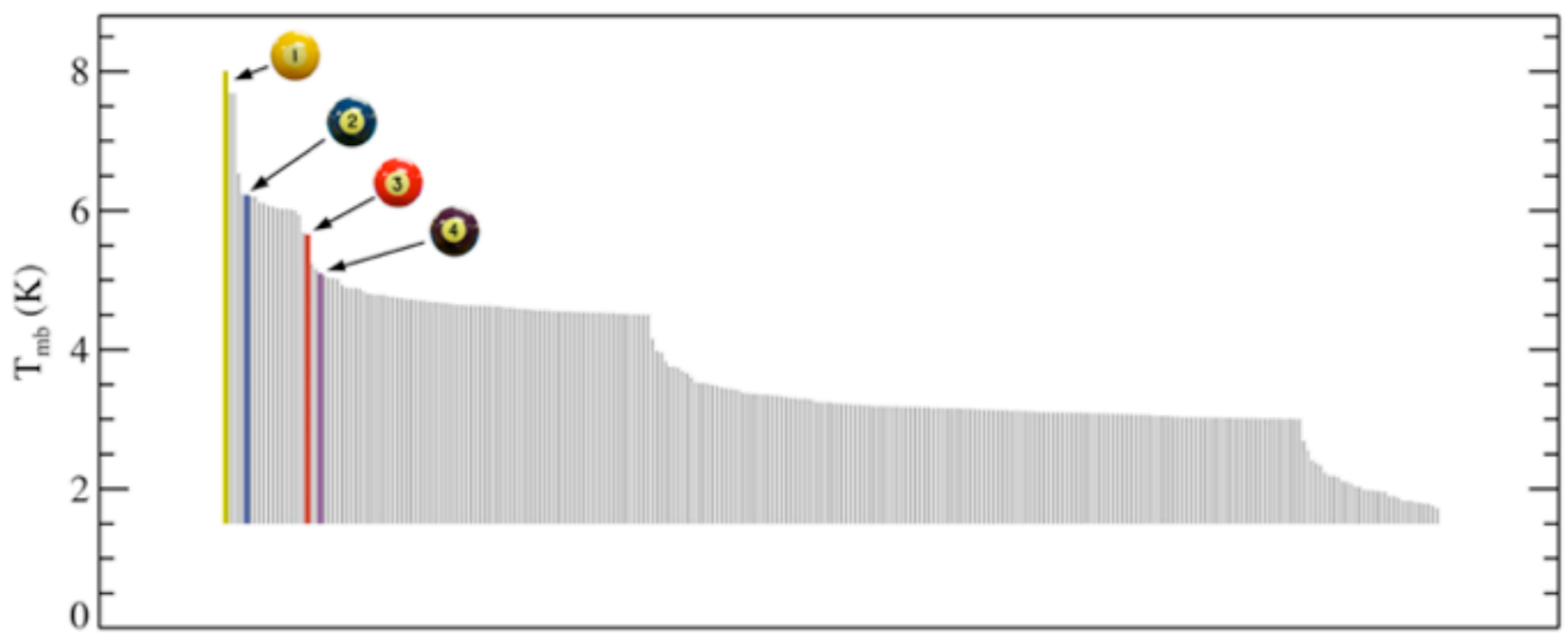
# CLUMPFIND vs. Dendrograms: LI 448

## Dendrograms



The online PDFs of these insets

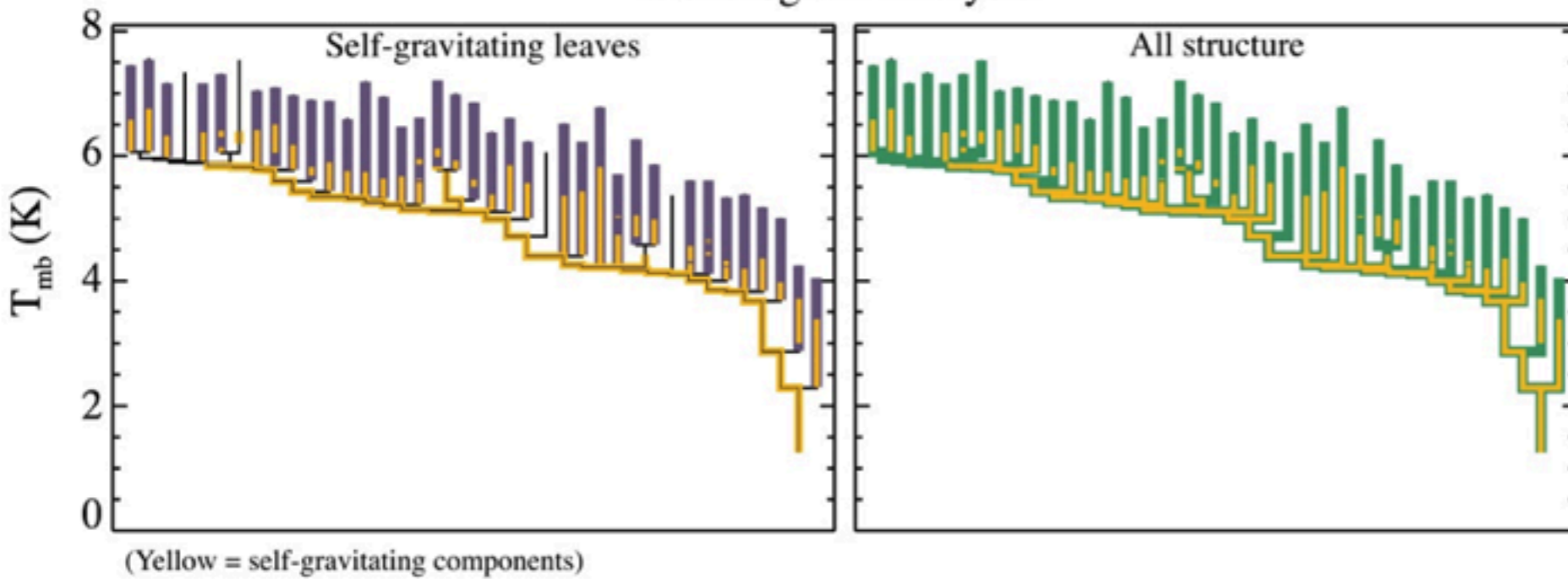
## “CLUMPFIND”



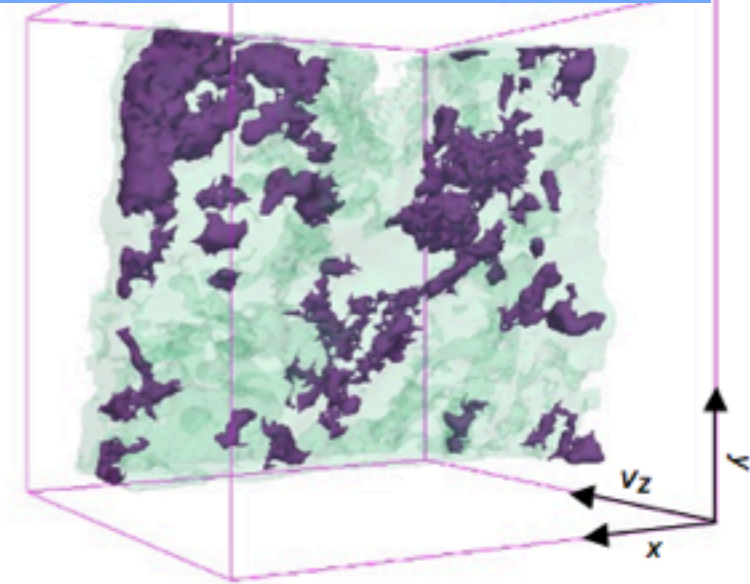


# CLUMPFIND vs. Dendrograms: Synthetic Data

## Dendrogram Analysis

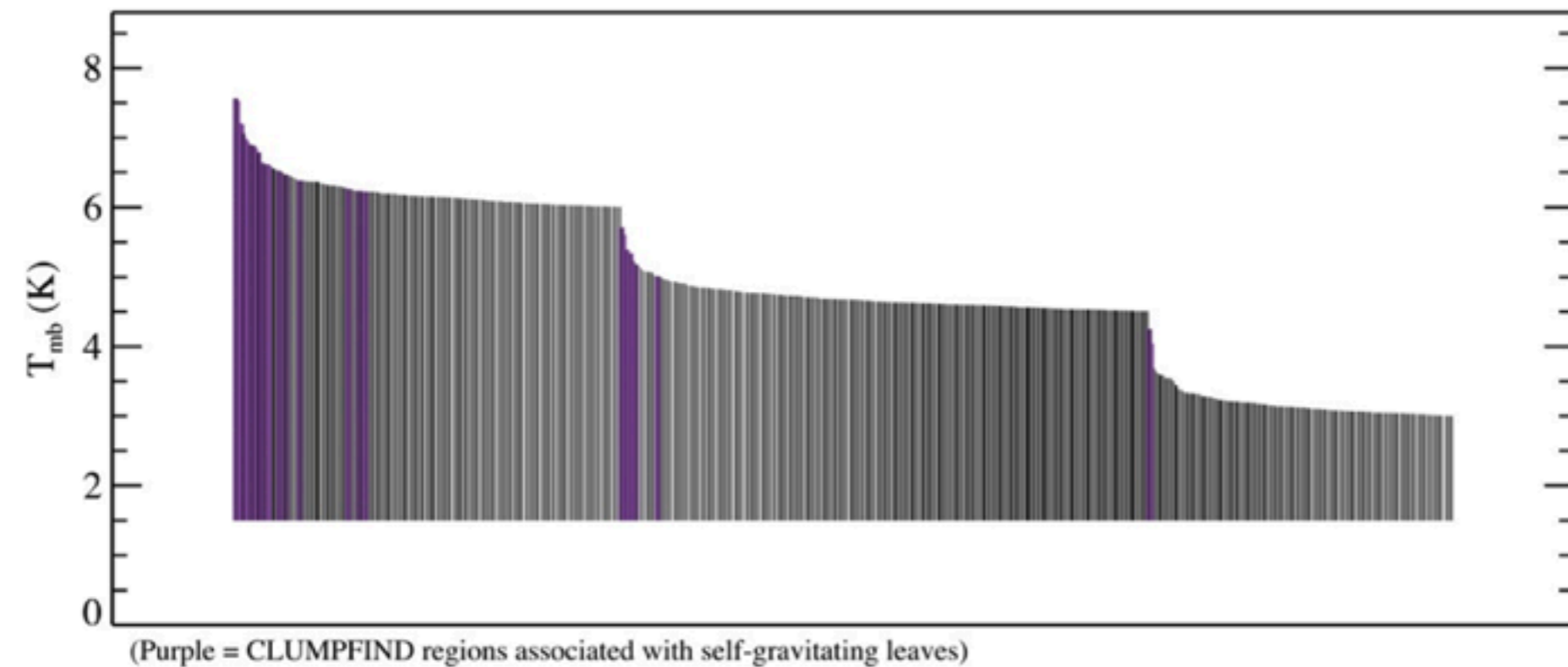


## Dendrograms

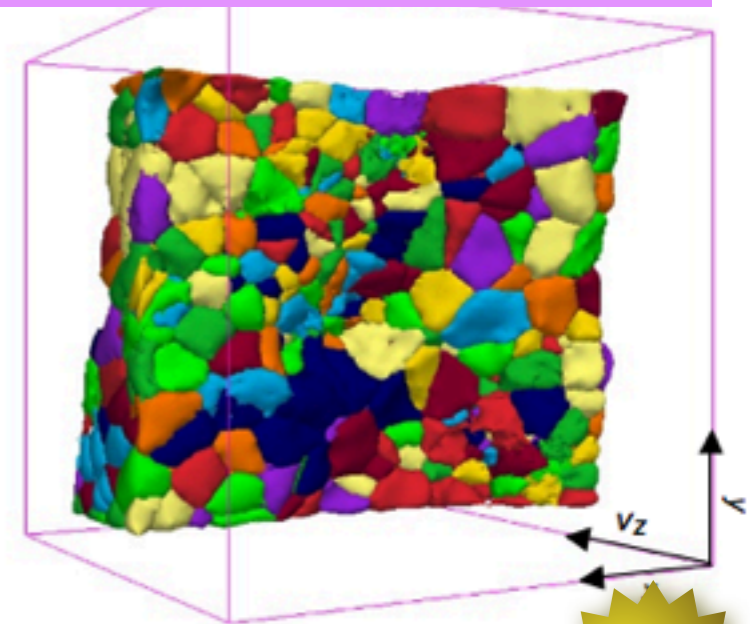


*i* The online PDFs of these insets are interactive, offer additional surfaces, and can be rotated and manipulated by

## CLUMPFIND Analysis



## “CLUMPFIND”



TASTE TEST



# HOMEWRECKERS

*Stars disturbing their ancestral homes*

*Alyssa Goodman (Harvard-Smithsonian Center for Astrophysics)*

*Héctor Arce (Yale University)*

*Lawrence Valverde (Harvard College)*



# M17



Hubble image of the Swan Nebula  
Photograph courtesy of NASA/STSCI/Jeff Hester, Arizona State University



# This is not real..but it could be.

